

Malin Bø Nevstad

Use of different imaging systems for ROV-based mapping of complex benthic habitats

Master's thesis in Ocean Resources

Supervisor: Geir Johnsen

Co-supervisor: Torkild Bakken, Martin K. Larsen, Aksel A. Mogstad

December 2022



ROV-photo by Malin Bø Nevstad.

Malin Bø Nevstad

Use of different imaging systems for ROV-based mapping of complex benthic habitats

Master's thesis in Ocean Resources

Supervisor: Geir Johnsen

Co-supervisor: Torkild Bakken, Martin K. Larsen, Aksel A. Mogstad

December 2022

Norwegian University of Science and Technology

Faculty of Natural Sciences

Department of Biology



Norwegian University of
Science and Technology

Acknowledgements

The work for this thesis took place at the Norwegian University of Science and Technology (NTNU), at the Department of Biology in the period from August 2021 to December 2022. Most of the work was conducted at Trondhjem Biological Station (TBS). Fieldwork was performed at NTNU's field station at Slettvik in Hopavågen, Agdenes and Karihavet, Nordmøre.

First, I want to thank my supervisor Geir Johnsen for this amazing opportunity to work hands-on with enabling technology and sharing his enthusiasm and encouragement. I also thank my co-supervisor Torkild Bakken for help and guidance identifying animals, concretizing the thesis, and discussing the results. Thank you, co-supervisor Martin Kvisvik Larsen, for your help with UHI data collection and underwater photogrammetry guidance. Thank you Aksel Mogstad for your guidance on UHI data collection and processing the UHI raw data. I want to thank you all for sharing your in-depth knowledge.

A big thank you to Glauca Fragoso for letting me use your ROV for this project. Learning the ROV and photogrammetry with you and your team has been a fun learning experience. I want to thank Eleni Diamanti for sharing your experience of UPG methods with me and teaching me all the cool tips and tricks. Thankyou Stephen Grant for assisting me with the spectrometer data when I was completely stuck, and to Marie Henriksen for helping me with the visualization of the reflectance plots. Thank you, Natalie Summers, for great advice (I followed it) and discussions of my results. I wish to thank everyone at TBS for your support and keeping your doors open for me during my stay here.

Thank you, Nils Aukan, for sharing your in-depth knowledge of Karihavet and allowing us to use your amazing photos. Thank you Nils Aukan and Peder Martinini from Kristiansund dykkerklubb for the help collecting specimens. Thank you Trond Larsen (Blueye) for sharing your knowledge and experience on the Blueye ROV and underwater photogrammetry.

Additional gratitude given to my peers at TBS. Thank you Mikkel Bjerkvoll, Maren Thu, Martin Overrein, Marte Sjøreng, Camilla Marnor and Anneken Nøland for the great discussions and fun fieldworks. Thankyou Amy Li for taking pictures and all your help during field- and labwork (Tether-master).

Thank you to Astrid Ellinor Godø and Tove Beate Leren at Akademiet Ålesund for cultivating my curiosity for biology and supporting me early on. I especially value our fieldtrips to different nature sites and cities, and especially thank you Tove for introducing me to the amazing people at TBS. You both inspired me greatly and I am so happy I got the experience to be your student.

I want to thank my mother for her endless support from the start. I can still remember telling you at the age of 11 that I wanted to be a marine biologist. Thank you for letting me stay 6 hours in the aquarium and babble about jellyfish to you and letting me binge-watch ocean documentaries when you'd rather watch the news.

Trondheim, December 2022

Malin Bø Nevstad

Abstract

This study uses mini-ROVs, small remotely controlled vehicles carrying cameras with different properties such as the underwater hyperspectral imager (UHI) and the high definition (HD) red, green, and blue (RGB) camera to map benthic habitats in both soft sediment and bedrock vertical walls in a poorly examined nature type (semi-enclosed bay), at a location called Karihavet in Nordmøre inhabiting species with cold-water (<7 °C) distribution only found in similar bays along the Norwegian coastline and the Svalbard-Barents Sea region. The discovery of these special habitats, present in Karihavet, were done by SCUBA divers and is an example of citizen science for mapping of species observations along the Norwegian coast. Semi-enclosed bays are a nature type that has been very little studied in terms of biology.

There was a clear change in salinity and temperature at 25 meters depth towards colder and denser water. At depths deeper than 20 meters the faunal species composition changed to include typical cold-water species from the Arctic. One such species that occurred at >24 meters depth was high occurrence of the bivalve *Chlamys islandica*, a scallop that has previously been a focused species for trawling in the Barents Sea (intensive trawling during 1987-1989). This study showed that biodiversity and coverage of filter feeding species indicated the depth range from 20-30 meters is an extremely productive zone in Karihavet, characterized with substrate covered with red coralline algae and bioclastic sediments.

The use of enabling technology to survey the ocean can be done over a big range of spatial levels. The observational pyramid uses layers of information from different platforms to systemize ocean observations. For this study the observational pyramid is applied to extract biological information from the comparison of physical samples (from SCUBA-diving) and different optical methods like RGB-ROV video analysis, underwater hyperspectral imaging (UHI) and underwater photogrammetry (UPG) across the same habitat.

Assessment of new modeling methods derived from RGB-camera imaging data called underwater photogrammetry (UPG) previously used in underwater archeological research were done mapping the seafloor from 35 meters depth soft sediments to a 10 meters depth vertical wall. UPG uses overlapping images to estimate object placement in 3D space and creates a 3D model derived from 2D overlapping images. The use of UPG enabled a continuous visualization of the video-data derived from ROV-video data without preprogrammed altitude control, known geolocations or lasers, but simple measurements of size estimation of objects, diversity indexes, habitat mapping and classification could be done. The method could register and place objects as small as calcareous tubeworms onto flat bedrock walls, obtaining sub-centimeter spatial resolution. More verification of accuracy of this method is needed to control the accuracy of the measurements derived from UPG, which will be the next step in the process of assessment of UPG for use in biological surveying of the seafloor and obtaining absolute size measuring.

Underwater hyperspectral imaging (UHI) was used to map the soft sediments to collect hyperspectral data of the area, and objects with different spectral properties were classified into six classes of animals, different algae groups, and sediment classes. Bioclastic sediments that consist of calcareous shell pieces of dead and living animals were possible to identify and map in a single class of objects of interest (OOI) due to its high-intensity spectral reflectance (λ). This class can be used to quantify production of filter feeding species like mollusks and calcareous tubeworms and estimate productivity. By demonstrating ROV-UHI mapping, this study contributes to establishing the use of UHI for benthic habitat mapping and estimating spatial coverage of species in the habitat.

Sammendrag

Denne studien bruker mini-ROV-er, små fjernstyrte kjøretøyer som bærer kameraer med forskjellige egenskaper som undervanns hyperspektral avbildning (UHI) og høy-definisjon (HD) rød, grønn og blå (RGB) kameraer for å kartlegge bunnhabitater med bløte sedimenter og berggrunn. Karihavet på Nordmøre er en naturtype som kallet poll. Disse karakteriseres som et saltvannsbasseng med avgrensede terskler ut mot åpne fjorder, som begrenser vannutveksling. Her kan det finnes arter med kaldtvannsutbredelse (<7 °C) bare funnet i tilsvarende poller langs norskekysten. Oppdagelsen av disse spesielle habitatene som finnes i Karihavet ble gjort av dykkere og er et eksempel på Citizen-science for kartlegging av artsobservasjoner langs norskekysten. Poller er en naturtype som har vært svært lite studert med hensyn til biologi.

Det ble målt klare endring i miljøvariablene saltholdighet og temperatur på 25 meters dyp mot kaldere og tettere vann. På større dyp enn 20 meter endret artssammensetningen seg til å inkludere arter med kaldtvannsutbredelse. En slik art som forekom fra 24 meters dyp var høye forekomster av muslingen *Chlamys islandica*, et kamskjell som tidligere har vært mye trålt i Barentshavet. Biologisk mangfold og stor forekomst av filtrerende arter som dekker større områder fra 20-30 m dyp indikerer en ekstremt produktiv sone i Karihavet.

Bruken av muliggjørende teknologi for å kartlegge havet kan gjøres over et stort spenn av skalaer i tid og rom. Observasjonspyramiden bruker lag med informasjon fra forskjellige plattformer for å systematisere havobservasjoner og trekke ut informasjon fra overlappende lag. I denne oppgaven blir observasjonspyramiden brukt for å hente ut biologisk informasjon ved sammenligning av forskjellige metoder som innsamlede prøver (fra dykkere) og forskjellige optiske metoder som RGB-ROV video analyse, undervanns hyperspektral avbildning (UHI) og undervannsfotogrammetri (UPG) i samme habitat.

Nye modelleringsmetoder hentet fra RGB-kamera kalt undervannsfotogrammetri (UPG) har tidligere blitt brukt i arkeologisk undervannsforskning, og i nyere tid blitt brukt til biologisk kartlegging. Denne metoden ble brukt til kartlegging av havbunnen fra 35 meters dyp bløte sedimenter opp langs en vegg til 10 meter dybde. UPG bruker overlappende bilder for å estimere plassering av objekter i 3D-rom og lager en 3D-modell fra 2D-overlappende bilder. Bruken av UPG muliggjorde en kontinuerlig visualisering av videodataene hentet fra ROV-videoen uten forhåndsprogrammert høydekontroll, kjent geolokalisering eller laserbasert skala beregning. Enkle målinger av størrelse av objekter, diversitetsindekser, habitatkartlegging og klassifisering ble gjort. Metoden kunne registrere og plassere gjenstander så små som kalkrørsormer på flate berggrunns-vegger, og oppnådde en romlig skala på mindre enn en cm. Mer verifisering av nøyaktigheten av denne metoden er nødvendig for å kontrollere nøyaktigheten til målingene som er hentet fra UPG, som vil være neste trinn i prosessen med å vurdere UPG for bruk i biologiske undersøkelser av havbunnen og oppnå absolutt størrelsesmåling.

Undervanns hyperspektral avbildning (UHI) ble brukt til å kartlegge habitater med bløte sedimenter for å kartlegge objekter med ulike spektrale egenskaper. Disse ble klassifisert i seks organismeklasser; dyregrupper, ulike algegrupper og sediment klasser. Bioklastiske sedimenter som består av kalkskallbiter av døde og levende dyr var mulig å isolere i en egen klasse på grunn av kalkholdige elementer som forårsaker høy intensitet i spektral reflektans (λ). Denne klassen kan brukes til å kvantifisere produksjon av plankton-filtrerende arter som muslinger og kalkholdige rørsormer for å estimere produktivitet. Ved å demonstrere ROV-UHI-kartlegging, bidrar i denne studien til å etablere bruk av UHI for bunnhabitatkartlegging og estimering av romlig dekning av arter i habitatet.

Abbreviations

2D	Two-Dimensional
3D	Three-Dimensional
AMOS	Centre for Autonomous Marine Operations and Systems at NTNU
AT	Aerial Triangulation
AUV	Autonomous Underwater Vehicle
BBA	Bundle Block Adjustment
BCS	Body coordinate system
CCS	Camera coordinate system
Cold-water species	Species living in temperatures <7 °C year-round.
DEM	Depth Elevation Model
DVL	Doppler Velocity Logger
FOV	Field of Vision
FPS	Frames per Second
HD	High-Definition camera
HI	Hyperspectral Imaging
IMU	Internal Measurement Unit
IOP	Inherent Optical Properties
Macrofauna	Animal species 1-50mm + including fauna species >50 mm.
MBE	Multi Beam Echosounder
OOI	Object Of Interest
R (λ)	Spectral reflectance measured as intensity per wavelength
RGB	Red, Green and Blue
ROI	Region Of Interest
ROV	Remotely Operated Vehicle
SAM	Spectral Angle Mapper
SfM	Structure from Motion
SVM	Support Vector Machine
TBS	Trondhjem Biological Station
UHI	Underwater Hyperspectral Imaging
UPG	Underwater Photogrammetry
USV	Unmanned Surface Vehicle

Table of contents

Acknowledgements.....	III
Abstract.....	V
Sammendrag.....	VII
Abbreviations.....	VIII
1. Introduction.....	1
1.1 Coldwater species habitats and distribution along the Norwegian coast	1
1.2 Benthic research and sampling.....	4
1.2.1 Physical sampling and ground truthing.....	4
1.2.2 Remotely operated vehicles (ROV).....	4
1.2.3 Marine acoustic- and optical sampling.....	4
1.2.4 Underwater hyperspectral imaging (UHI)	6
1.2.5 Underwater photogrammetry (UPG)	6
1.3 Karihavet; hydrography and history.....	7
1.3.1 History and connection to surrounding fjords	7
1.3.2 Water exchange and hydrography	8
1.4 Experimental aims.....	10
2. Material and methods.....	11
2.1 Study area.....	11
2.2 Remotely operated vehicle (ROV) transects	14
2.3 <i>in-situ</i> ROV-Sensors	15
2.4 Ground truthing (GT).....	17
2.5 Processing of camera data	21
2.6 Environmental data.....	26
3. Results.....	27
3.1 ROV-transects.....	27
3.2 UHI transects of soft sediment seafloor in Faksvågen.....	33
3.3 Underwater photogrammetry of vertical wall structures in Faksvågen and Nastadholmen..	35
3.4 Ground-truthing and laboratory work	41
3.5 Castaway-CTD.....	47
3.6 Habitat description.....	47
4. Discussion	50
5. Conclusion	59
References	60
Appendix.....	72

1. Introduction

1.1 Coldwater species habitats and distribution along the Norwegian coast

Coldwater species, defined as species with comfortable water temperature $<7\text{ }^{\circ}\text{C}$ (Strøm, 1936 in Sneli, 2007, and Gulliksen and Svensen, 2004) have survived in special micro-habitats along the Norwegian coast since the last ice age 10,000 years ago (Sneli, 2007, naturforvaltning, 2007). These special habitats are semi-enclosed bays which are smaller fjords or “fjord-arms” characterized by shallow inlets ($<20\text{ m}$) and deep basins ($<100\text{ m}$) where water exchange with the deeper basin is restricted, resulting in stagnant water with low oxygen content ($<2\text{ ml}^{-l}$) in the seafloor water (naturforvaltning, 2007) and low temperatures in the deep basin lower than surrounding fjord water (Sneli, 2007, Marion, 1996). These bays can also be affected by high levels of freshwater run-off from the surrounding land resulting in a layer of brackish water in the surface affecting water mixing of the water masses (Sneli, 2007).

Many semi-enclosed bays with shallow inlets and deep cold-water basins are found along the Norwegian coast, but very little research is done especially on the biology of the bays (Sneli, 2007, naturforvaltning, 2007). Partially cause of this commercial aquaculture favoring bays with opposite characteristics of higher temperatures and shallower basins (4-8 meters) for oyster-farming (Sneli, 2007), and such assessments on bay ecosystems are higher in priority for these bays and bringing research equipment into these bays in many cases may be challenging due to the shallow sills. With measured bottom temperatures it is possible to predict which bays may contain cold-water species, but very little data on bottom temperatures on bays is collected and usually done as single-point measurement for construction assessment purposes that does not give insight on annual variation in the water masses (Relling and Otnes, 2000, Sneli, 2007).

Species inhabiting semi-enclosed bays with shallow inlets are especially threatened by changes in hydrography, due to the already restricted water exchange with the surrounding fjords (naturforvaltning, 2007). Changes in sills from sediment movement can lead to increased- or decreased water exchange in- and out of the bay (Sneli, 2007, naturforvaltning, 2007, Hansen et al., 2008). Pollution from land such as nutrient runoff from agriculture and sewer systems are also a big threat to semi-enclosed bays and might lead to eutrophication (naturforvaltning, 2007). Sudden changes resulting from rockslides or human construction can have great consequences on the bay environmental conditions (Marion, 1996, naturforvaltning, 2007). Macrofauna are animal species 1-50 mm (standardization, 2012). In this thesis this will also include species bigger than 50 mm. Some macrofaunal species of Karihavet with cold-water distribution were in focus for this thesis and were compared with morphologically similar boreal species.

Chlamys islandica (O. F. Müller, 1776) (Figure 1.1. a) is a filter feeding species of clam in the family Pectinidae. *C. islandica* is the northernmost clam species found in the Barents Sea with a circumpolar distribution and was trawled around Svalbard by fisheries in 1987-89 at Bjørnøya (Gulliksen and Svensen, 2004, Sakshaug et al., 2009, Gulliksen et al., 2009). This bivalve is found from 8-1300m depth along the Norwegian coast, but clam beds of this species occur mainly between 10-60m (Wiborg, 1963, Moen and Svensen, 2020). The clam prefers habitats with strong currents and low temperatures ranging from $-1.8 - 8\text{ }^{\circ}\text{C}$ (Gulliksen and Svensen, 2004) and found on coarse soft sediments like sand and gravel in steep hills where it will be attached by byssus threads (Ekman, 1953). *C. islandica* will tolerate slightly higher temperatures and is registered at locations with $15\text{ }^{\circ}\text{C}$ (Sundet, 1998 in Johansson et al., 2004), but temperatures $12-13\text{ }^{\circ}\text{C}$ and higher was found to increase the mortality of the clams (Jonasson et al., 2004). This species can reach a width of 13 cm (Moen and Svensen, 2020). The shell surface of the clam has densely placed thin radial keels and high variation in color between

individuals (Orange, light pink and red, with the left side more red and right side more browngray). Both shell valves are of similar morphology, but the left auricle is larger than the right auricle (Moen and Svensen, 2020). After high pressure from trawling in the early 1980s the *C. islandica* stock collapsed in the Barents Sea and Svalbard after only ten years (Gulliksen and Svensen, 2004, Gulliksen et al., 2009). This was due to little knowledge on the recruitment capacity of the bivalve, which is a slow-growing species compared to other commercial bivalve species which resulted in harvest exceeding recruitment capacity (Gulliksen et al., 2009). In current time, trial fishery on *C. islandica* is reopening in the Barents Sea using new harvest technologies to minimize the invasiveness of the previously highly intrusive benthic trawling (Holseth, 2022).

Aequipecten opercularis (Linnaeus, 1758) (Figure 1.1. b) is a species of clam found in the northeastern Atlantic Ocean to Northern Norway. *Aequipecten opercularis* is found from a few meters depth down to 200 m along the Norwegian coast. Adult specimens of this bivalve can swim, and usually is found on soft sediments like sand and fine gravel. This clam has 18-22 radial keels on each of its shell halves, and right shell halves have a bigger overlapping auricle. The width of this clam can reach 9 cm. This clam has varying colors from brownish red, violet, yellow or gray, and is morphologically similar to *C. islandica* (Moen and Svensen, 2020).

Neptunea despecta (Linnaeus, 1758) (Figure 1.1. c) is a northerly distributed species of snail and one of the biggest species of marine snails along the Norwegian coast. *N. despecta* can be found in the northern Atlantic Ocean, in the Arctic and along the entire Norwegian coast. This species is found from 10 – 1200 meters depth on mainly soft sediments, often with symbiont anemones of *Hormathia*. The snail has a distinct spiral keels on its shell and can reach a height of 20 cm (Moen and Svensen, 2020).

Buccinum undatum (Linnaeus, 1758) (Figure 1.1. d) is a snail (gastropod) found on soft- and hard sediments from the littoral zone to a depth of 1200 m. It is often found in high abundance in kelp forests. This species can tolerate brackish water with low salinity levels. The snail is distinguished from *N. despecta* by having a wavy shell pattern, and reaches a height of 11 cm (Moen and Svensen, 2020). This snail is the most common large gastropod along the Norwegian coast and Svalbard (Berge and Johnsen, 2020).

Two species of cold-water anemones belonging to the *Hormathia* genus (Gosse, 1859) (Figure 1.1. c) is registered in Karihavet (Moen and Svensen, 2020, Aukan, N., prs. com., Artsdatabanken, 2022). These species are *Hormathia digitata* (O.F. Müller, 1776) and *Hormathia nodosa* (Fabricius, 1780). The two species are morphologically similar but are distinguished by *H. digitata* having an orange mouth and a wrinkly foot surface, while *H. nodosa* having the same pale-pink color across all its body and warty foot surface. *Hormathia digitata* reaches a size of 8 cm diameter of its foot, while *H. nodosa* has been found to be 4.5-6 cm diameter. *Hormathia digitata* is often found attached to shells of dead- and living animals like *N. despecta* and *B. undatum* (Moen and Svensen, 2020). This is less common for *H. nodosa*, and this species is usually attached to hard substrate on the seafloor, often rocks interspersed on soft sediments (Gulliksen and Svensen, 2004).

Ctenodiscus crispatus (Bruzellius, 1805) (Figure 1.1. e) is a species of sea star with circumpolar distribution and contribute largely to the biomass of some locations of glacial marine clay in the Barents Sea (Gulliksen et al., 2009, Moen and Svensen, 2020). Along the Norwegian coast this echinoderm is found as far south as Vestland county. The pale-yellow body of the sea star is lined with spikes, all the way to its short arms. The sea star reaches a diameter of 10cm. This species can be found from 10-2000m depth (Moen and Svensen, 2020).



Figure 1.1 Some photos taken in Karihavet of cold-water and boreal species a) *Chlamys islandica* with non-coldwater similar species b) *Aquiptecten opercularis*. c) *Neptunea despecta* is a cold-water mollusc here with *Hormatia* indet. indicated by arrow. d) Norwegian *Buccinum undatum* in similar area. e) *Ctenodiscus crispatus*. Photos: Nils Aukan, 2021-2022, with permission.

1.2 Benthic research and sampling

Traditionally most sampling methods of benthic organisms below the littoral zone have been intrusive like trawls, bottom sledges, dredges grabs and box corers or SCUBA-based sampling (Eleftheriou and Moore, 2005). Technological advances allow for the use of non-intrusive methods eliminating the risk of destroying a habitat as well as minimizing the aspect of single blind point-sampling. This allows researchers to observe and monitor the spatial distribution of organisms, enabling the obtaining of a total area coverage of the habitat or ecosystem (Smith and Rumohr, 2005).

1.2.1 Physical sampling and ground truthing

Ground truthing (GT) is a way of ensuring data validity by manual processing of the data or a subset of the data by an expert, such as physical examination of morphology and corresponding analysis of species composition (Sørensen et al., 2020). This can be a time-consuming process requiring specialists analyzing the data. Collecting physical samples might not be possible in every scenario, and with the advance in technology the need for physical samples is reduced as more non-intrusive methods are applied (Dumke et al., 2018, Sørensen et al., 2020). Trawling in transects and grabs taking single point measurements can hit “hotspots” in the benthic mosaic or “dead zones” that could affect habitat and biodiversity descriptions for large zones (Underwood and Chapman, 2005). Use of enabling technology will increase spatial coverage while achieving a high spatial resolution increasing knowledge of spatial distribution of organisms within mosaics and achieve more accurate description of these. Optical methods can be used as verifications for acoustic methods and can be used for identifications of objects of interest (OOI).

1.2.2 Remotely operated vehicles (ROV)

Remotely operated vehicles (ROV) are underwater robots with an operator on land, usually connected by a tether for communication between the ROV and the surface unit (Sørensen et al., 2020, Ludvigsen et al., 2007, Mogstad and Johnsen, 2017). These platforms can be used for a range of operations, from retrieving physical samples of specimens, sediment samples or water samples, and collect optical, acoustic and chemical data. The operational boundaries of the ROV is a balance between payload capacity, component durability and operational depths, maneuverability defining size and price of the ROV (Sørensen et al., 2020). Mini-ROVs are small ROVs with high- or specialized maneuverability, requiring less personnel to operate, but at the cost of lower payload capacity and/or shallower operational depth (Summers et al., 2022).

1.2.3 Marine acoustic- and optical sampling

Technological advances open up a new world of methods for surveying the seafloor, but also brings new challenges to the table in terms of data acquisition, processing and visualizing (J. L. Garrett et al., 2021). The observational pyramid is an approach to combine information from different instrument-carrying platforms using satellites, mini satellites, aerial drones, unmanned surface vehicles (USV), autonomous underwater vehicles (AUV) and ROV (e.g., using hyperspectral imaging as a common sensor system) at different scale- and time periods. This allows for observation over several spatial scales of the ocean surface, water column and seafloor to collect in-depth information of the habitats (Sørensen et al., 2020, Johansen, 2022 from: , J. L. Garrett et al., 2021). Figure 1.2 shows the concept of spatial coverage for a) physical sampling, where the focus is on point sampling like e.g., grabs and SCUBA-based analysis with high spatial resolution, b) optical methods like UHI and UPG obtaining sub-centimeter spatial scale of OOI and c) acoustic methods covering big spatial areas but non-specific on biological- information. Bigger ROV's can survey deeper parts of the ocean but are unable to survey closed-off and narrow bays due to the need for large equipment like boats and are unable to survey the shallow habitats due their size. Smaller ROVs are used instead to survey areas like these, allowing for a close-up view of the seafloor and the habitats they contain.

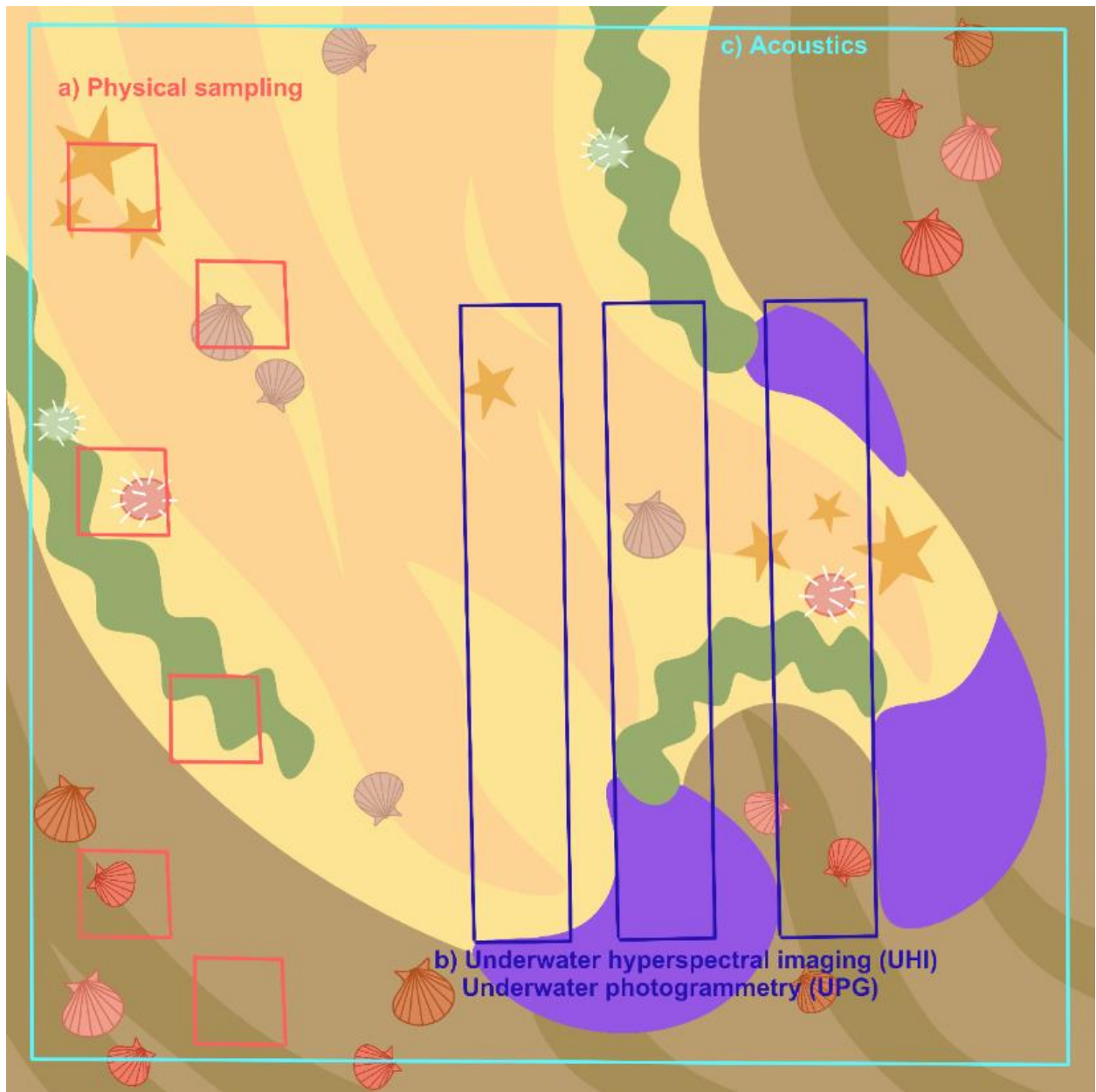


Figure 1.2 The difference in spatial extent of information collected by a) physical samples e.g., from grabs. Physical samples collect high-resolution information on species in one- or more point samples, trawl paths or by SCUBA diving (limited to 0-30 m). b) Optical methods such as underwater hyperspectral imaging (UHI) or underwater photogrammetry (UPG). Optical methods can collect fine-scale information of macrofaunal species across sediment types covering greater distances than physical sampling while preserving the life at the seafloor. c) Acoustic methods (e.g., multibeam- and single beam echo sounders) spanning greater spatial scales collecting bathymetry- and sediment information across a high spatial scale but do not give specific information on species distribution. Illustration: Malin Bø Nevstad, 2022.

1.2.4 Underwater hyperspectral imaging (UHI)

Underwater hyperspectral imaging (UHI) is a technique of measuring *in-situ* spectral reflectance (λ) (optical fingerprints) per image pixel (Johnsen et al., 2013, Mogstad et al., 2022). It measures visible light, or radiance in the 400-700 nm range. This is measured as a continuous light spectrum of 1 nm spectral resolution, in comparison to digital cameras measuring three different wavebands in the red, green and blue (RGB) part of the spectrum. These UHI data gives a higher spectral resolution to observe difference in optical signatures of different objects of interest (OOI) (Sørensen et al., 2020, Mogstad et al., 2022).

Spectrometers measure the $R(\lambda)$ in an area of $\sim 1 \text{ mm}^2$. In comparison, the UHI measures a larger area from 1 cm^2 to 800 m^2 , which determined by the distance from the OOI and the spatial resolution of 5mm per pixel (Mogstad et al., 2022). The spectrometer is often used under controlled conditions in the lab for verification of $R(\lambda)$ of OOI providing ground truth data. The spectrometer is used for gathering precise, detailed and accurate measurements, often measured ca. 2 mm away from the object (Johnsen et al., 2013, Mogstad and Johnsen, 2017) The information acquired by the spectrometer can in turn be used as GT to recognize similar pixels in the UHI transects.

The information collected by the UHI can be affected by a range of parameters, of these some can be adjusted for by adapting the trajectory of the carrying platform. These parameters include light available reaching the camera after being reflected off the seafloor. This is again determined by water content, artificial or ambient light and the water masses' inherent optical properties (IOPs) affecting spectral light beam attenuation coefficient $R(\lambda)$. IOPs of the water column changes the waters spectral absorption and scattering coefficients. The IOPs are determined by the water molecules, phytoplankton pigments, particulate detritus, minerals and colored dissolved organic matter (CDOM) (Johnsen et al., 2013). In low-light environments, additional light sources must be added to collect UHI data. The distance from the camera to the OOI is important for the spatial- and spectral resolution (Summers et al., 2022). The spectral attenuation of light in the water column is not negligible and is accustomed for by deploying a reflectance standard in-situ to correct for the attenuated light due to IOPs (Mogstad et al., 2019).

1.2.5 Underwater photogrammetry (UPG)

Structure from motion (SfM) is an approach in utilizing 3D photogrammetry, where overlapping camera- and video is used for 3D reconstruction of moving objects or scenes (Price et al., 2019). It works by utilizing stereovision to interpret depth of objects in the field of vision (FOV) (Sørensen et al., 2020). This method has become considerably more advances throughout the years and has been increasingly used both by aerial drones for mapping of large spatial areas, and by ROVs underwater archeological sites (Nornes et al., 2015). In recent years UPG has been used increasingly for biological surveys to obtain sub-centimeter spatial resolution of benthic habitats and macrofaunal biology (Price et al., 2019). In the underwater environment, the distance between the OOI and the camera is limited by the clarity of the water (Diamanti et al., 2021).

UPG has previously been conducted for archeological surveys using simple "off the shelf" digital cameras such as the GoPro Hero 2 (Capra et al., 2015). The fast development of cameras with enhanced spatial resolution provides more detailed information. This results in an increase in utilization of UPG for benthic habitat mapping and monitoring (Nocerino et al., 2019).

1.3 Karihavet; hydrography and history

1.3.1 History and connection to surrounding fjords

Karihavet (63°025 N, 7°965 E) near Kristiansund, Nordmøre, Norway is a semi-enclosed bay between Aspøya and mainland Straumsnes (Brakstad et al., 1975, pers. comm., Aukan, 2021-2022). Karihavet consists of three shallow sills at ca. 6 meters depth in the south restricting exchange of water to the 70m deep bay (pers. comm., Aukan, 2021-2022). These sills limit the water exchange with the Tingvoll fjord. Figure 1.3 shows a map of Karihavet and surrounding fjords.

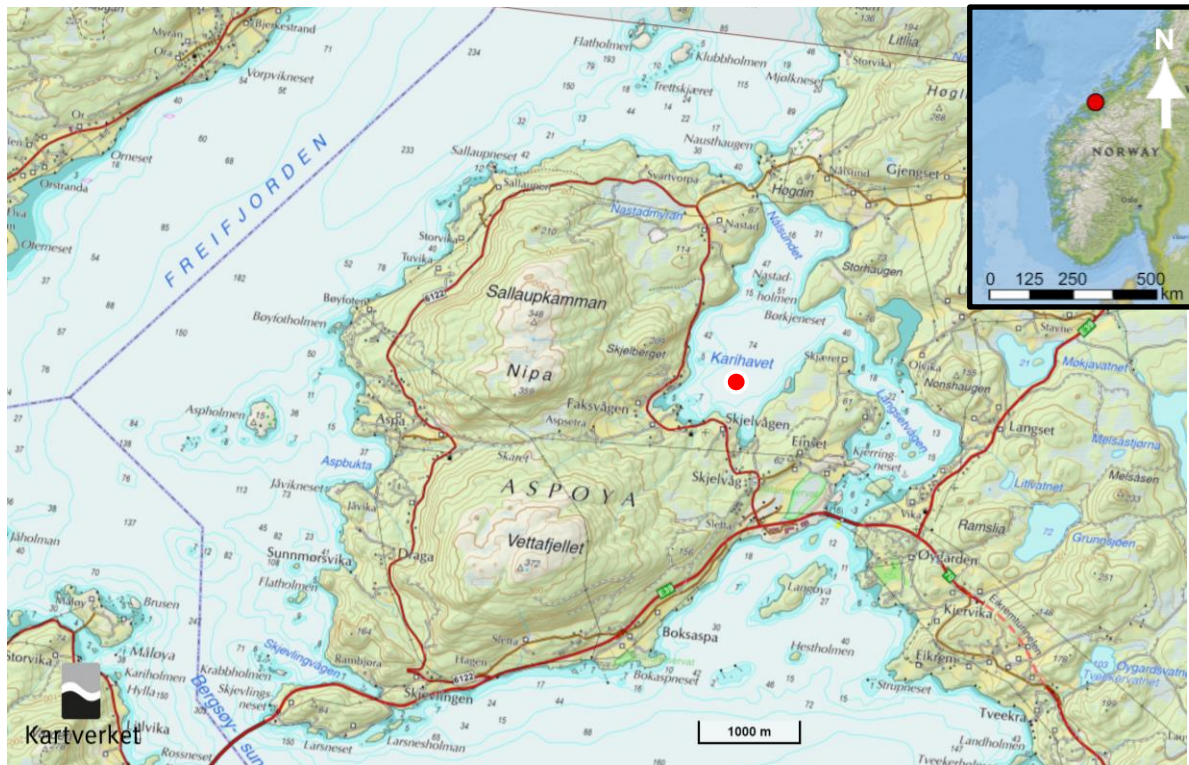


Figure 1.3 Map of the study area. Red circle indicate Karihavet. Adapted from "Kartgrunnlag: Kartverket (Creative Commons Attribution ShareAlike 3.0)", 2022, and ESRI National Geographic World Map 2021.

In 1901 a shallow 1.5 m deep- and 148m long channel (Nålsundet) was dug out in the north of the bay (Figure 1.4) (Brakstad et al., 1975). This enabled water exchange with the coastal fjordsystem (Freifjorden) to Karihavet (Brakstad et al., 1975).



Figure 1.4 Nålundet (direction Freifjorden), the northern human-made inlet across the previously narrow isthmus. This channel allowed for water exchange between the outer fjordsystem of Freifjorden and Karihavet. Photo: Malin Bø Nevstad, 2022.

The reason for opening this channel between the coastal Freifjord and Karihavet was due to row- and sailboat transport between the bay and the outlying fjord/coastal area. People used this channel to safely transport goods by sea to Kristiansund and for travelling to fishing spots. Previous to the channel being constructed, this area was used for pulling boats across the narrow isthmus by local farmers (Brakstad et al., 1975).

Due to the glaciers during the last ice age (10,000 years ago) pressing big landmasses down, land elevation in Strømsnes has been slowly rising. Findings of moraines from glaciers across Aspøya and Kvisvik, north of Karihavet. In Kvisvik the marine seabed threshold was found to be over 100m above current sea level (Brakstad et al., 1970).

1.3.2 Water exchange and hydrography

During the early 1980s and 90s several surveys were conducted of the biology and biogeochemical properties of Karihavet. This was done as part of mapping the areas before building new road infrastructure including the Strømsneset bridge. There is little surveying done in Karihavet after this, and information on its physical properties are restricted to the surveys done in the 80s and 90s on oxygen content, temperature and a general description on the habitats (Relling and Otnes, 2000).

In basins with inlets considerably shallower than the depth of the basin (Figure 1.5), the exchange of water is restricted to the upper meter (20-30m). Due to the limited exchange of salt water in Karihavet with the surrounding fjords, as well as natural freshwater sources such as rivers, Karihavet has been observed to contain a brackish layer of water on the surface in earlier surveys done in the area. Oxygen measurements were done of the deep water (40-65 m) of Karihavet both in 1982 and 1986 showing a reduced oxygen concentration from 5.5 ml^{-l} in May 1982 to 2.4 ml^{-l} in September/October 1982 (Brun, 1982, Relling and Otnes, 2000). In 1986 the oxygen content were measured to be 3.5 ml^{-l} in July and 2.7 ml^{-l} in September/October (Aure and Stigebrandt, 1989). Oxygen concentrations were also measured in 1989-90 where the recorded oxygen percentage was lower than 0.7 ml^{-l} for depths

>40 m for the period May – November (Relling and Otnes, 2000, Thendrup, 1991). Temperatures were recorded as low as 4.5 °C at 60m in 1982, with surface temperatures of 4.6 °C in May and 10.7 °C in September/October at >40 m depth (Brun, 1982). Due to the freshwater contribution from surrounding rivers Karihavet freezes up at the surface during winter (Brakstad et al., 1975). Compared to fjords with good oxygen conditions $>3 \text{ ml}^{-l}$ for fauna the oxygen levels of the deeper waters in Karihavet are very low and indicates stagnating water masses under 30 m depth (Buhl-Mortensen et al., 2006).

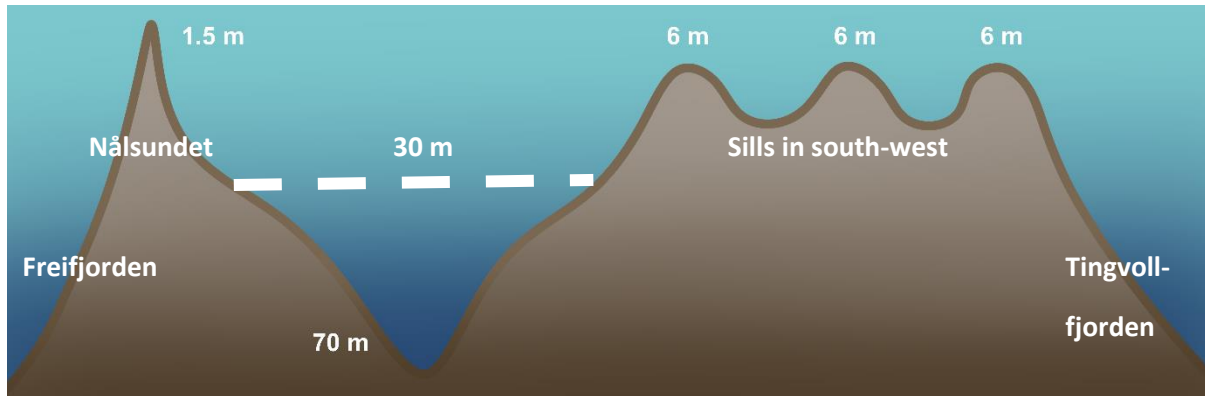


Figure 1.5 Sills in Karihavet restricting water exchange to the semi-enclosed bay with shallow sills and a deep basin. The shallow inlets restrict the deeper water of Karihavet from freely flowing into the surrounding fjords, and water exchange occurs from around 0-30 m. Illustration: Malin Bø Nevstad, 2022.

Very little information is found on the conditions of Karihavet before the construction of Nålsundet channel from the isthmus in the 1900s. Similar semi-enclosed bays may have similar conditions to Karihavet and contain cold-water species. By looking at inlet depth and deepest depth Sneli (2007) predicted some locations possibly containing cold-water species. One such location is Hamnesfjorden, located in Halsafjorden north of Karihavet. This bay has an inlet of 7m depth, and a deepest depth of 135 m (Sneli, 2007). This bay had a reduced oxygen concentration at 120-125 m depth in 1985, with lowest concentrations measured were 2.3 ml^{-l} in May (Brun, 1986 in: Relling and Otnes, 2000). Surveys done in Hamnesfjorden indicated that most regions of the fjord had little marine fauna with sediments smelling of hydrogen sulfide, but the inner part of the fjord were noted as having more marine fauna and less smell of hydrogen sulfide (Brun, 1986).

1.4 Experimental aims

Can ROV-based optical habitat mapping (biogeochemistry) be used to perform monitoring of biodiversity and distribution of objects of interest – this in contrast to the usual single-point measurements?

Main goal:

Utilizing different camera systems on a small-ROV to identify and map spatial distribution of organisms in complex benthic habitats.

Sub goals:

#1 Use ROV-UHI to map spatial distribution of organisms in complex benthic habitats.

#2 Assess the use of ROV-RGB for construction of photomosaic by underwater photogrammetry.

#3 Compare environmental variables such as temperature and salinity with species occurrence and biodiversity.

2. Material and methods

2.1 Study area

Karihavet contains some cold water species usually found in the arctic (Gulliksen and Svensen, 2004). These micro-habitats were used in this thesis to explore and assess species distribution over large areas (1-30m²). Species found during field campaigns were verified with pictures *in-situ* from Nils Aukan to supplement (Aukan, 2021-2022).

During the fieldwork in November 2021 several potential sites were visited to explore the accessibility and potential for sampling data with ROV-platform methods. Nils Aukan provided knowledge of different sites with high density of cold-water species in Faksvågen (Figure 2.1, a-c) was decided to be the most accessible site of interest in term of logistics and was used as the main point of interest. CTD measurements were taken by going to the site with a paddleboard to the locations. During the fieldwork in November 2021 the inlets in south-east as well as Nålsundet were visited.

In March 2022 a boat (Libra 33 ft, 6 m², Calypso owned by Kristiansund Diveclub) was used as a launching platform for the ROVs to reach the middle of the bay as well as allowing data collection at Nastadholmen (Figure 2.1, d). Faksvågen was also revisited (Figure 2.1, c).

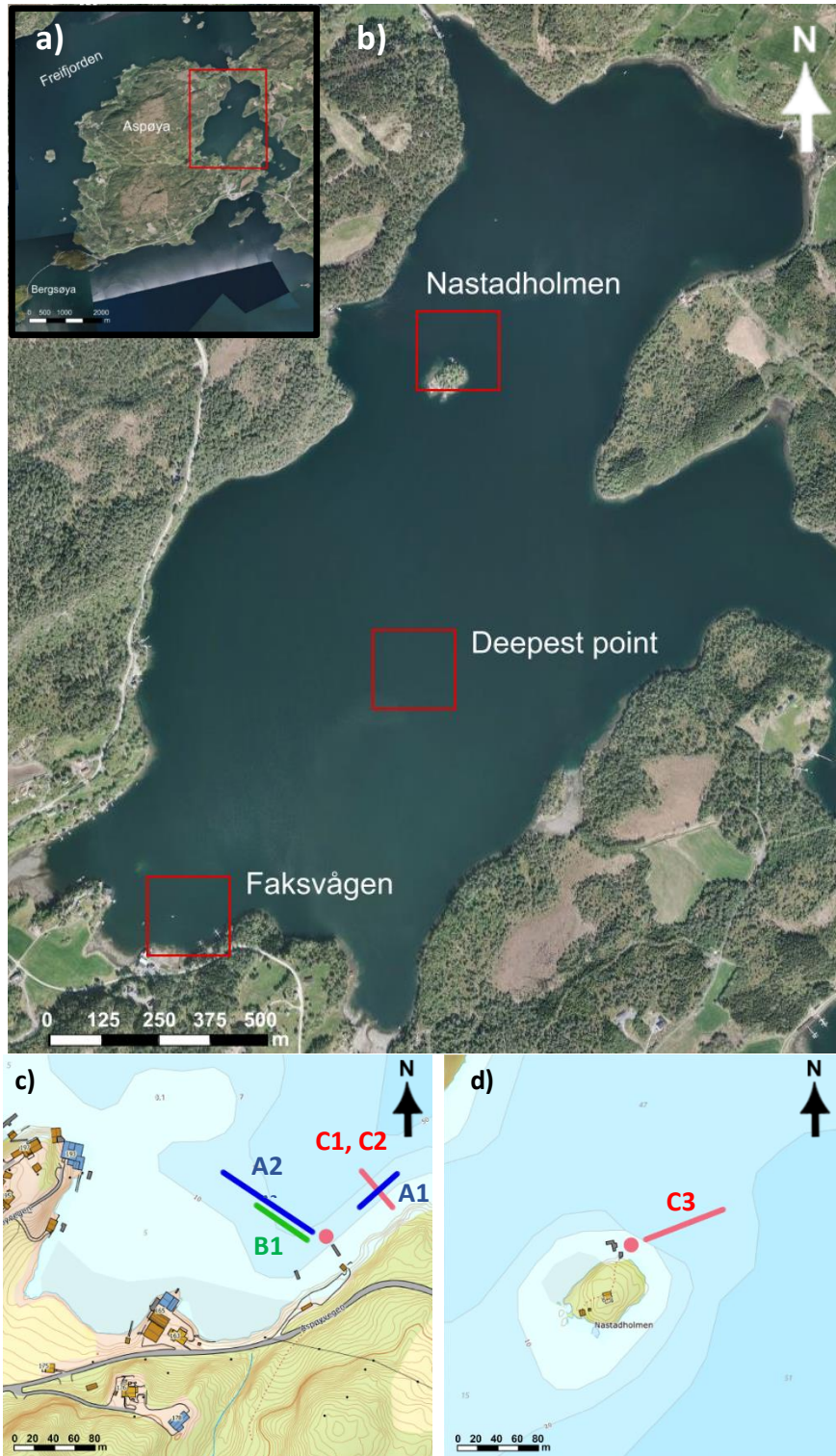


Figure 2.1 a) Karihavet relative to surrounding fjord systems. b) Karihavet and marked areas of interest. ROVs were deployed in Faksvågen and Nastadholmen. CTD was deployed at all three locations (Faksvågen, Nastadholmen and Deepest point). c) Faksvågen was mapped using Blueye Pioneer (A1 & A2) and (B1) ROV-UHI in 2021. This site was also mapped in 2022 with the Blueye X3 (C1 & C2). d) Nastadholmen was visited in 2022 and mapped using the Blueye X3 (C3). Lines visualise relative position and direction of the transects. Lines do not represent real distance covered. Methods of driving each transect is shown in Figure 2.4. Maps modified from Norwegian Mapping Authority 2022.

Several instrument-carrying robotic platforms were used for the collection of data. These platforms are listed in Table 2.1 showing an overview of when the platforms were used, and for the data collected using different sensors. This allowed for collection of data across a range of horizontal to vertical surfaces.

Table 2.1 shows an overview of the Blueye mini-ROV-platforms used for the fieldwork. The platforms are different versions and configurations of ROVs carrying different payload sensors shown in the Setup column (Blueye, 2022). Each of the platforms have been assigned a code and color for visualization in this thesis.

Platform	Fieldwork	Setup	Collected data	Code
Pioneer (ROV-RGB)	15 th - 17 th November 2021	Single internal wide-FOV camera (1080p/30fps, no tilt), 360-camera, IMU	Single video w/ navigational data, 360-video transect.	A (blue)
Double Pioneer with UHI (ROV-UHI)	15 th - 17 th November 2021	Double ROV with wide-FOV front-facing cameras (1080p/30fps) rig system with downwards-facing altimeter, UHI and RGB payload camera	UHI transect + RGB transect with corresponding altimeter data.	B (green)
X3 (ROV-RGB)	9 th – 11 th March 2022	Internal wide-FOV camera (1080p/30fps) with ± 30 degree tilt + stereo camera, IMU (Table 2.4)	Blueye video, navigational data + mounted footage.	C (red)

2.2 Remotely operated vehicle (ROV) transects

The ROVs were used to collect imaging of the seafloor following different trajectories (Figure 2.1). Since the Single-ROVs carried sensors with no communication with the ROVs internal system, the length of the transects were limited by the ROV battery capacity and maximum video length of the external cameras (10-12 minutes of continuous footage). An overview of collected transects is shown in Table 2.2. This table also contains coordinates of CTD measurements taken from the deepest point in Karihavet.

Table 2.2 Deployment start locations in Karihavet visited during fieldwork 15th -17th of November 2022 and 9th – 11th of March 2022. Transects named UHI_ represent transect done by ROV-UHI and Pioneer in same trajectory. Depth (in meters) based on internal depth sensor of the corresponding ROVs. Cells with single depth value did horizontal transects (see Figure 2.4, A), while cells containing a range represents depth-transects in given direction. Weather is based on logged information from visual observations on-site.

Location	Coordinates	Transect	Date	Depth (m)	Weather
Faksvågen-west (Figure 2.1 c)	(63°02048 N, 7°95941 E)	B1+ A2	15.11.2021	17	Sunny.
Faksvågen-east (Figure 2.1 c)	(63°02092 N, 7°96006 E)	A1	17.11.2021	20	
		C1	10.03.2022	12 - 0	Overcast, partially sunny. Strong winds.
		C2	10.03.2022	10 - 32	
Nastadholmen (Figure 2.1, d)	(63°03269 N, 7°96618 E)	C3	10.03.2022	35-14	Overcast, small rain towards end of field day. Strong winds.
Deepest point (Figure 2.1 b)	(63°02525 N 7°96516 E)	CTD only.	10.03.2022	0 – 70	Overcast. Strong winds.

During the fieldwork in November 2021 the mini-ROV Blueeye Pioneer carrying a 360-camera (Insta 360 model X2, Figure 2.2, a) was used to survey selected habitats in Karihavet with a near-vertical wall down to around 35 m deep. The video data collected by this drone covered an area of coverage around 60m vertically, but due to the lack of positioning sensors in the ROV the exact length of the transect is unknown. The ROV was kept driving at a constant speed and it was attempted to keep a constant distance of 1 meter from the OOI.

The ROV-UHI is a specialized platform consisting of two Blueeye Pioneers (Figure 2.2, b). The two ROVs are synched and operated as one unit. The ROV-UHI carries a downwards-facing UHI and altimeter to record hyperspectral transects of the seafloor. The ROV-UHI keeps approximately 1m distance from the seafloor during data collection. This is done by utilizing data from the altimeter as an altitude-control.

Based on the trials done in November, another fieldwork was conducted in March 2022 focusing on collecting stereo-videodata for underwater photogrammetry. During this fieldwork a newer model of the Blueeye ROV called the X3 was used. The new model of the Blueeye ROV included the internal camera tilt (± 30 degrees vertical tilt) (Blueeye, 2022). This ROV was used to carry a Gopro stereo-camera (Figure 2.2, c and Figure 2.3 b).

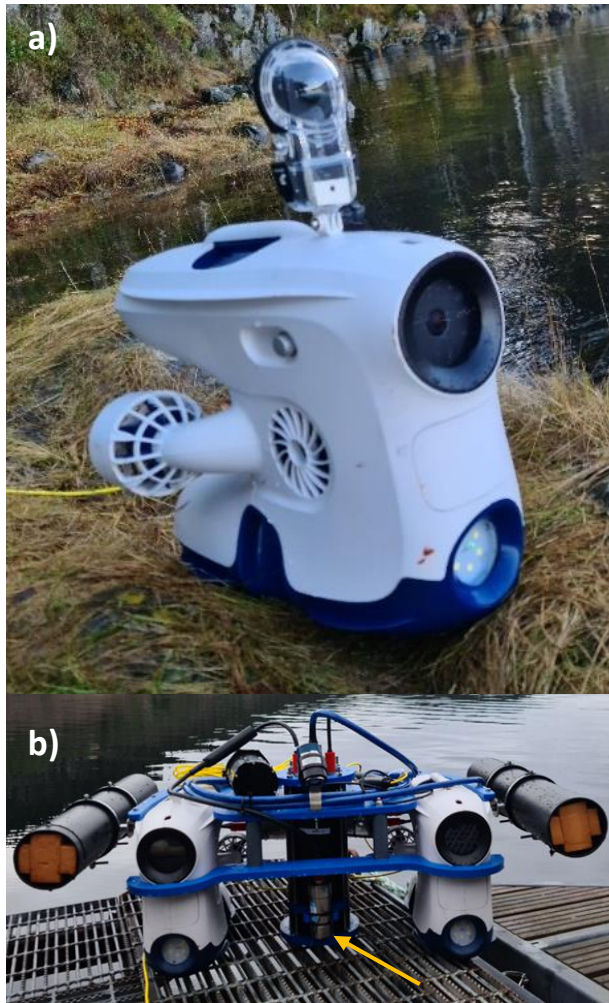


Figure 2.2 a) The setup for the Blueeye Pioneer used during the November 2020 fieldwork. This ROV carried a 360-camera on the external mount (See Figure 2.3 a) and Table 2.3). Photo: Malin Bø Nevstad, 2021. b) The ROV-UHI called the Double-Blueye carrying the down-facing UHI and altimeter (Indicated by arrow). c) The setup of the Blueeye X3 carrying a forward-facing GoPro stereo camera (see Figure 2.3 b) and Table 2.3) system on top of the ROV. Photos: Malin Bø Nevstad, 2022.

2.3 *in-situ* ROV-Sensors

The 360-camera (shown in Figure 2.3 a) with underwater housing (Depth rating <40 m) was used to observe the surrounding area to provide information in addition to the ROVs field of view (FOV). The camera was mounted on top of the Blueeye Pioneer ROV as shown in Figure 2.2 a). The 360-camera did not communicate through the ROV platform and had to be switched on by hand in the surface. The 360-video footage was used to observe the 3Dimensionality of the seafloor the ROV was operating in, enabling for the continuous observation of the full areal coverage outside the FOV of the ROV. This is a feature not possible for the front-facing camera and proved valuable insight to the topography of the surveyed area as well as capturing the natural light climate vs. the area exposed to artificial light sources introduced from the ROV.

The UHI camera consists of two cameras (Depth rating <2000 m) where one is a regular digital camera (RGB) and the second is a push-broom scanner (the UHI) recording in a full spectral resolution (Mogstad et al., 2022). The UHI records images where each pixel in the image contains a full spectrum in contrary to normal RGB cameras.

As shown in Figure 2.2 c) the GoPro Hero 3 dual system stereo camera (Depth rating <60 m) was mounted on top of the Blueeye X3. The attachment was possible to attach at different angles (shown in Figure 2.3 b), and to ensure similar angle between missions a level object was used to position the stereo camera when mounting it to the ROV.

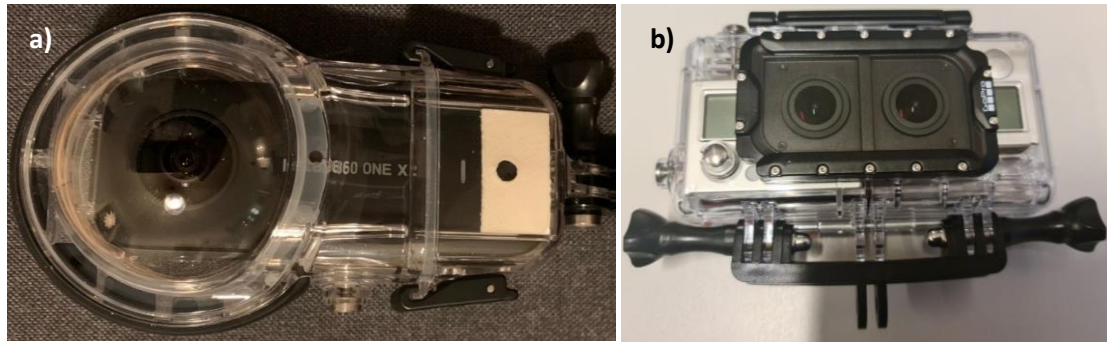


Figure 2.3 The a) Insta360 One X2 360-camera in an underwater housing with depth rating <40 m. Photo: Geir Johnsen, 2022. b) Two GoPro Hero 3 Black in a dual system diving housing used in Karihavet March 2022. The two cameras are connected by a dual system plugged into the back side of the cameras. Photo: Malin Bø Nevstad, 2022.

Table 2.3 Cameras used during fieldwork and their function as well as their model.

Sensors	Model	Function
Underwater hyperspectral imager	UHI-4 Ecotone	Collects UHI transects and corresponding RGB images.
360-camera	Insta360 One X2	Collect 360-video of seascape by combining two 180° cameras in an underwater (<50m) housing.
Internal Blueye camera	RGB HD 1080/30fps, 115° vertical FOV	Collect HD video for model construction and analysis.
GoPro stereo camera	GoPro Hero 3 Black dual system	Collect synchronized stereo video for model construction.

During fieldwork in November 2021, the Blueye Pioneer (Figure 2.4, A) was used to survey a near-vertical wall of Faksvågen, moving horizontally along the wall. The ROV also completed a transect following the trajectory of the Double Blueye Pioneer ROV-UHI (Figure 2.4, B). In March 2022, the Blueye X3 (Figure 2.4, C) completed transects following the depth gradient in Faksvågen and Nastadholmen.

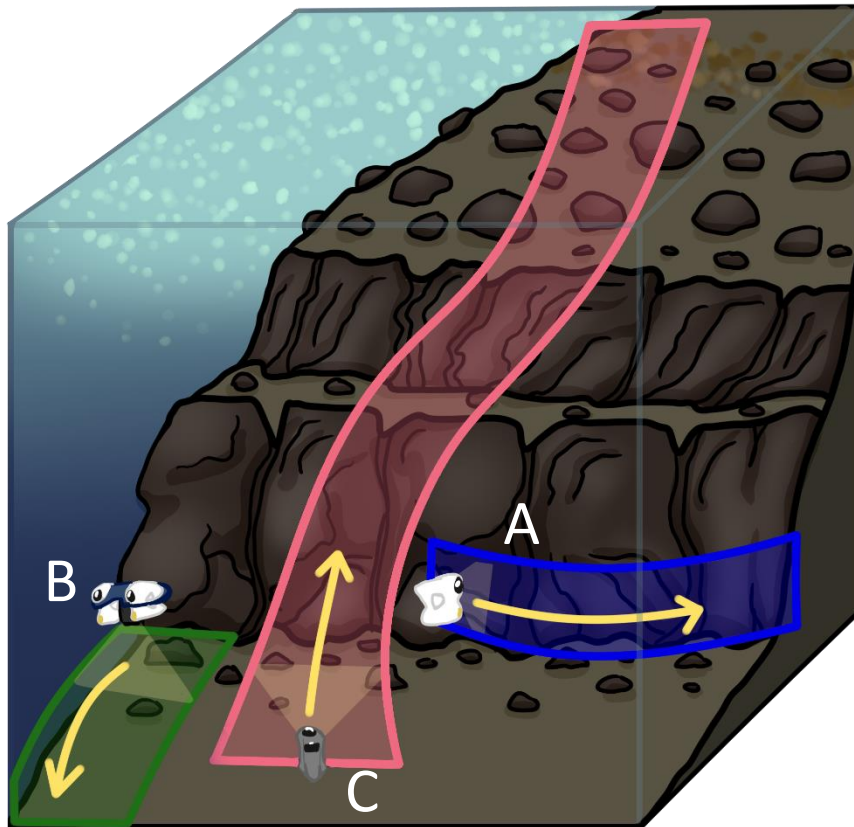


Figure 2.4 Different ROV survey methods of operating and navigating in Karihavet. The A) Blueye Pioneer (white ROV) was used to survey the wall at 32-13m horizontally. The B) ROV-UHI operated on horizontal seafloor. The C) Blueye X3 (grey ROV) was used to follow the wall from 32-0m. The figure is not to scale but illustrates the trajectories of the different ROVs transect lines. Illustration: Malin Bø Nevstad, 2022.

2.4 Ground truthing (GT)

To verify the data collected by the camera systems a) physical samples (OOI) were collected, identified, and measured for physical properties (length and width) and spectral reflectance (λ) *in-vivo*. b) A physical checkerboard-reference plate was placed *in-situ* for camera parameter calibration and to verify scale in ROV-UPG transects. c) A reference plate reflecting 99% of incoming light (in 400-700 nm range) was placed to compare *in-situ* UHI spectral reflectance $R(\lambda)$ vs. *in-vivo* spectrometer spectral reflectance $R(\lambda)$ from collected OOI in the lab.

a) Physical samples of organisms

At location Nastadholmen (March 2022, Figure 2.1 d), SCUBA-based diving was used to collect *in-situ* close-up images of OOI and specimens for further identification of different species of echinoderms, molluscs, cnidarians and poriferans. This was done by Nils Aukan and Peder Martinini from Kristiansund Dykkerklubb. Focused specimens to collect were macrofaunal species that were large enough to show up on the ROV's video. Divers were instructed to collect specimens along a transect line from 35-0m depth, starting from the deepest point. The Blueye X3 was used to accompany the divers, and recorded depth and temperatures as the divers collected species as shown in Figure 2.5.



Figure 2.5 Divers collecting clams at 32 meters depth. Picture is taken by the Blueye ROV accompanying the divers along the transect at Nastadholmen. Photo: Malin Bø Nevstad, 2022.

The specimens were sorted and brought alive to the lab using large saltwater containers with fresh saltwater at approximately in situ temperature. Saltwater containers with OOI were transported from Karihavet to Kristiansund, then to Trondheim Biologiske Stasjon (TBS) by car (ca. 7 hrs) the following day. The organisms were kept in constant saltwater flow at TBS where the length and width of individual animals were measured (Figure 2.6). After the lab work the specimens were passed on to the NTNU University Museum for deposition in the scientific collections.

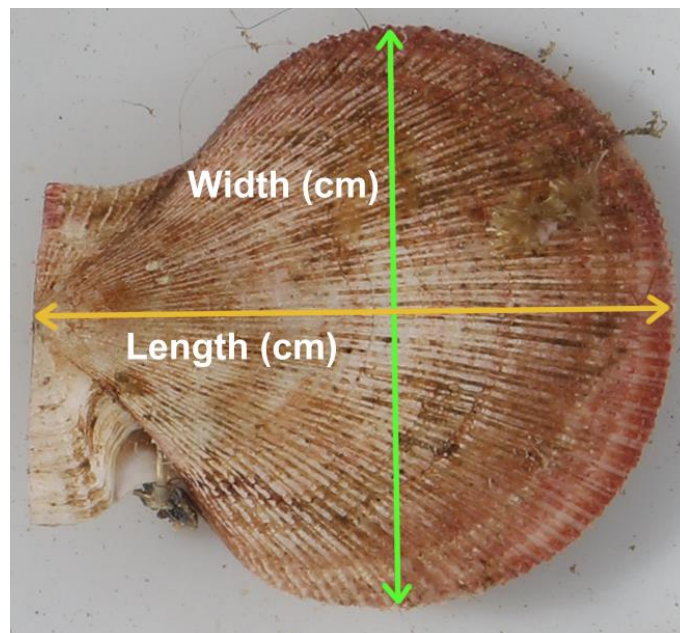


Figure 2.6 *Chlamys islandica* measured length (Orange) and width (Green) in cm in the lab. Photo: Malin Bø Nevstad, 2022.

Spectrometer to measure *in-vivo* spectral reflectance (λ) of specimens

A QE-pro spectrometer with reflectance fiber, halogen light source, spectral resolution of ~ 0.5 nm (Figure 2.7) was used to measure the spectral reflectance (λ) of the organisms in the lab (Done as described by Summers et al., 2022).

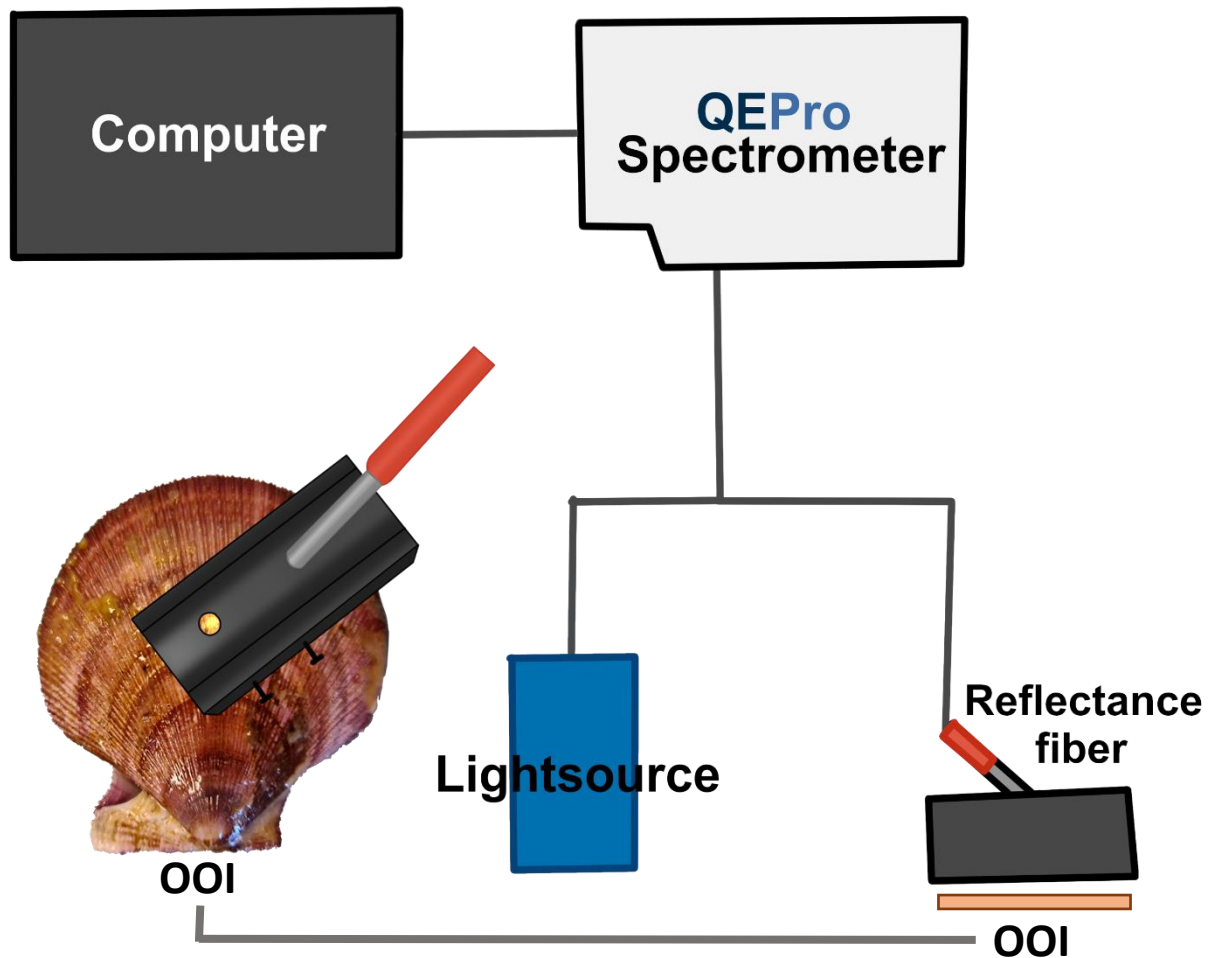


Figure 2.7 QE-pro spectrometer is used in the lab to take point-measurements of spectral reflectance ($R(\lambda)$) of object of interest (OOI) with high accuracy. These measurements are the organism's spectral fingerprint and is used to classify species in the UHI transect data based on similar trends in spectral fingerprint. The spectrometer is attached to a light source and reflectance fiber probe and converts the optical data to digital numbers to be displayed on the computer. Illustration: Malin Bø Nevstad, 2022.

b) Calibration of camera parameters and verification of OOI scale in ROV-UPG using a checkerboard-reference board

A checkerboard-reference plate (Figure 2.8) was deployed along the ROV transects in March 2022 to control scale of the UPG models and for camera calibration. The square-pattern was printed on waterproof paper and attached to a metal plate with tape. Each square (white and black) was printed to a 4x4 cm size. The checkerboard-reference plate was weighted down with lead weights on the back and deployed using a rope from the surface.

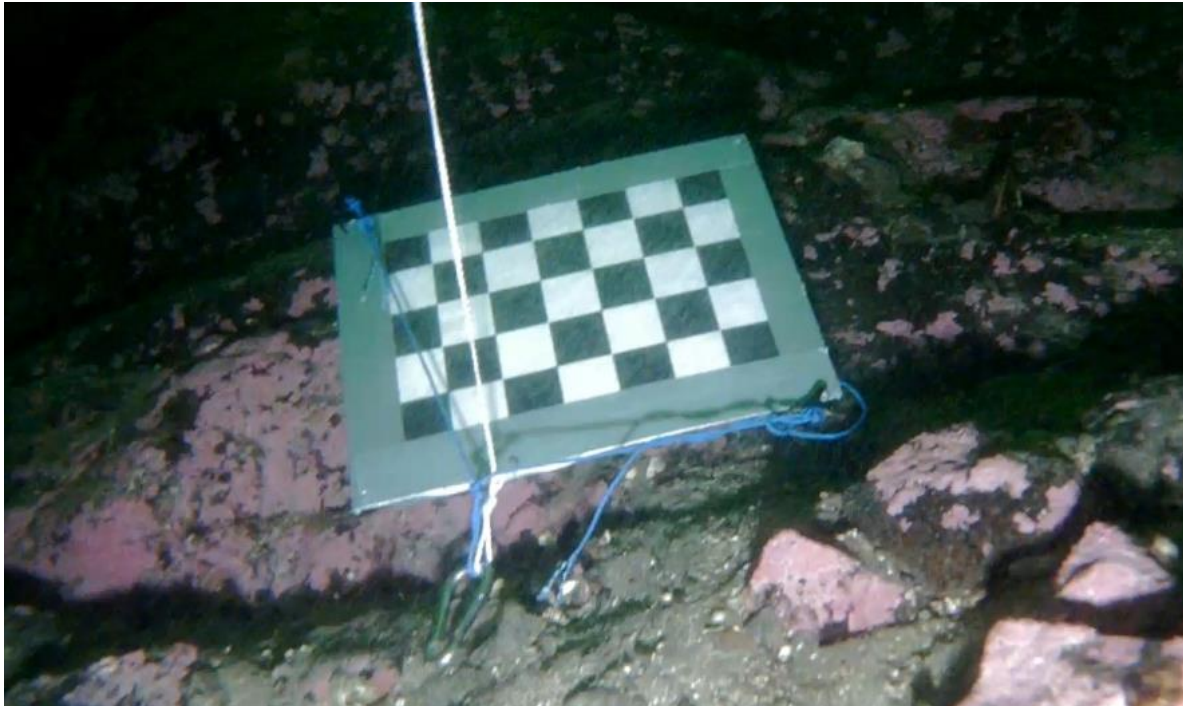


Figure 2.8 shows the checkerboard-reference plate *in situ* at Nastadholmen. The checkerboard was placed on the seafloor at 18.5 m as good as possible by using weights attached to the plate and ropes to keep the checkerboard side of the plate facing up. This checkerboard was recorded by the ROV to use for scale of OOI and camera calibration in UPG models. Photo: Malin Bø Nevstad, 2022.

The checkerboard-reference was filmed from different angles and distances to collect *in-situ* camera calibration data to be used when processing the ROV-video and stereo camera video. This ensured proper calibration of internal and external camera parameters by using known scalebars (size of squares) to calibrate cameras in Matlab Camera Calibration Toolbox (Appendix 3). This checkerboard was also used to place known scale-bars in the UPG models to obtain scale.

c) Correction for inherent optical properties (IOPs)

For UHI-transects a white reference-plate was deployed to measure *in-situ* spectral reflectance (λ) of pixels with no OOI's absorbing or reflecting light (a white surface). This reference-plate reflects 99% of incoming light from 400-700 nm. This makes it possible to make a connection between incoming light (from lamp) and the attenuated light by water constituents like phytoplankton, colored dissolved organic matter (CDOM) and total suspended matter (TSM) (Summers et al., 2022, Mogstad et al., 2022).

2.5 Processing of camera data

2.5.1 RGB HD-video analysis

Video transects were collected and analyzed for organisms showing up in the transect. This was done by looking through the videos manually and recording sightings of species across depths, not focusing on the number of individuals, but rather their relative coverage and change in coverage across different depths. The video transects also worked as species identification and reference for scale (of organisms) for underwater photogrammetry and hyperspectral imaging data.

The 360-camera video was analyzed in parallel with the ROV video from the same transect. The 360-camera enabled the observation of the habitat in a 360-degree coverage while also sampling the video data in the FOV of the ROVs internal camera. From approximately 10 meters depth into the deeper water masses most light of long wavelengths were attenuated, giving a green hue to the water which indicated high concentrations of CDOM from freshwater run-off in the surface layer. The natural light environment in the deeper water masses was not sufficient for filming without an artificial light source. On the Blueeye ROVs the light sources are located at the bottom of the front of the ROV, illuminating the FOV of the Blueeye's internal camera (Figure 2.9).

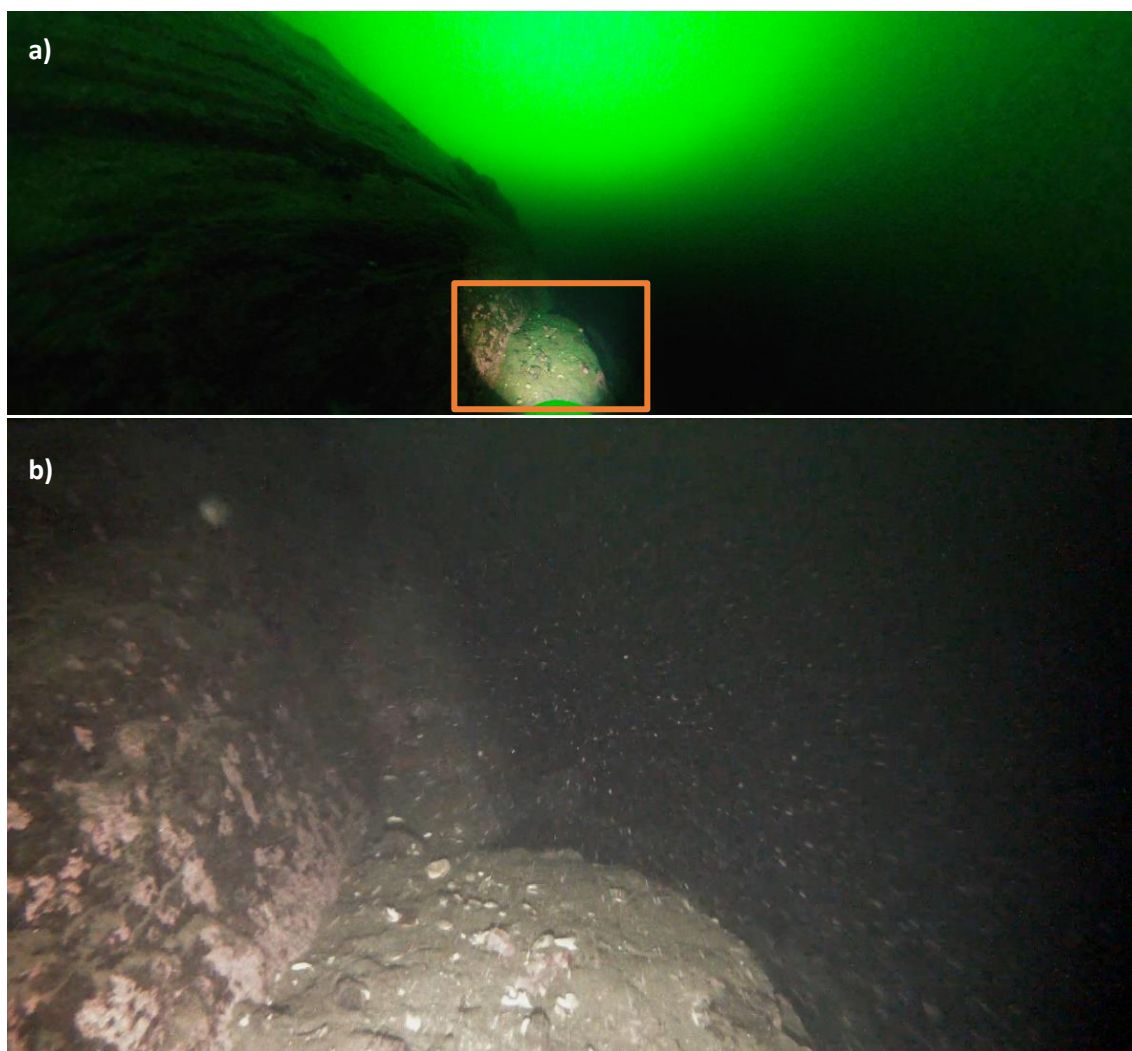


Figure 2.9 Wall transect A1 images demonstrating a) 360-camera footage illustrates how the FOV of the Blueeye camera is lighted up by artificial illumination, while the area around is illuminated by ambient light with a greenish hue due to high concentrations of CDOM from freshwater run-off in surface layer. b) Shows a closeup of the Blueeye Pioneer's internal camera in the same area with artificial light. Photo: Malin Bø Nevstad, 2021.

2.5.2 Underwater hyperspectral imaging data

These ROV-UHI transects were pre-processed in Immersion (Ecotone, 2021). The processed UHI transect was analyzed using ENVI (Version 5.6.2). A spectral library containing reflectance spectra of animals, algae and sediments were used to classify pixels in the transect to make ROIs. This was a way to ensure the best fitting pixels in the transect was used for the classification. Spectral Angle Mapper (SAM) classification is one of the most used classification tools in remote sensing. SAM measures the angle between complex spectral signatures where the signatures are compared as n-dimensional vectors (see Bjerkvoll, 2022). Support Vector Machine (SVM) is a supervised classification method used for complex- or noisy data derived from statistical learning theory where support vectors which are data points closest to a decision surface that maximizes margin between classes (see Hsu et al., 2003). A standard SAM and SVM classification algorithm were run of the transect to obtain the number of pixels coverage for sediments, animals, and algae. The UHI data was used to provide information of species and habitat over a given area with OOI, based on their specific optical fingerprint.

2.5.3 Underwater photogrammetry derived from RGB-ROV

Several trials in the execution of collecting image data for UPG was conducted during the fieldwork in November 2021 and during field training in Slettvik, NTNU's fieldstation (63°35 N, 9°32 E). From the experience gained during fieldwork in November in Karihavet together with the field training from Slettvik a mission was set up as shown in Figure 2.10. This allowed for the best use of the Blueye's depth sensor giving depth data while also reducing the uncertainty of not having positioning data. This also optimized the area captured by the FOV of the stereo camera mounted to the top of the ROV.

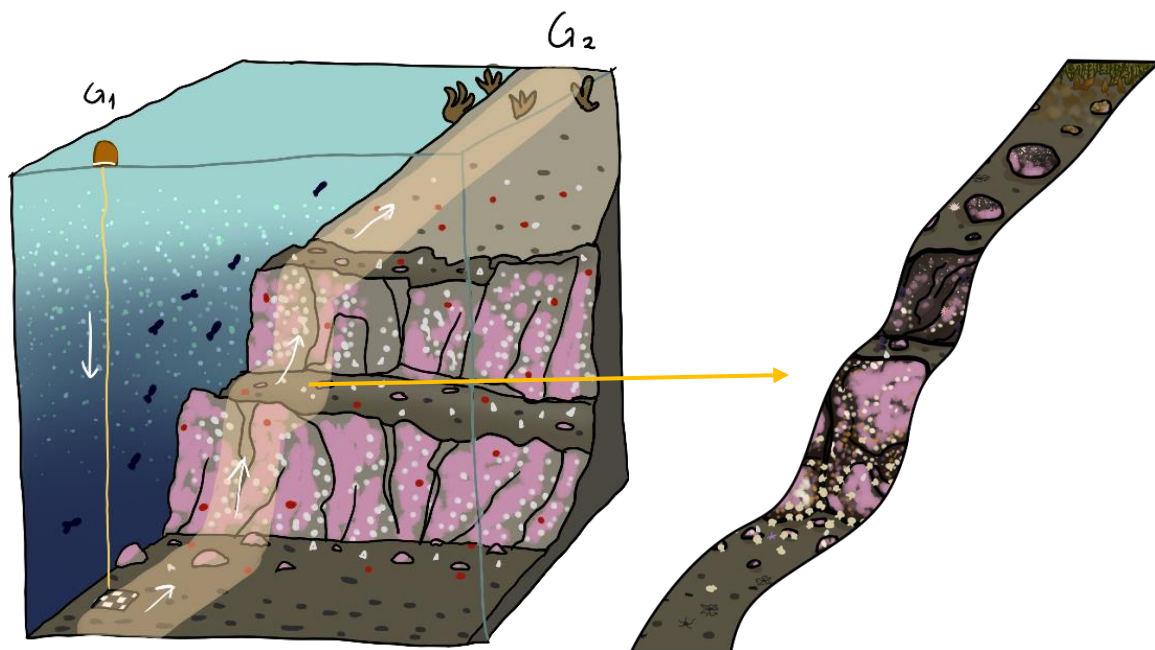


Figure 2.10: Biology study design for underwater photogrammetry collected with ROV March 2022. G1 shows point of descent for the ROV. G2 is the point of resurfacing after following predetermined heading along a depth gradient. This shows the path of the ROV and the reconstruction of this transect as a photomosaic to observe in detail the change in spatial distribution of organisms across a depth gradient. Illustration: Malin Bø Nevstad, 2022.

As shown in Figure 2.10 the ideal mission was having a point of descent to below the bedrock wall with a reference plate and following the wall up to the surface. In practice, the checkerboard was deployed close to the boat which was at 12m and 19m depth respectively for site Faksvågen and Nastadholmen. Due to this, not all transects done had the checkerboard-reference plate for

referencing scale as it proved a challenge to collect transects from deeper regions and be able to include the checkerboard-reference in the same transect. This was due to the need to drive a specific heading manually while also correcting for overhangs and protruding rocks along the transect, altering the course slightly to miss the checkerboard-reference plate from the point of descent. Because of this challenge as well as the restricted capacity of the stereo camera battery not all transects contained a scale reference.

As shown in Figure 2.11 there are several prerequisite steps to gathering UPG data. These steps ensure the quality and usability of the data, while also minimizing the need for additional manual steps. One such step was the introduction of the Agisoft navigational data converter by Blueye. Prior to accessing this tool, the navigational data was manually adapted to fit the Agisoft data. This step was converted to an almost automatic process, where it is only required for the user to input which dataset is needed and what adaptation should be done for the dataset. The output is a navigational datafile compatible with the frames used by Agisoft.

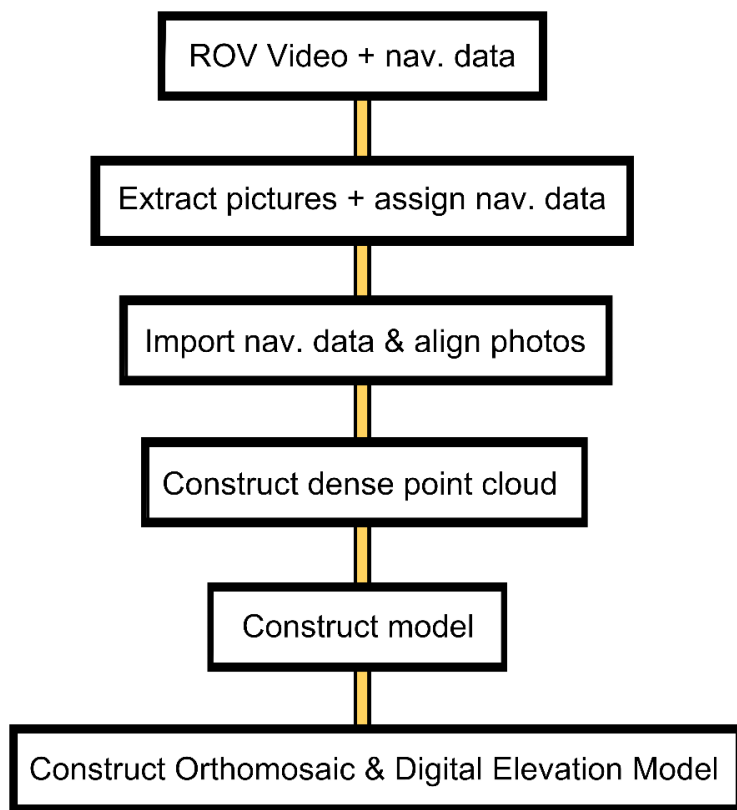


Figure 2.11 Workflow from extracting frames from ROV video data in photogrammetry software Agisoft. Here the steps illustrate the general workflow, where overlapping images are extracted from the ROV and aligned with corresponding navigational datapoints. From the aligned frames a point cloud is made, which shows the initial placement high-reconstruction accuracy points from neighboring images based on movement of objects across frames and navigational data. From a point cloud a dense point cloud was constructed increasing number of points and increasing resolution of the cloud. From a dense point cloud models, Digital elevation models (DEM) and orthomosaics can be constructed. All of this can be produced based on the ROV video footage and internal navigational sensor data. Illustration: Malin Bø Nevstad, 2022.

Processing steps for 3D photogrammetry executed following Agisoft Metashape Professional User Manual, and a detailed description of the workflow is shown in Appendix 3. The video-data from all cameras were loaded into Agisoft Professional, where the initial step of extraction of image frames from the video was done. The transect was filmed in dark environments, and a mask was applied to remove the darkest regions of the images to facilitate the first step of photogrammetry called alignment. Navigational data from the ROV with assigned depth, yaw, pitch and roll values for each image frame was imported into Agisoft and assigned to the corresponding image. During alignment Agisoft uses the navigational data and features across images to find the position of the camera for each image and estimates the camera orientations. The alignment is done using aerial triangulation (AT) and bundle block adjustment (BBA) (Agisoft, 2022). The image alignment is visualized as a tie point cloud called a sparse point cloud and is needed for the estimation of depth in the image (depth maps) (Figure 2.12).

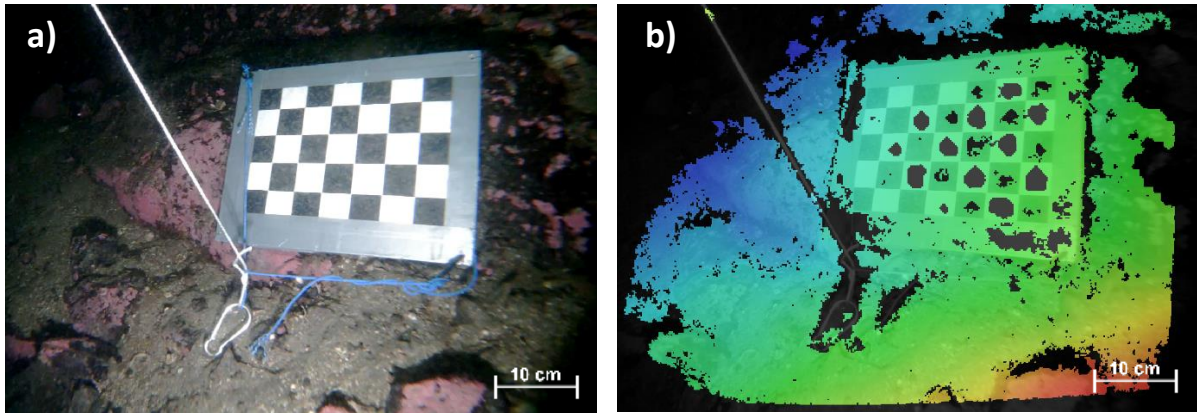


Figure 2.12 Example of the depth map estimated by Agisoft from a) a single image (Blueye internal camera) in a transect. Each image in the transect has b) a corresponding depth map. Here, red is regions of the image estimated to be close to the camera, while blue regions is estimated to be further away from the camera.

The sparse point cloud consists of points estimated by the Agisoft algorithms in a 3D space. This is illustrated in Figure 2.13, showing the estimated location of the camera for each image (Figure 2.13, a) and the estimated pixel positions in the 3D space (Figure 2.13, b). This also illustrates the overlap between images needed for estimation of depth and placement of pixels. With each placed pixel there is also a level of uncertainty in the placement, and the outer edges of the images contain the least overlap, resulting in the lowest certainty of correct placement. Knowing this, a gradual selection of pixels with high uncertainty in placement was filtered out, and the edges of the model was trimmed to reduce data amount while leaving the overlapping areas of higher certainty in the transect.

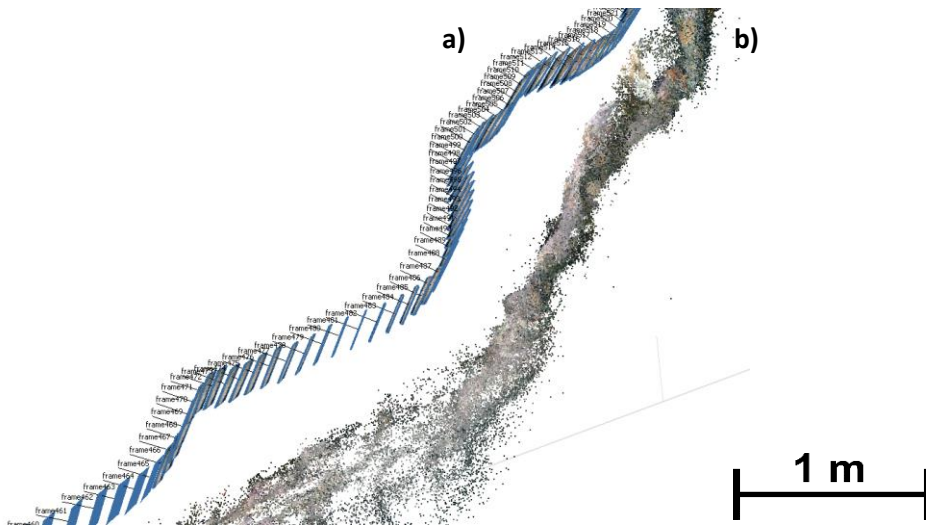


Figure 2.13 a) Overlapping images (blue squares) from the ROV is used to construct a b) sparse point cloud (points) in Agisoft. Features in images are placed in 3D space based on the movement of the feature across neighboring images.

Dense point clouds are built based on the estimated camera positions, images and more features are extracted from the images were constructed from the sparse point clouds after optimizing of cameras and cleaning of low-reconstruction accuracy points. From the dense point cloud, a 3D surface (mesh) and 2.5D depth elevation maps (DEMs) could be generated (Agisoft, 2022). Orthomosaics were generated by projecting image data onto the DEM or mesh. Figure 2.14 a) shows a selected set of neighboring images in a transect used for b) reconstruction accuracy of the dense point cloud and the c) 3D reconstruction of the same area.

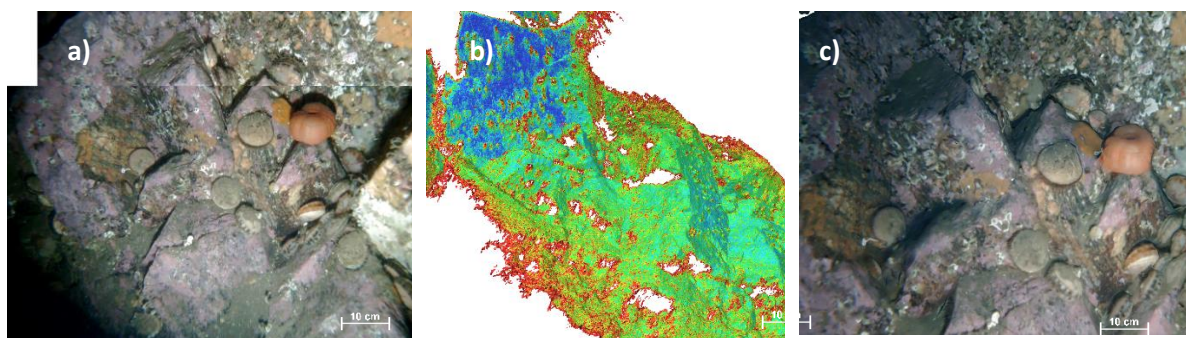


Figure 2.14 Location C3, 26.5 m depth (Figure 2.1, d). This figure is shown from the perspective of the ROV camera. a) Example of frame overlap from ROV video. b) Dense point cloud confidence of same location in the model. Here regions of low reconstruction accuracy is colored red, while mild reconstruction accuracy is colored green, and high reconstruction accuracy is colored blue. c) 3D reconstruction (mesh + texture) of same location in the transect.

Known scale-bars were fitted to the dataset during processing in Agisoft for the underwater photogrammetry. This allowed for scaling the model, giving the estimated length (in cm) of OOI in the model (Figure 2.15).

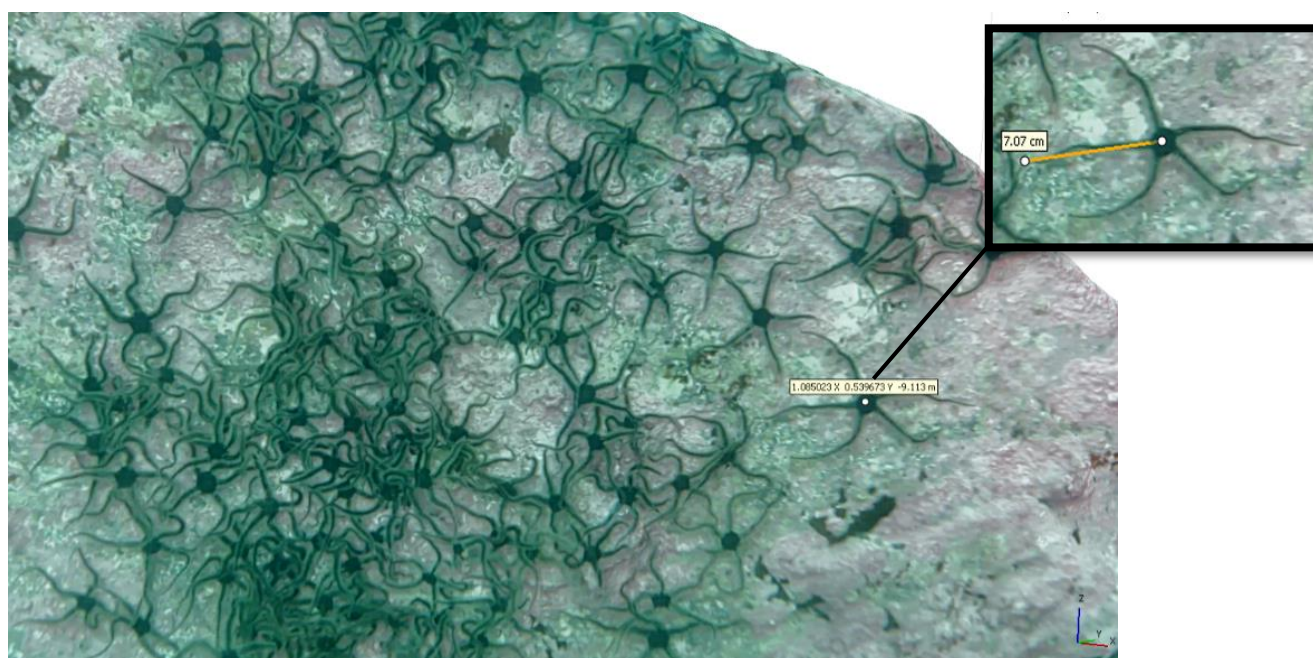


Figure 2.15 showing measuring distance between two points without the use of laserpoints, here, from the center of the brittle star's body to the tip of the arm (7 cm arm length). This model is a trial model from Slettvik, February 2022.

The feature of measuring lengths of OOI can also be applied to portions of- or the full transects in themselves to measure length in 2D image and in 3D. By constructing a polyline across the middle of the transect a cross-section visualization of the transect can be made.

2.6 Environmental data

A SonTek CastAway-CTD (Conductivity, temperature, and depth) with integrated GPS was used to measure the temperature (T), salinity (S) as a function of conductivity to be converted to salinity and depth (Pressure cell converts bar to meters). Several measurements were done at different parts of the bay with a approximately 700m distance between them to capture vertical zonation from the surface to the deepest point of the bay. The same CTD was used during both field campaigns (Figure 2.16).



Figure 2.16 360-image of the SonTek CastAway-CTD during vertical profiling of temperature and salinity in Karihavet during fieldwork November 2021. Photo: Geir Johnsen, 2021, with permission.

Temperature- and salinity within depth profiles at the deepest point in 2022 (Figure 2.1 b). By using a CTD and seeing the change from different seasons it is possible to tell what kind of water masses at different depths and observe if there is any change in existing thermoclines and pycnoclines. CTD profiles were visualized using programming software Python with matplotlib package.



A CTD profile was done in November 2021. Due to technical issues the coordinates of the CTD measurement were not recorded on site. The point sample is estimated to be within a 700m radius of the deepest point in Figure 2.1 with a depth of 62m.




3. Results




3.1 ROV-transects




Most of the Blueye ROV transects were trajectories covering areas with steep slopes or rocky terrain. High concentrations of zooplankton in the surface layers (0-10m) obscured the view of the ROV making analysis of the footage challenging. Analysis of the ROV video is shown in Appendix A1 (Table A1). Table 3.1 shows an overview of selected macrofaunal species at registered depths from the analysis of the ROV video footage. Selected macrofaunal species highlighted by this table was observed across the depth gradient, were easily distinguishable in ROV-video transects or key species in focus for this thesis. Small anemones (*Goniactinia prolifera*) were observed from 0 – 20 meters growing on the sea floor and on animals.




Table 3.1 with overview of major macrofaunal species observed in the ROV-transects and corresponding distribution in depth. Selected macrofaunal species highlighted by this table was observed across the depth gradient, were easily distinguishable in ROV-video transects or key species in focus for this thesis. Full table in Appendix 1 (Table A1). Images by Nils Aukan, 2022, with permission.



Name (Latin)	Depth (m)	Picture
Calcareous tubeworms	0-35	
<i>Chone infundibuliformis</i>	27-35	

<p><i>Oxydromus flexosus</i></p>	<p>27-35</p>	
<p><i>Aquiptecten opercularis</i></p>	<p>24-31</p>	
<p><i>Chlamys islandica</i></p>	<p>24-31</p>	

<p><i>Modiolus modiolus</i></p>	<p>14-31</p>	
<p><i>Hormathia</i> spp.</p>	<p>24-33</p>	
<p><i>Urticina</i> sp.</p>	<p>14-35</p>	

<p><i>Ctenodiscus crispatus</i></p>	<p>30-34</p>	
<p><i>Marthasterias glacialis</i></p>	<p>10-11</p>	
<p><i>Ophiura sp.</i></p>	<p>14-35</p>	

<p><i>Echinus esculentus</i></p>	<p>2-25</p>	 <p>(Nevstad, 2022)</p>
<p><i>Gracilichinus acutus</i></p>	<p>2-17</p>	
<p><i>Strongylocentrotus droebachiensis</i></p>	<p>10-30</p>	

<p><i>Buccinum undatum</i></p>	<p>15-33</p>	
<p><i>Neptunea despecta</i></p>	<p>25-31</p>	

3.2 UHI transects of soft sediment seafloor in Faksvågen

The UHI transect collected November 2021 of roughly 14.8m (Figure 3.1 a) was corrected for ROV distance from seafloor and a smaller portion of the transect was isolated for spectral classification (Figure 3.1 b). This section of transect (referred to as sub-transect from here on) was selected due to similar distance from the seafloor. The sub-transect had a length of 2.3m

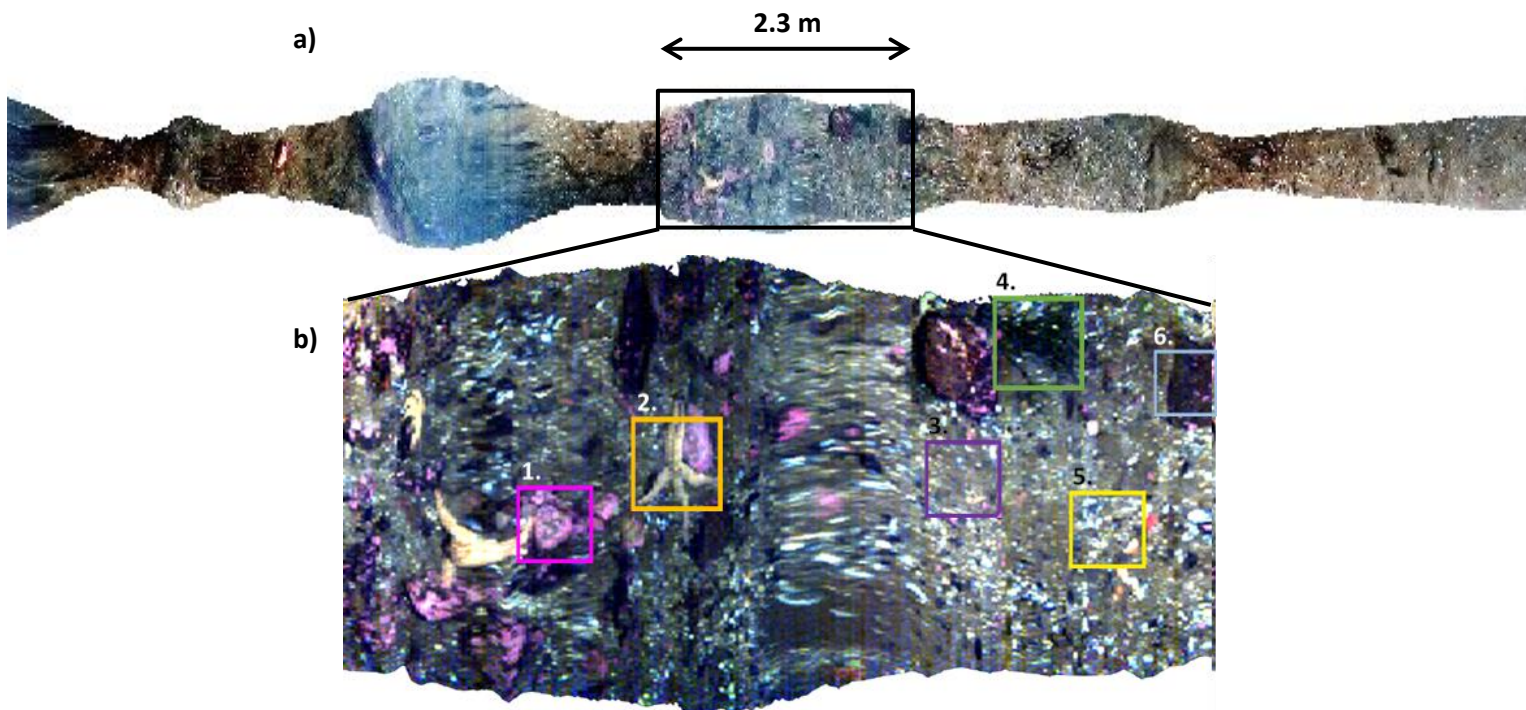


Figure 3.1 Location Faksvågen, UHI photomosaic of transect B1, a) full transect of 14.8m length with box indicating which portion of the transect was used for classification and b) resized sub-transect of 2.3m length with objects of interest 1. Coralline algae 2. Sea stars 3. soft sediment (gray pixels) 4. brown algae (dark pixels) 5. bioclastic sediments (white) and 6. rocks (dark pixels).

A spectral library to be used for spectral classification of the sub-transect was created by manually defining regions of interest (ROI) by selecting pixels of known organisms. Six classes were made, with ROIs picked from coralline algae, sea stars, soft sediments (gray particles), brown algae, bioclastic sediments (shell pieces) and rocks (hard sediments) (Figure 3.1 b). Figure 3.2 shows the mean reflectance spectra (in % $R(\lambda)$) of pixels within each ROI class.

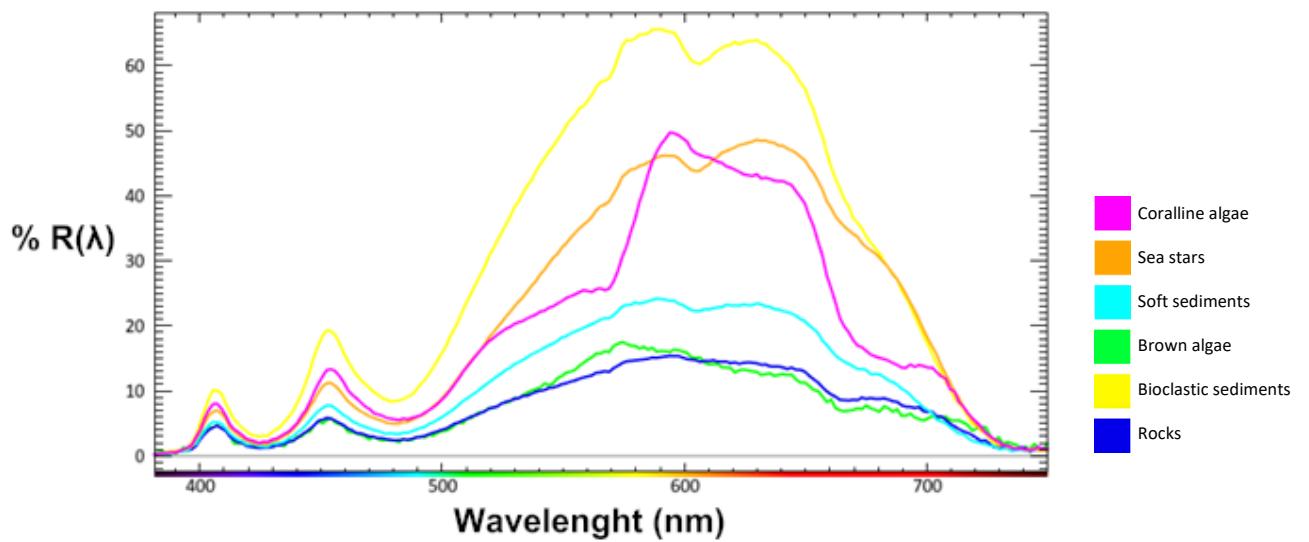


Figure 3.2 Mean in-situ reflectance spectra (% $R(\lambda)$) of each ROI class from the UHI sub-transect based on 20-30 handpicked pixels from the sub-transect. These signatures are hand-picked and used as classification library for the automated classifications in Figure 3.3 (a-b).

For spectral classification of the transect two supervised classification methods were done utilizing the same ROI-library. The resulting classification is shown in Figure 3.3, with overview of classified pixels and coverage (%) in Table 3.2.

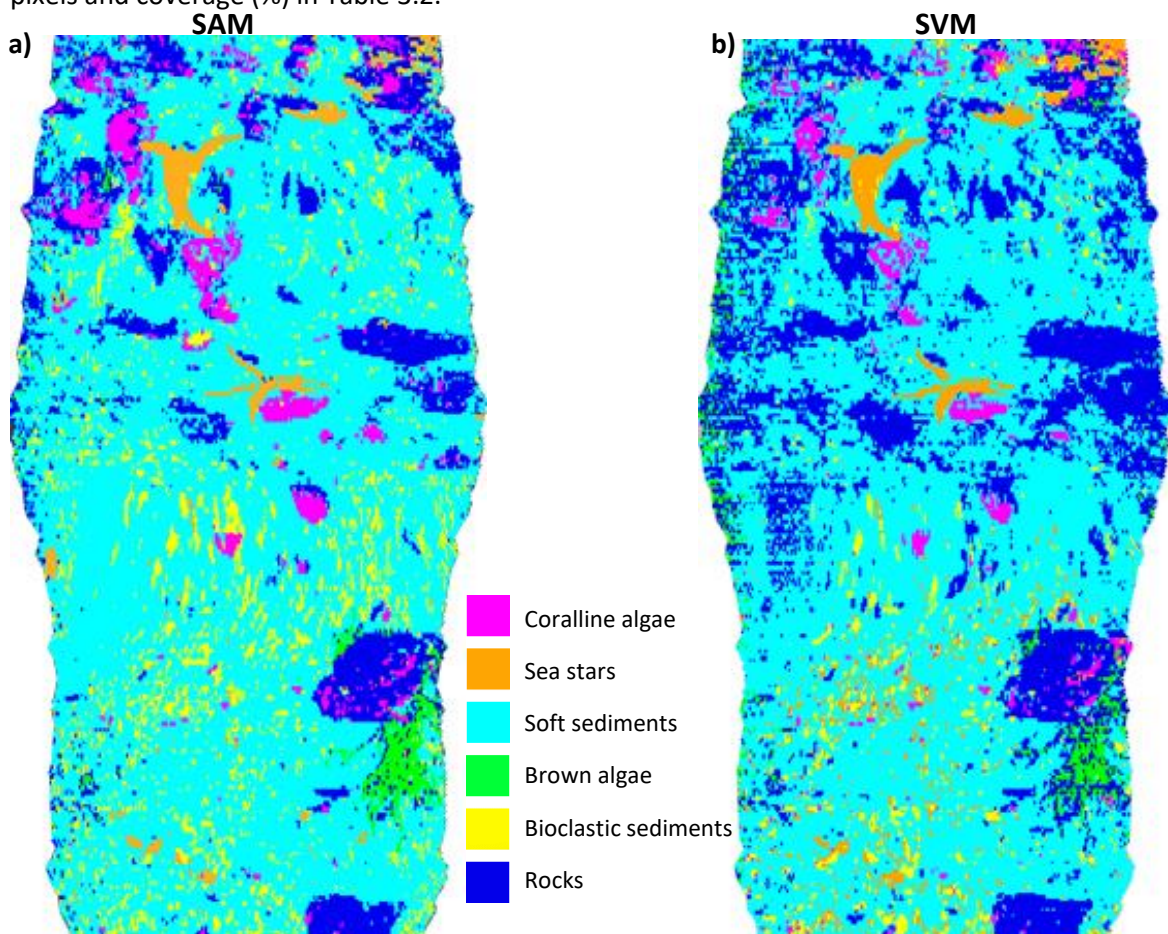


Figure 3.3 Results of the a) SAM-classification and b) SVM-classification as a result of using hand-picked ROIs to classify pixels (classification indicated as pixels marked in different color groups, see Figure 3.2).

Table 3.2 Results of the SAM-classification and SVM-classification algorithms in pixels classified per class and estimated % coverage of total pixels mapped in figure 3.1 b). Unclassified pixels are regions outside of the transect and when removed gives coverage % of transect.

SAM-classification			SVM-classification		
Class	Pixel count	Percent (%)	Class	Pixel count	Percent (%)
Coralline algae	3999	4.1	Coralline algae	2886	3.0
Sea stars	2509	2.6	Sea stars	3901	4.0
Soft sediments	69709	71.9	Soft sediments	63029	65.0
Brown algae	1482	1.5	Brown algae	2134	2.2
Bioclastic sediments	7851	8.1	Bioclastic sediments	3096	3.2
Rocks	11352	11.7	Rocks	21856	22.6
Total	96902	100.0	Total	96902	100.0

3.3 Underwater photogrammetry of vertical wall structures in Faksvågen and Nastadholmen

Three transects in total (A1, C2 and C3 from Figure 2.1 c and d) were selected for producing UPG models displayed in this section (Table 3.3). Due to different length of trajectories the number of frames vary between the models, as well as number of points during initial alignment. All models are processed according to the description given in Appendix 3 in exception of model from transect A1 which did not have navigational data. This was due to the use of navigational data not being supported by Agisoft Metashape Standard used prior to obtaining Agisoft Professional.

Table 3.3 shows the ROV-transects processed in Agisoft and the number of image frames, points (separated by , per hundred) in sparse point cloud and estimated areal of coverage. Model A1 does not have areal as the model was created using Agisoft Metashape Standard, which did not support the use of navigational data, and therefore not obtaining spatial scale.

Transect name	# of image frames	# of points in sparse cloud alignment	Areal (m ²)
A1 (Sub-transect)	73	37,084	
C2	709	1,097,213	39.3
C3	818	1,355,446	51.2

Trial models done in December 2021 to test the method shown in Figure 3.4 of OOI *Urticina* sp. on a wall in Faksvågen.

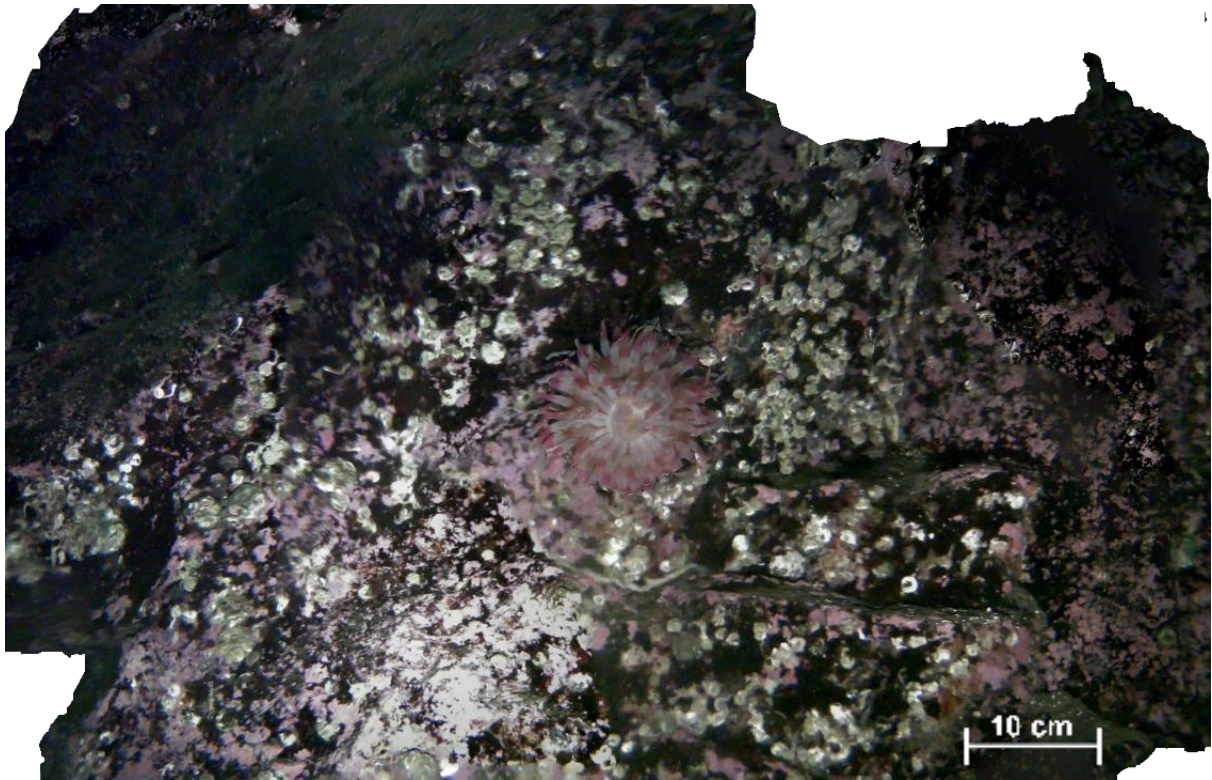


*Figure 3.4 Initial test of UPG done December 2021 with 86 overlapping images from November 2021 Blueye Pioneer video data. Orthomosaic of wall-transect a1 (sub-transect) seen from front (eye of the ROV). This transect does not have scale as the navigational data from the ROV was not used in this model. Anemone (*Urticina* sp.) in center estimated to be approximately 10 cm in diameter, and an estimated scalebar for 10 cm is added to the figure. Model constructed in Agisoft Metashape Standard.*

Long transects were challenging to visualize in a 2D figure due to varying degree of horizontal- and vertical shape of the models. The different sections of the model can be isolated and visualized in fitting view for further analyzing and processing. DEM was constructed based on dense point cloud of transect X2 and was visualized by color defined by depth (Figure 3.5 a), and hillshade to visualize model structure was added (Figure 3.5 b). Orthomosaic of transect C2 was also visualized with the same bird's eye view-viewpoint (Figure 3.5 c, setting "top XY" in Agisoft, see Appendix 3).

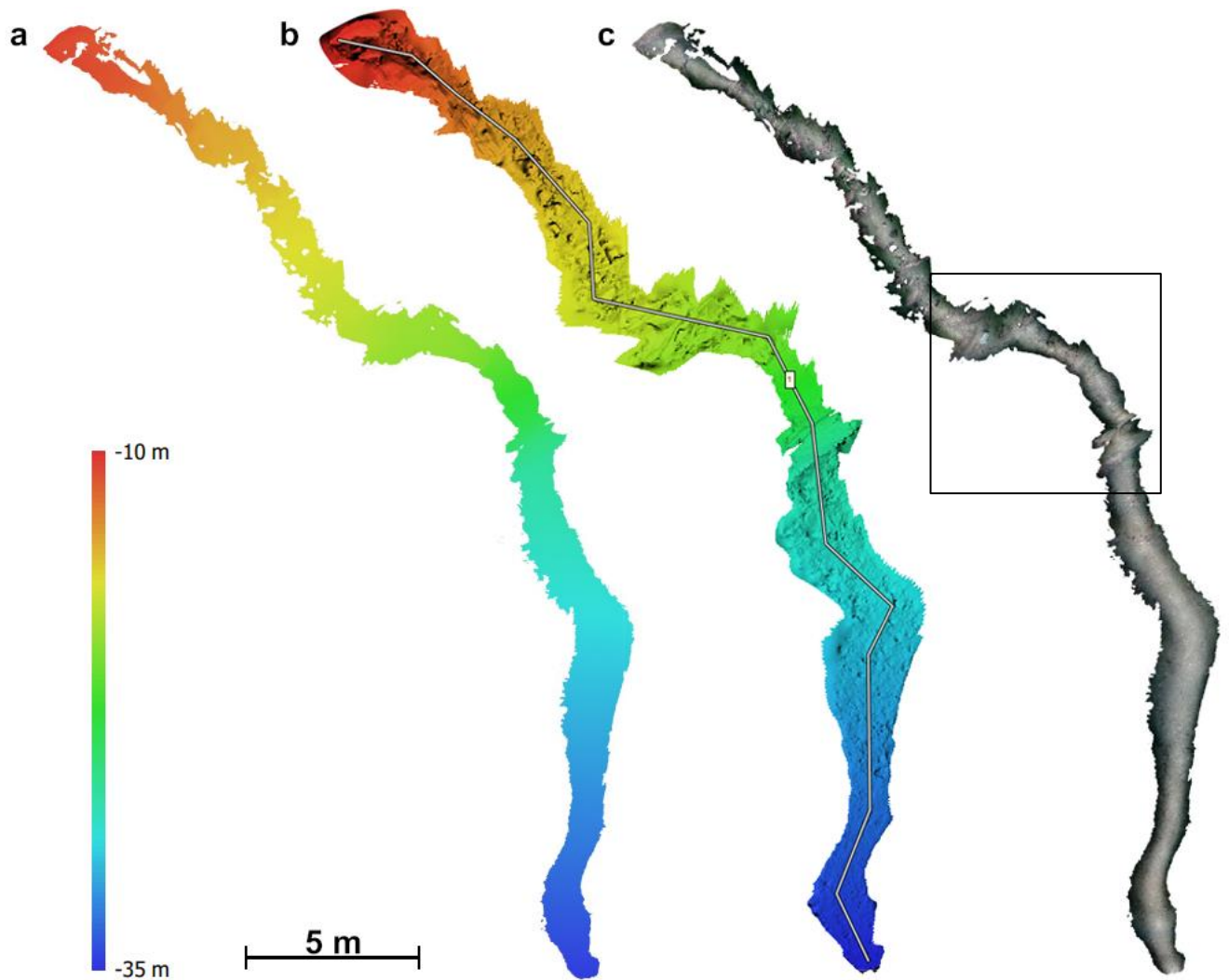


Figure 3.5 ROV transect C2 in Faksvågen consisting of 1,097,213 overlapping images. a) Depth elevation model (DEM) in meter depth, b) DEM with hillshade (shadow from model structure) and polyline (combination of multiple lines across transect) to visualize the depth profile in Figure 3.11 and c) Orthomosaic, with a black frame marking out the sub-transect shown in Figure 3.7 a). Model constructed in Agisoft Metashape Professional.

By drawing a polyline across the middle of the DEM a depth profile of the transect could be made (Figure 3.6). This shows the change in depth and distance. This visualizes the selected area covered by the polyline in a similar fashion of a cross-section.

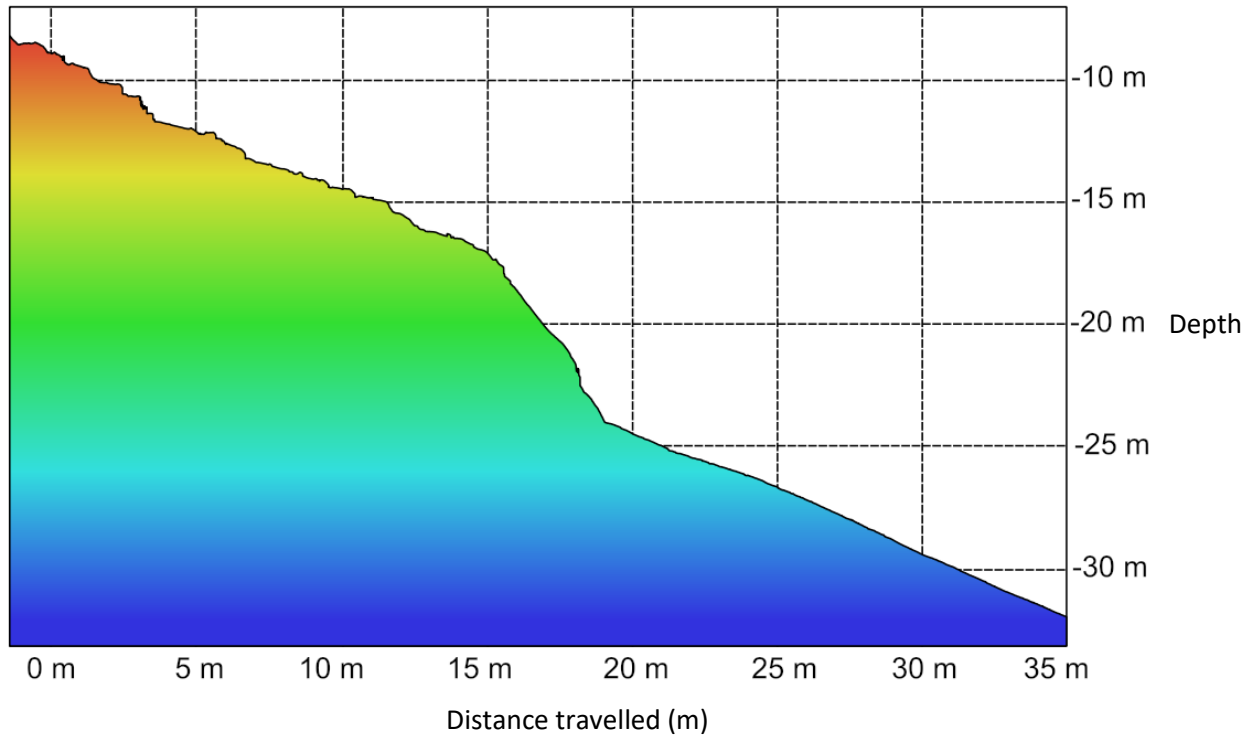


Figure 3.6 Depth profile 10-35m depth of transect C2 in Faksvågen based on the polyline manually placed in the depth elevation map (DEM) of the transect based on navigational data assigned to 1,097,213 overlapping images. X-axis shows the estimated distance travelled (m). Created from model constructed in Agisoft Metashape Professional.

For visualization purposes the C2 transect was isolated into a shorter sub-transects as shown in Figure 3.7.

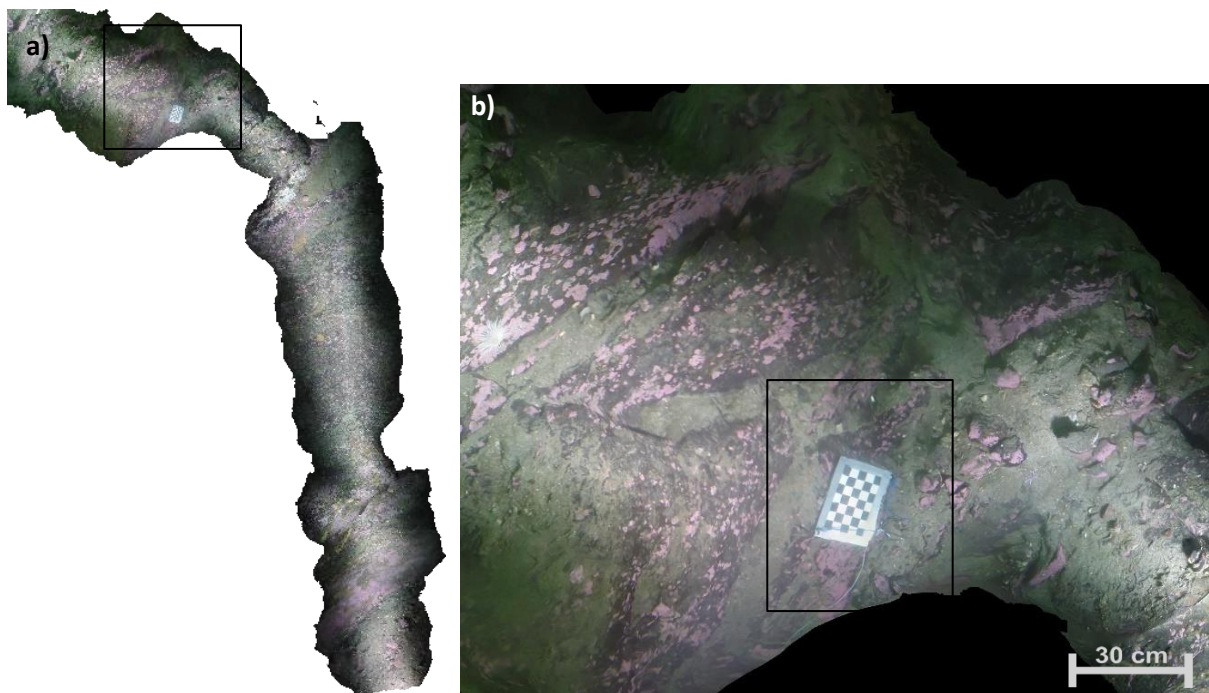


Figure 3.7 Orthomosaic of C2 from Faksvågen in Figure 3.10 isolated to a) The sub-transect (approximately 250,000 points derived from approximately 175 images) in top-XY visualization and b) closeup of the checkerboard-reference area. The box indicates area isolated for a detailed visualization in Figure 3.8. Model constructed in Agisoft Metashape Professional.

Figure 3.8 demonstrate how isolating transects into sub-transects for higher-detailed visualization of models when using heatmaps and hillshading for depth and mesh texture visualization.

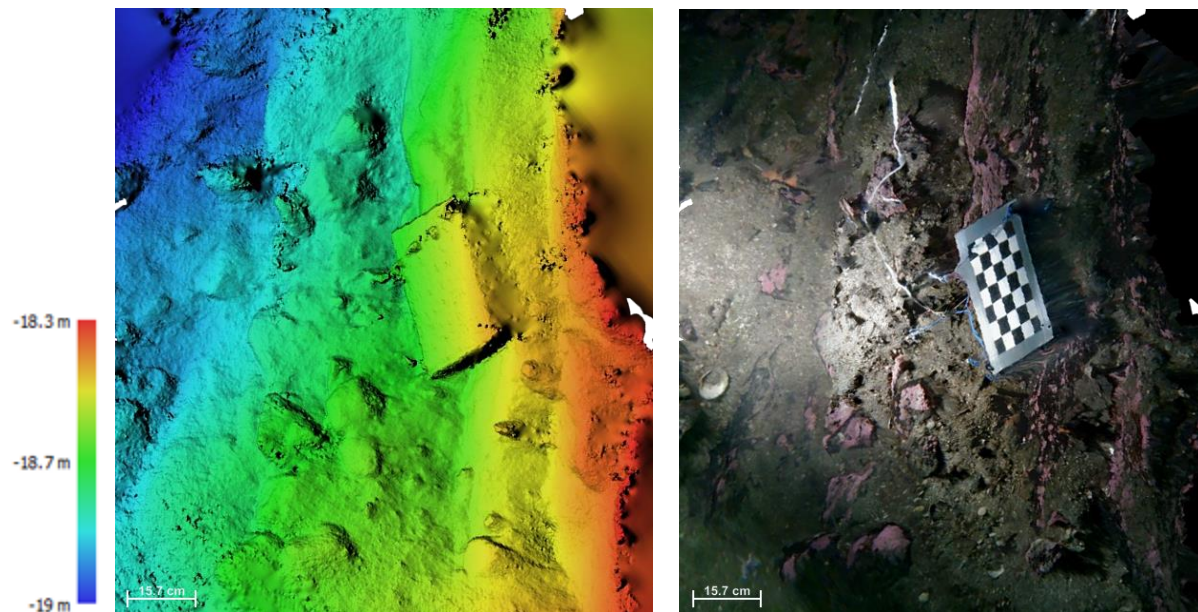


Figure 3.8 shows a close-up of the checkerboard-reference in transect C2 from Faksvågen in a) depth elevation map (DEM) and b) Orthomosaic in XY-visualization. Model constructed in Agisoft Metashape Professional.

Contours were created in Agisoft to visualize the changing depth in the model (Figure 3.9).

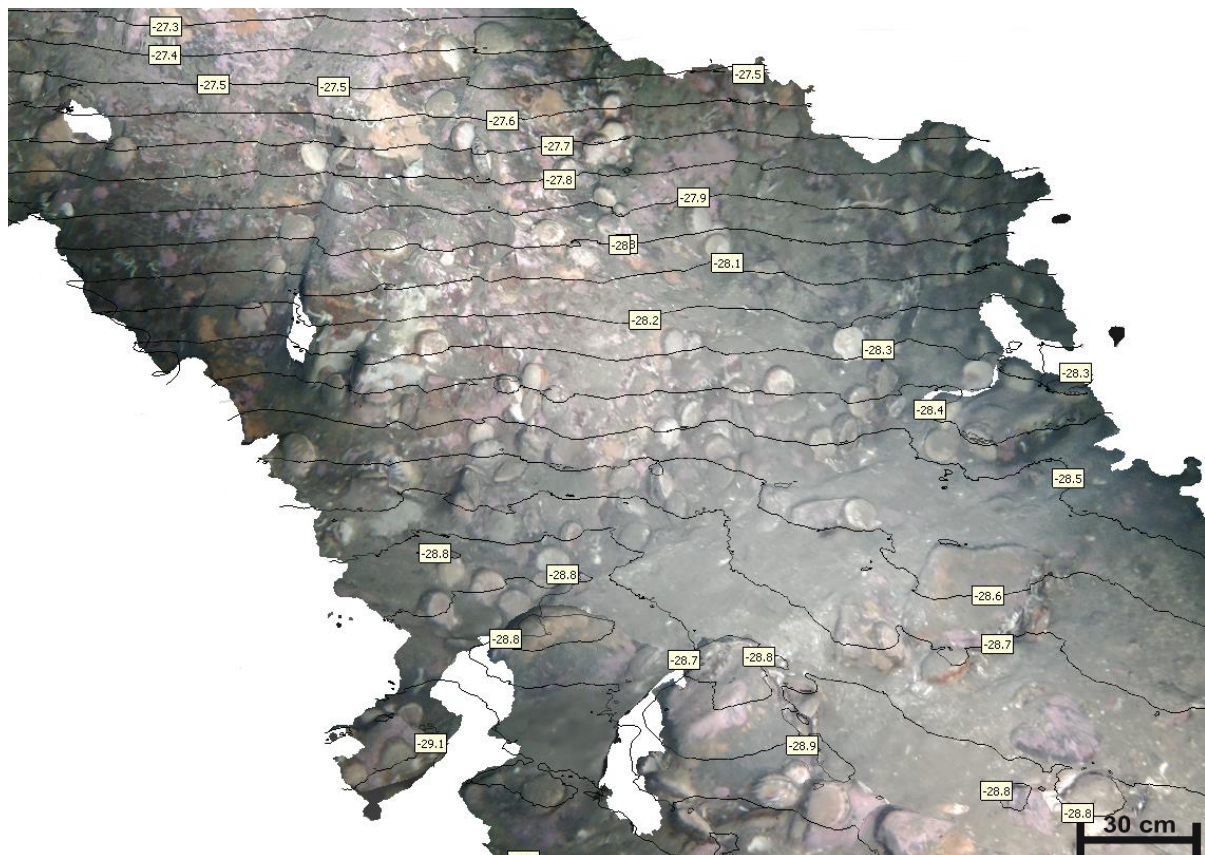


Figure 3.9 A portion of C3 model from Nastadholmen with depth contours indicating depth (in negative meters, black lines) generated in Agisoft. This habitat is possibly showing a high density of cold-water species *C. islandica*. Model constructed in Agisoft Metashape Professional.

From the models it was possible to measure the width and length (in cm) of OOI. Clams from 27-29m depth in the C3 transect were measured length and width of (Figure 3.10).

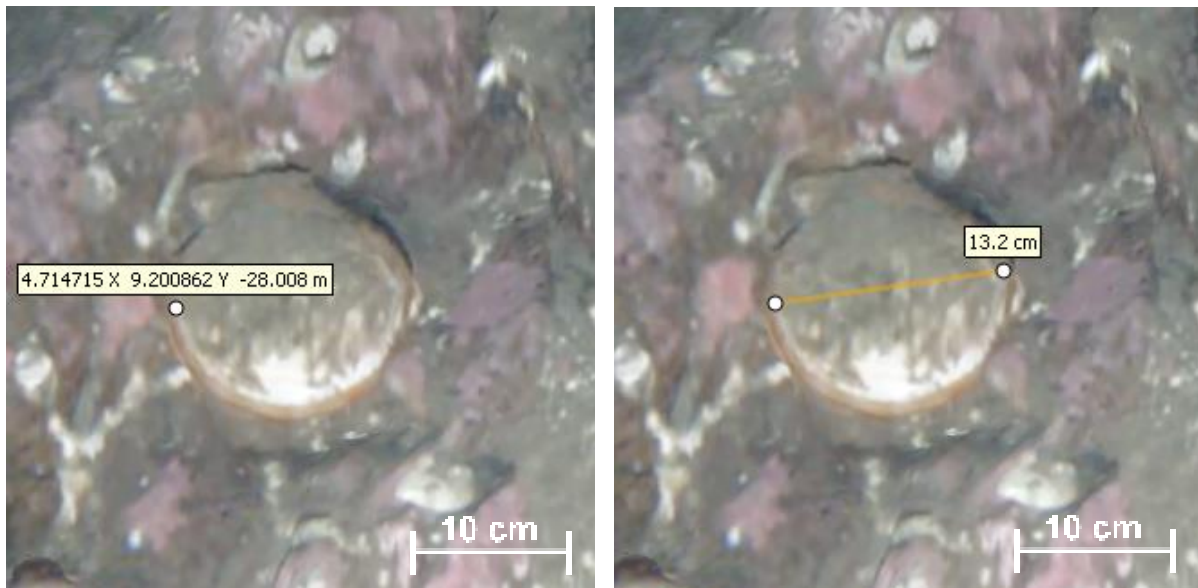


Figure 3.10 showing measured depth and size of bivalves *C. islandica* in transect C3 in Agisoft. This clam is at 28m depth and had a measured width of 13.2 cm \pm 0.5 cm in the model. Model constructed in Agisoft Metashape Professional.

Macrofaunal species along the transect were measured to compare with measurements *in-vivo*. Specimens were selected from regions of the model with high reconstruction accuracy. The measured specimens also had to have distinguishable edges to assure correct regions measured. A mean length and width was calculated for all groups with a \pm 0.5 cm inaccuracy given by Agisoft reconstruction uncertainty (Table 3.4).

Table 3.4 Calculated average measured sized of specimens within transect R25 done as illustrated in Figure 3.10. For echinoderms, the sea urchins (*E. esculentus* and *G. acutus*) were measured in diameter, and the brittlestars (*Ophiura sp.*) were measured from central disk to tip of the arm similar to specimens measured *in-vivo*. Only one specimen of *B. undatum* was captured clearly enough in the transect to be measured in length, but it was not possible to measure the width of this specimen as the view was obscured. Full table of measurements shown in Appendix 2, Table A2.2.

Molluscs	Length (cm)	Width (cm)	Echinoderms	Length (cm)
Average <i>C. islandica</i>	10.1 \pm 0.5	9.3 \pm 0.5	Average <i>E. esculentus</i>	6.2 \pm 0.5
Average <i>M. modiolus</i>	20.4 \pm 0.5	10.2 \pm 0.5	Average <i>G. acutus</i>	7.4 \pm 0.5
Average <i>B. undatum</i>	6.5 \pm 0.5		Average <i>Ophiura sp.</i>	7.1 \pm 0.5

3.4 Ground-truthing and laboratory work

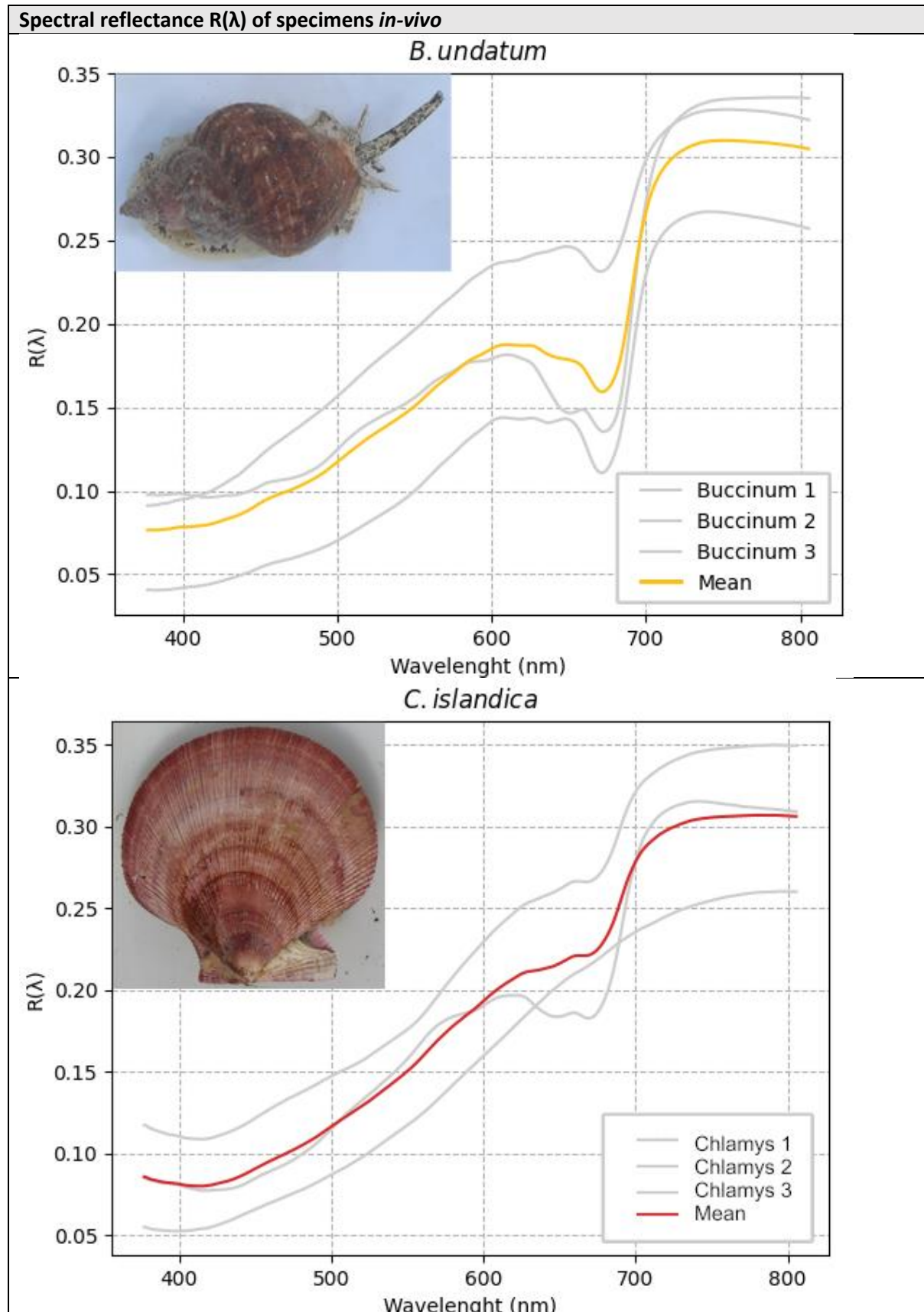
Animals sampled along the transect at Nastadholmen (March 2022) were measured in lab for their size and the *in-vivo* $R(\lambda)$ were measured for up to three sites on the body. To facilitate the comparison of size of macrofauna in transect the measured length and width was averaged, displayed in Table 3.5. In this table the biggest specimen within each species is also added to easier compare with measurements of the same species within the UPG models.

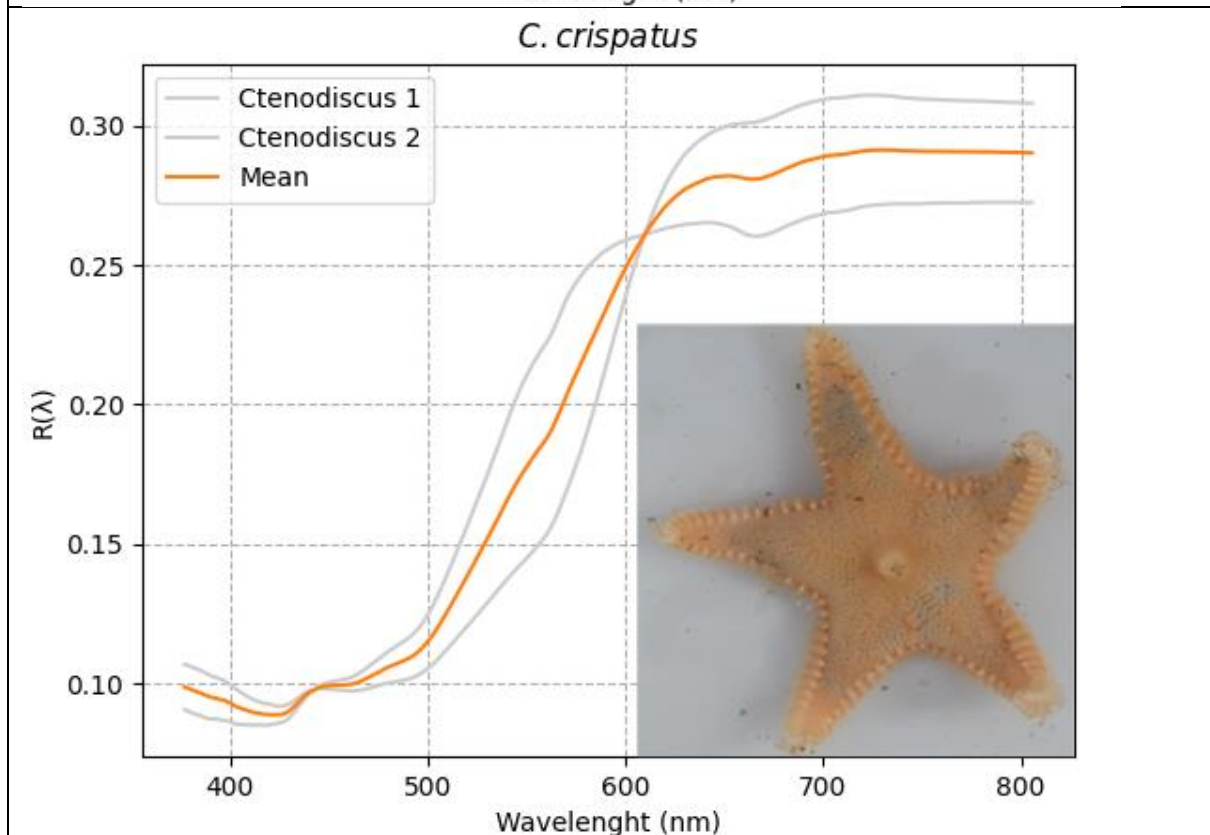
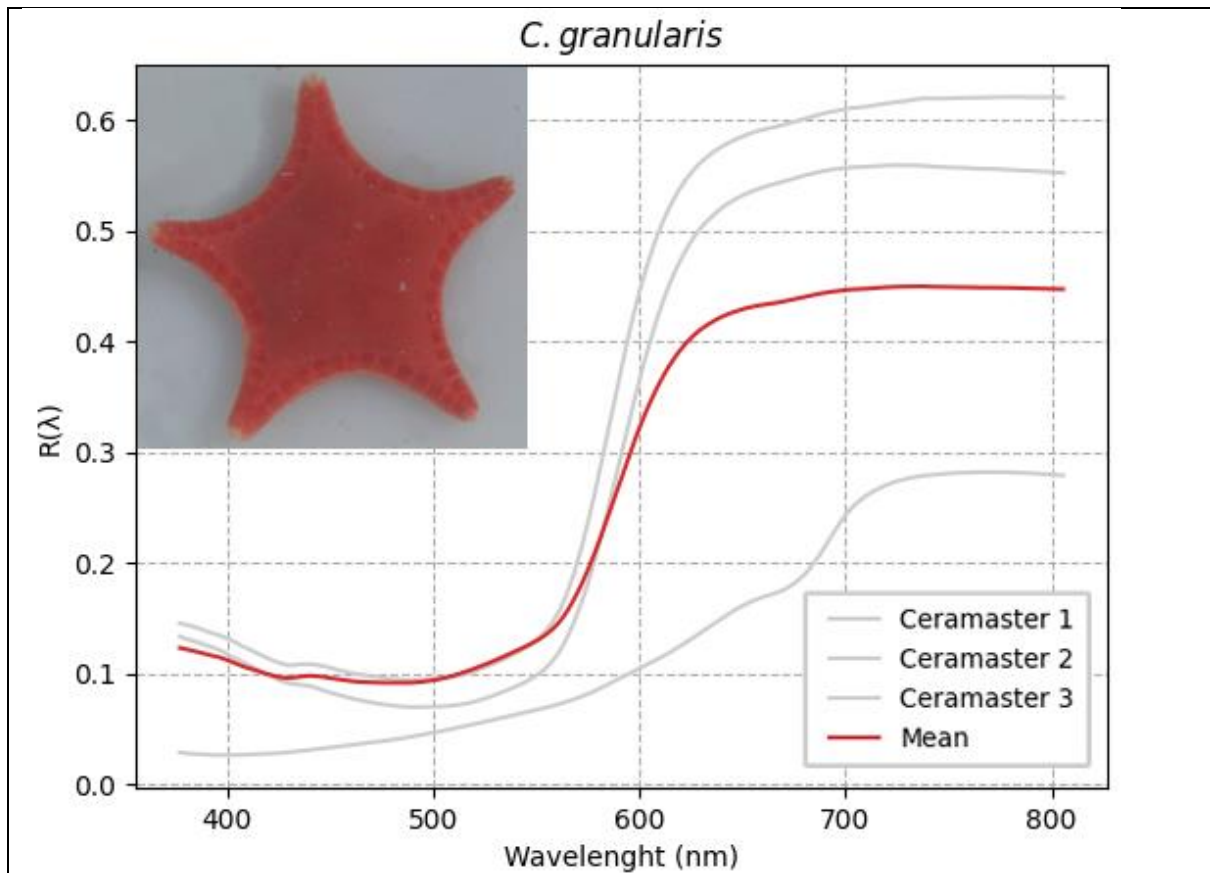
Table 3.5 Highest- and average length and width of selected macrofauna species measured in lab. Some of the species collected were cold-water species, like *C. islandica*, *Hormathia* spp., *C. crispatus* and *N. despecta*. Columns containing echinoderm species had a measurement from central disk to arm for sea stars, and diameter of body for sea urchins given in the width column. Average length is left blank for echinoderms.

Morphogroup	Species name	Average length (cm)	Average width (cm)	Longest specimen (cm)	Widest specimen (cm)
Bivalva	<i>Aquiptecten opercularis</i>	5.9	5.9	5.9	5.9
Bivalva	<i>Chlamys islandica</i>	7.9	7.4	9.4	8.7
Bivalva	<i>Modiolus modiolus</i>	13.4	6.8	15.7	8
Cnidaria	<i>Hormatia</i> spp.		3.4		3.8
Echinodermata	<i>Ctenodiscus crispatus</i>		3.1		4.1
Echinodermata	<i>Echinus acutus</i>		7.0		7.6
Echinodermata	<i>Marthasterias glacialis</i>		23.7		23.7
Echinodermata	<i>Strongylocentrotus droebachiensis</i>		3.7		5.2
Gastropoda	<i>Buccinum undatum</i>	7.1	3.7	8.1	3.9
Gastropoda	<i>Neptunea despecta</i>	7.1	3.7	14.4	7.5

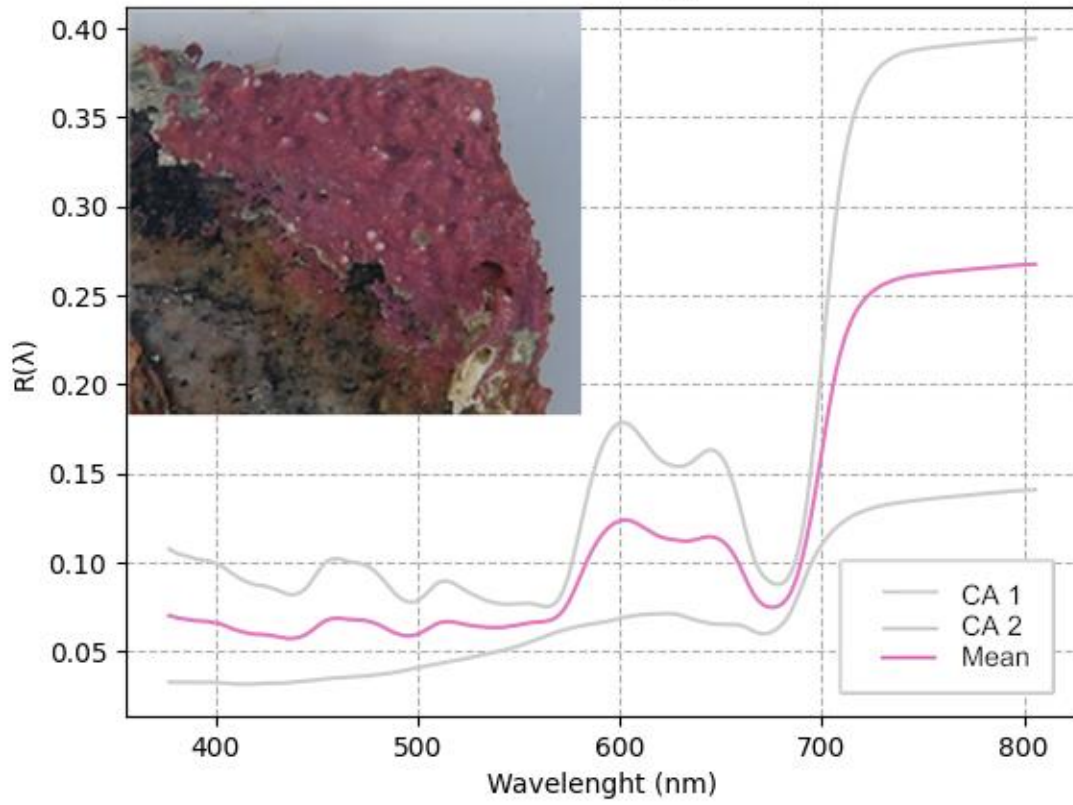
Measurements of $R(\lambda)$ *in-vivo* were done using the QE-pro spectrometer on the live specimens. By selecting three different areas on the organism, the variation of pigment content was considered. This was converted to a reflectance-spectra and shown in Table 3.6.

Table 3.6 Animals (in alphabetical order) sampled during the fieldwork in March 2022 in Karihavet with measured in-vivo spectral reflectance $R(\lambda)$. Spectral reflectance measured using the spectrometer on selected specimens in lab for ground truthing of $R(\lambda)$. Photos: Amy Li., 2022 with permission.

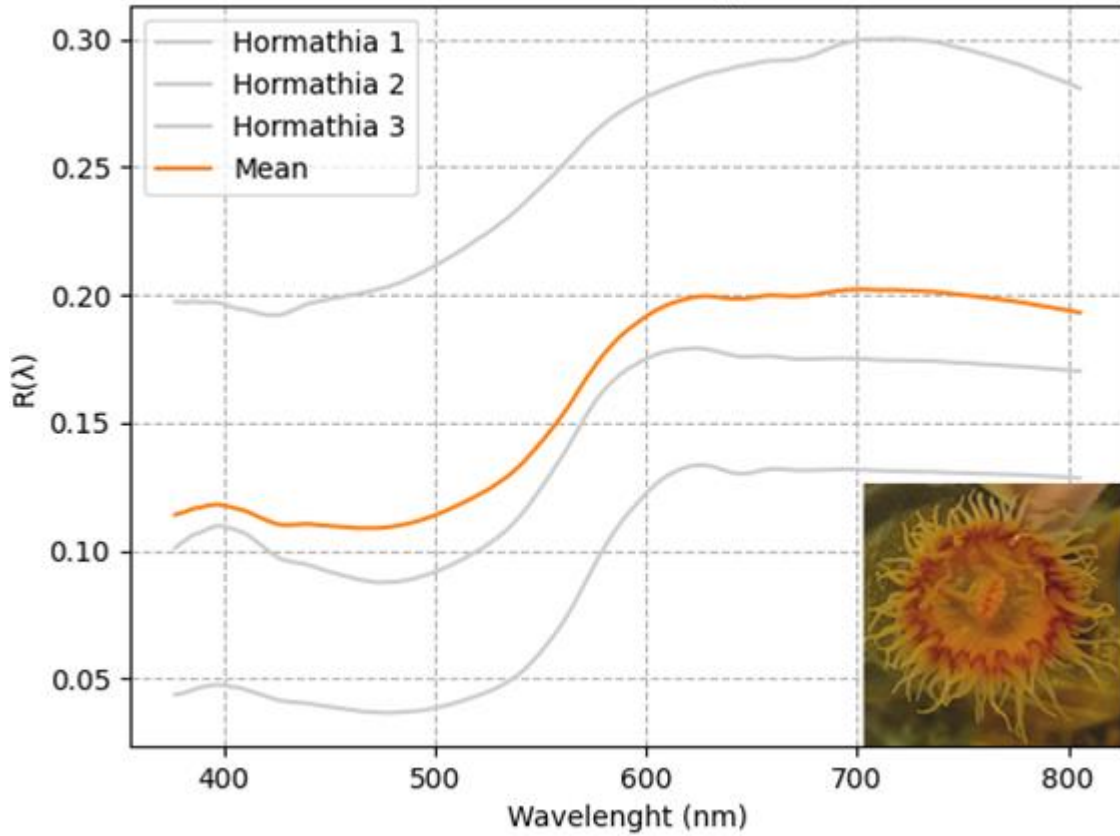


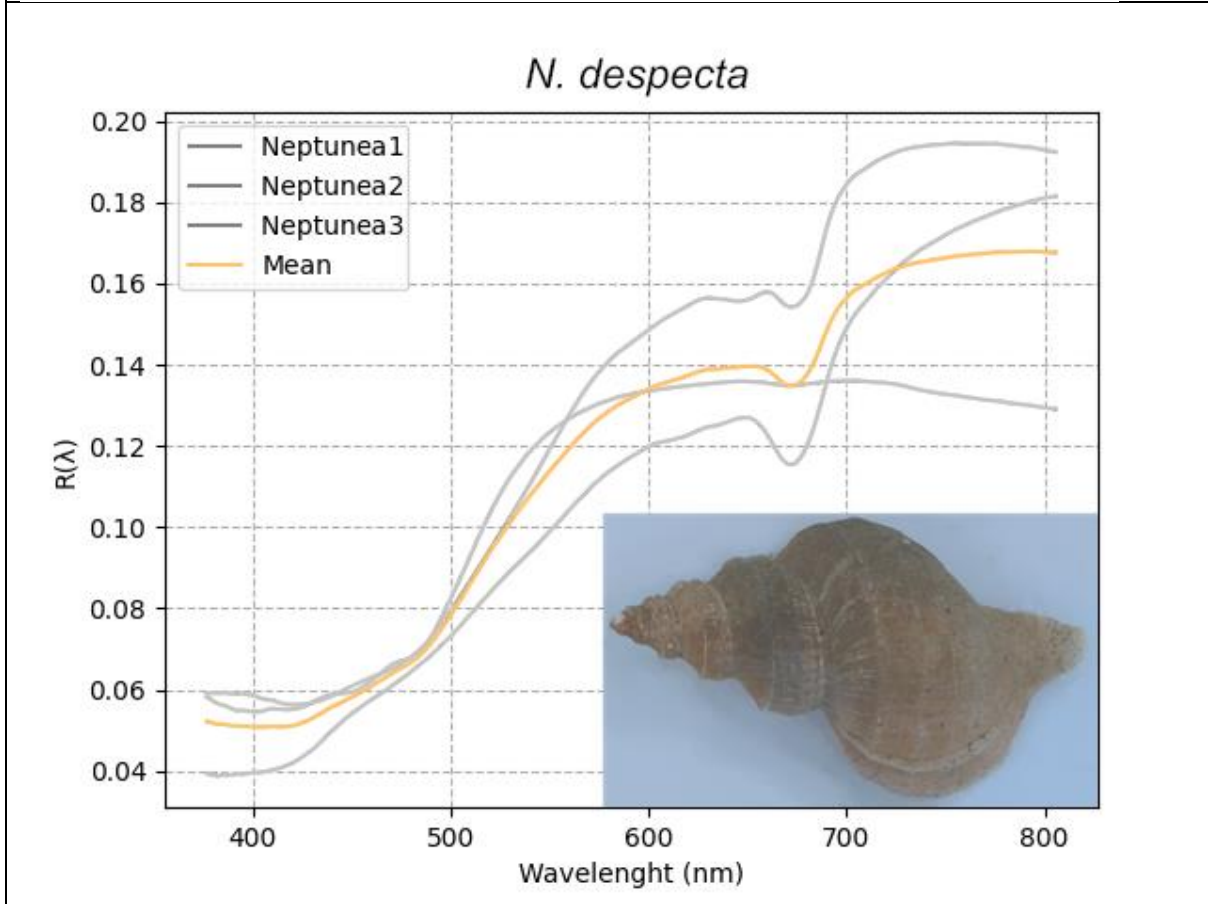
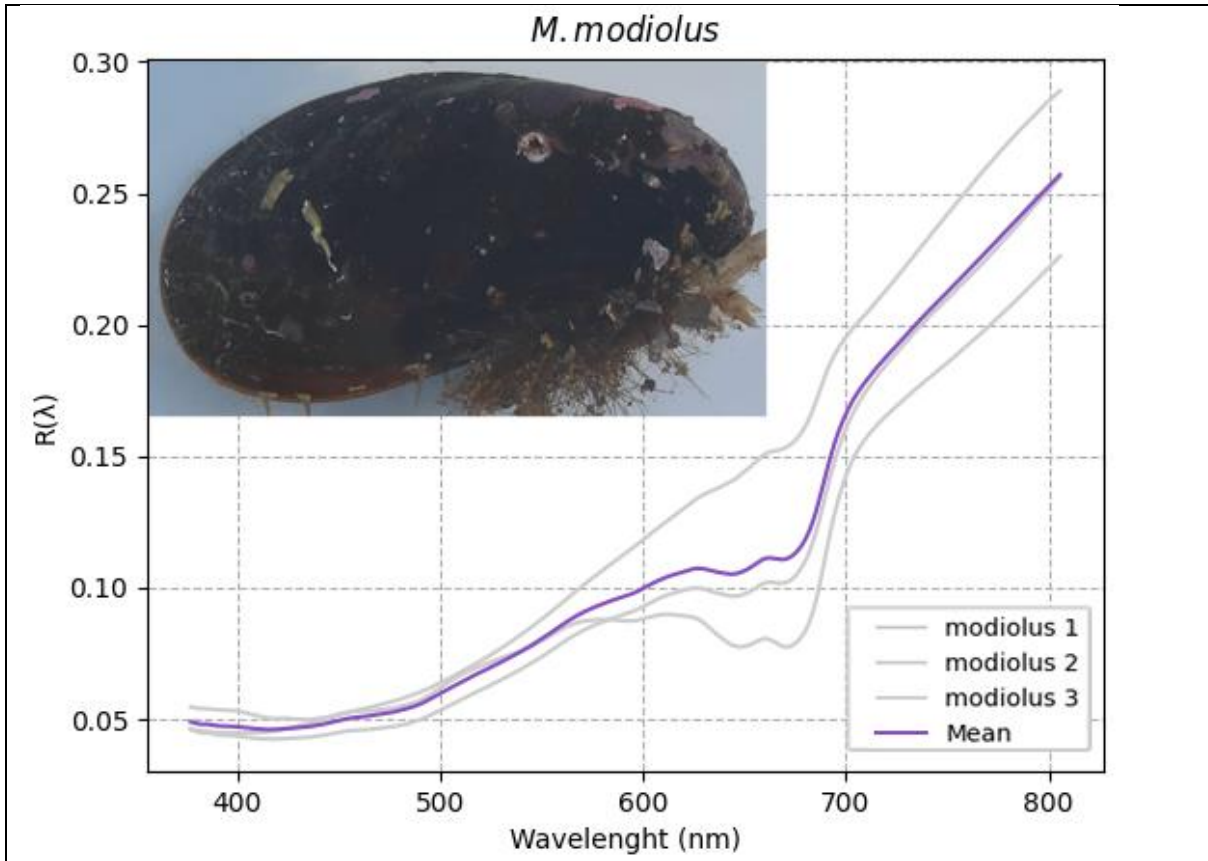


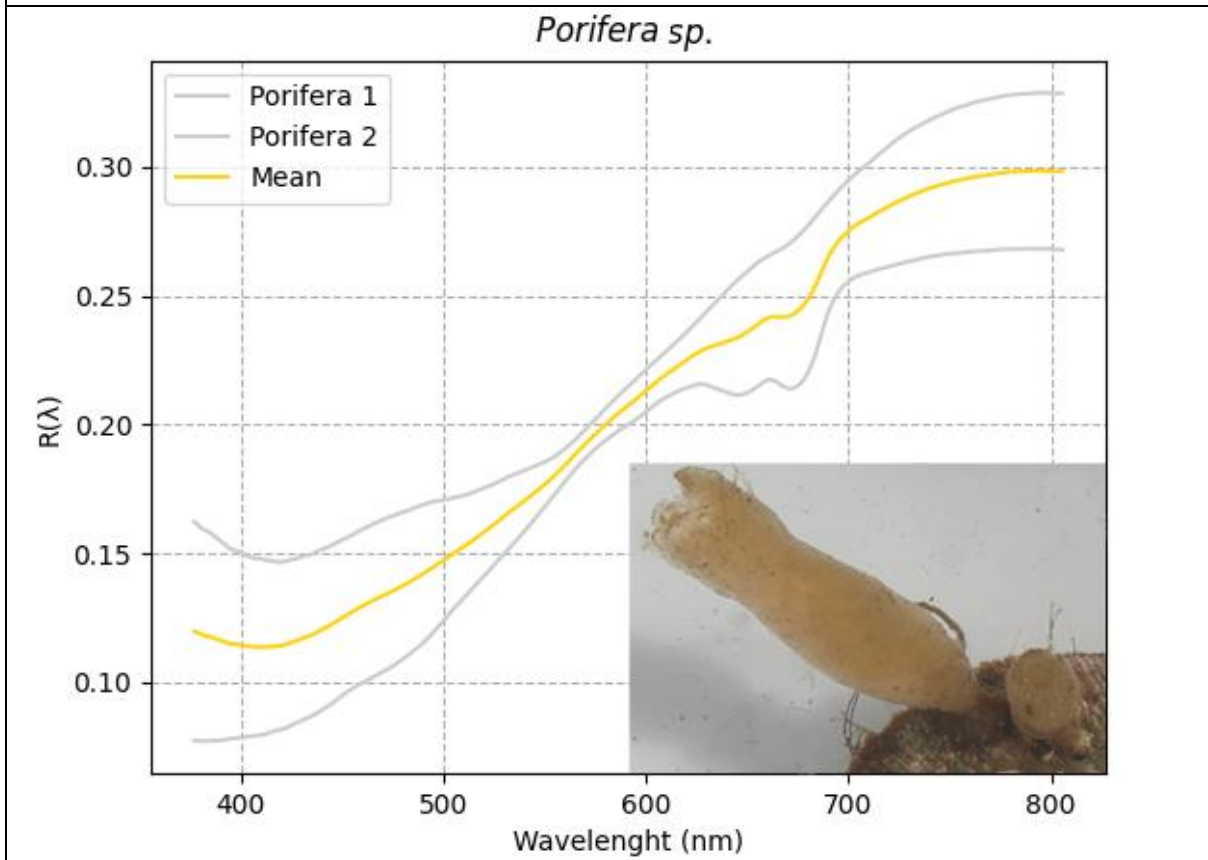
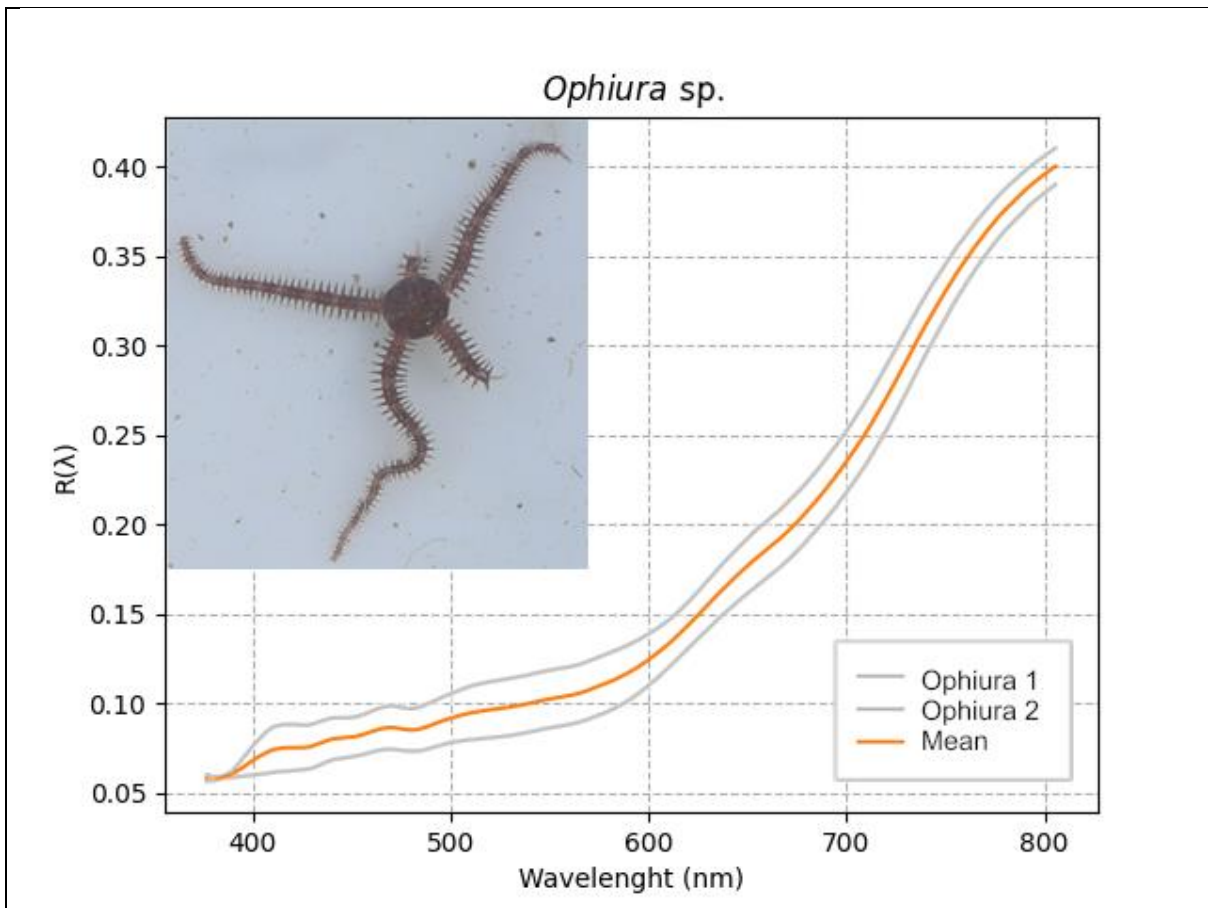
Coralline algae



Hormathia spp.







3.5 Castaway-CTD

CTD profile was done in the deepest point (See figure 2.1 b) of the bay in November 2021 to a depth of 62m (Figure 3.11, a). This was repeated in March 2022 reaching a depth of 70m (Figure 3.11, b).

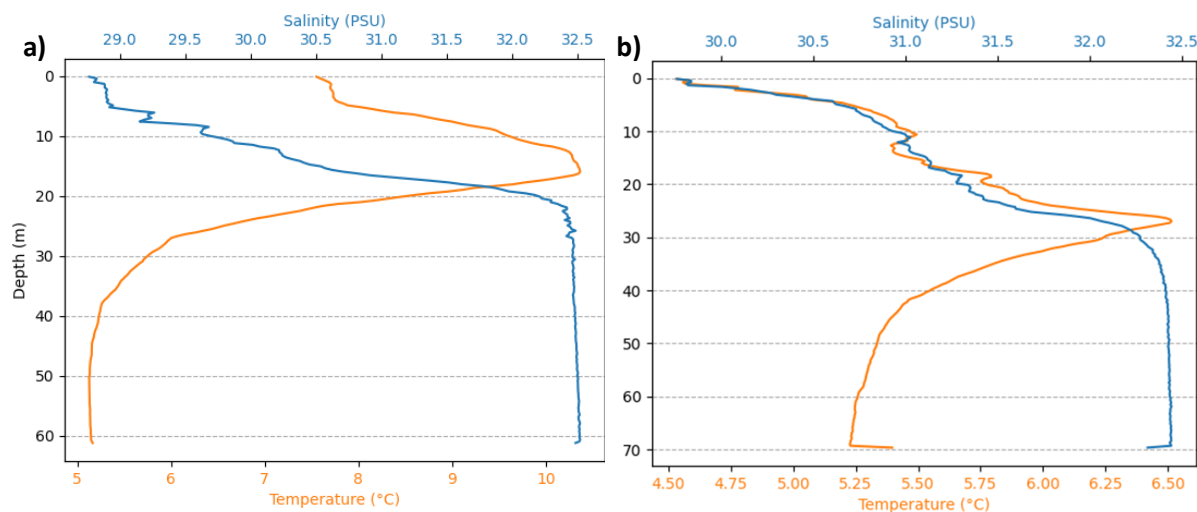


Figure 3.11 CTD measurements salinity (Practical salinity unit PSU) and temperature (C °) per depth (m) done at the deepest point (\pm 700 m) of Karihavet in a) November 2021 and b) March 2022. Further details see figure 1.5 on sills in Karihavet.

3.6 Habitat description

RGB-ROV-video analysis and physical samples were used to display an overview in habitats across the depth gradients and sediment types. A full overview of observed morpho groups and species from the RGB-video analysis can be found in Appendix 1, with an overview shown in Figure 3.12. Less data was acquired from 0-6 meters due to cloudy water (from zooplankton) at these depths strongly reducing visibility. A clear *Ascomphyllum nodosum* belt was present at rocky hills at 0-1 meters with *G. acutus* inhabiting the wrack belt. From the surface to 10 meters sand, gravel and mixed small rocks were covered with a layer of turf algae with a decreasing coverage of turf with increasing depth. Rocks were increasingly dominated by red calcareous algae (*Corallinales*) on the surfaces not exposed to direct sunlight (usually underside of the rocks) with increasing depth. The vertical wall started at approximately 10 meters with the first section having a low to medium coverage in coralline algae and calcareous tubeworms. Some areas of the wall had shelves with soft sediment and contained pieces of shells from mollusks as well as the bivalve *M. modiolus*.

There was a clear increase in coverage of coralline algae and calcareous tubeworms at approximately 20 meters. 25 – 35 meters is the depth region where *C. islandica* and *A. opercularis* were observed, where there is a change from vertical wall to slow-sloping soft sediments with interspersed rocks. The clams occur on both the wall in between cracks, on top of the hard sediment and on the soft sediment with rocks. *Hormathia* spp. was observed from 25 – 35 meters on both hard and soft sediment. *Ctenodiscus crispatus* and *O. flexuosus* were observed from 30 – 35 meters on soft sediments. *Ophiura* sp. was observed along the entire transect on soft sediment and shelves. Macrofaunal observations are shown in Figure 3.12.

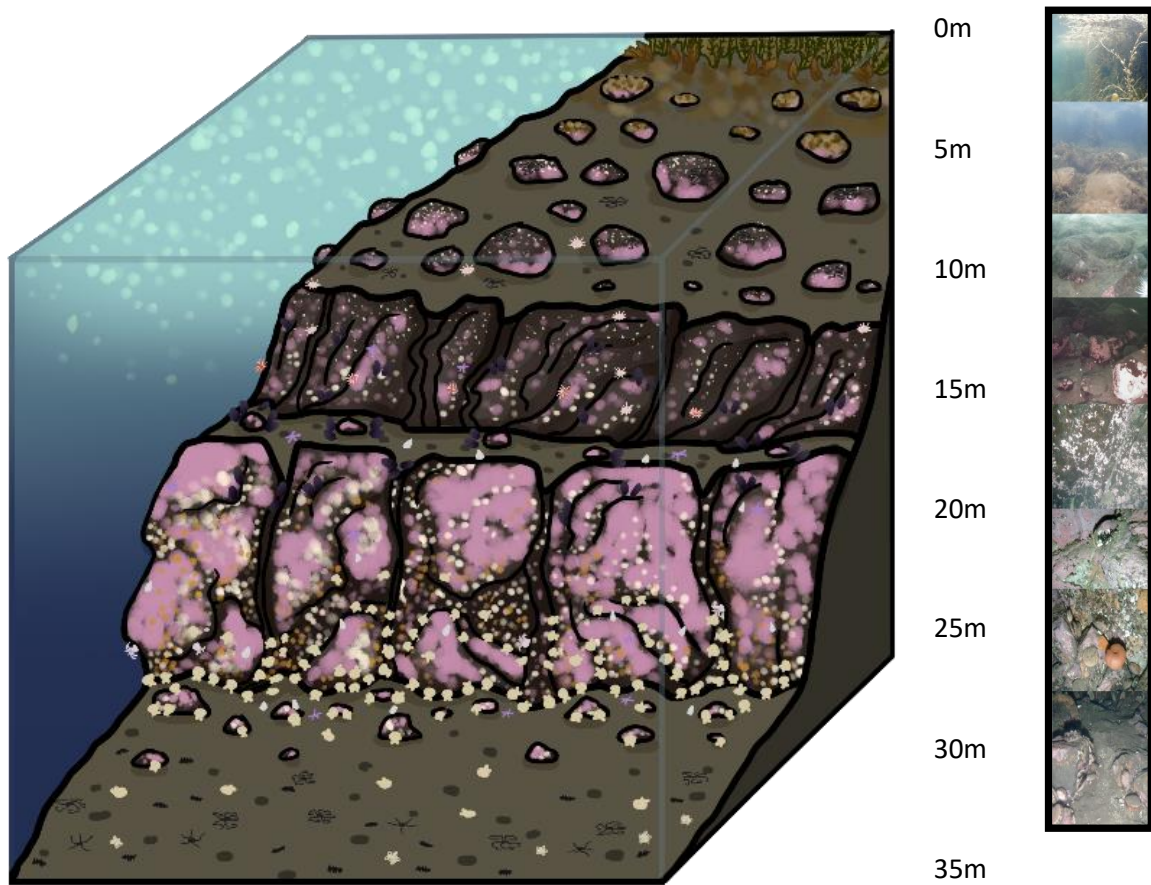


Figure 3.12 Difference in distribution and morpho group occurrence observed in the ROV transects from 0-35m. ROV still-images on the right were extracted from the video footage to use as reference for the figure. Not to scale. Illustration: Malin Bø Nevstad, 2022.

Shannon-Wiener biodiversity index based on data from photogrammetry model

A Shannon-Wiener biodiversity index (H) and evenness index (E) was done based on the observed macrofaunal species counted in 60x60 cm (2D-lines) squares in the models (Figure 3.13). The squares were placed evenly spaced in the transects depth profile to capture different difference in organisms at different depth (14, 20 and 34 m), sediment types and sediment rugosity (Table 3.7). Shannon-Wiener index were calculated for the three sites (Shannon and Weaver, 1949, Norse and Crowder, 2005).

$$\text{Shannon-Wiener diversity index } H = \sum [(p_i) * \ln(p_i)]$$

$$\text{Evenness-index } E = \frac{H}{\ln(S)}$$

Where P_i is the total number of counted individuals in species divided by total number of species and S is the number of species.

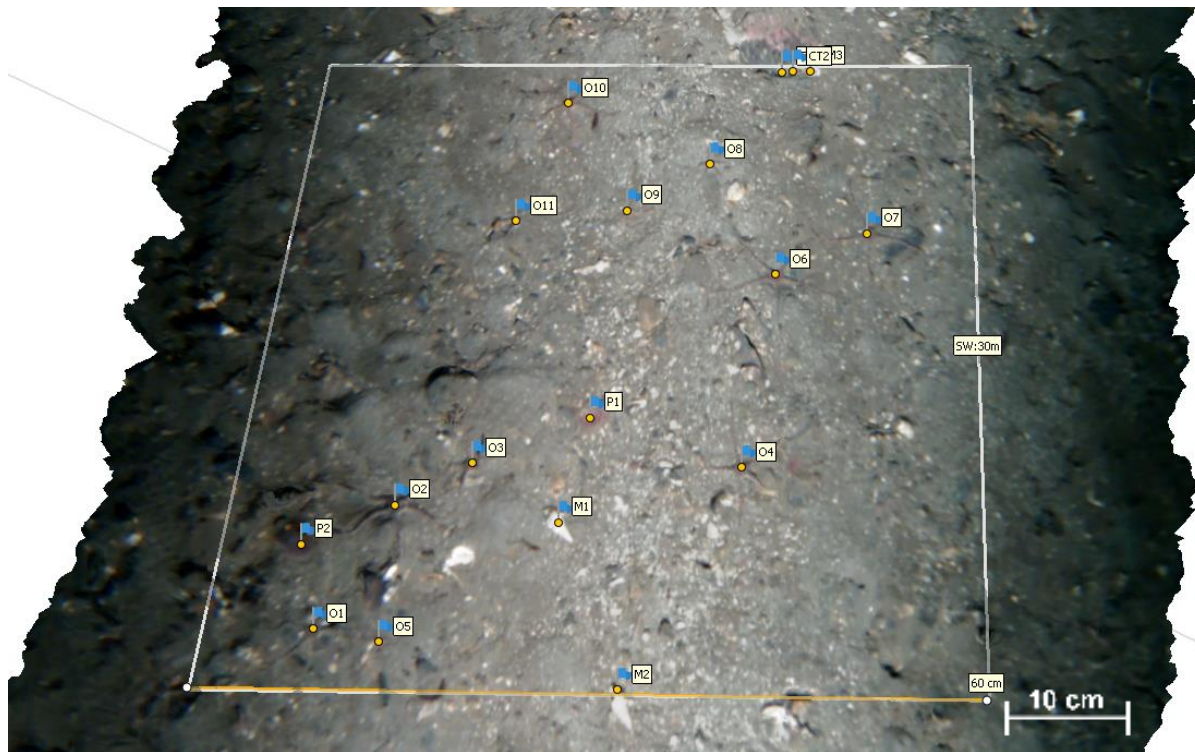


Figure 3.13 Counting of number of individuals of visible macrofaunal species at 34m depth soft sediment in transect C3 in a 60x60 cm square. Each flag (blue) indicates a counted organism. Each distinct species was assigned a code to keep track of counted organisms.

Table 3.7 Overview of Shannon-Weiner biodiversity index from counted as far into species taxa observed in each 60x60 cm square at 14-, 20- and 34-meters depth in transect C3 from Nastadholmen. The diversity index (H), the natural logarithm of number of species ($\ln(S)$) and evenness index (E) is calculated for each square from formulas on page 47. Serpulidae sp. Consists of two species that were indistinguishable in the image, Placostegus tridentatus & Spirobranchus triqueter. Bryozoans were counter per "colony" distinguished by clear borders.

Depth (m)	Taxa	Frequency	H	Ln(S)	E
14	Bryozoa indet.	9	0.56	1.1	0.51
	Ophiura sp.	4			
	Serpulidae sp.	63			
20	Balanus Balanus	9	1.35	1.95	0.69
	Asciacea indet.	6			
	Bryozoa indet.	2			
	Echinus esculentus	1			
	Pododesmus sp.	7			
	Serpula vermicularis	2			
	Serpulidae sp. (Placostegus tridentatus & spirobranchus triqueter)	36			
34	Ophiura sp.	11	1.09	1.39	0.78
	Gastropoda indet.	3			
	Myxicola infudibulum	2			
	Serpulidae sp.	2			

4. Discussion

Underwater hyperspectral imaging (UHI) was used in this study to estimate coverage of different taxa of benthic organisms and substrate, among these photosynthetic macroalgae (red and brown), benthic organisms (sea stars) and sediment classes (rocks, soft sediment and bioclastic sediments). Bioclastic sediments were observed to have a high reflectance compared to other sediments and organisms due to its white surface, and this information can be used to quantify high production in an area based on coverage of this sediment type to indicate areas with high density of plankton filter-feeders. This high production area may resemble production in deep water coral reefs (Mogstad et al., 2022).

Underwater photogrammetry (UPG) was used combined with mini-ROV to map benthic habitats and macrofaunal species across a variation of sediment types and 3D structures. Simple measurements based on the constructed models provide additional information on size of objects, project sloping of the terrain, visualize the benthic habitats and simple biodiversity estimations.

Cold-water macrofaunal species were found at shallower depth than similar habitats in the Barents Sea, confirming that Karihavet is a special location of specific semi-enclosed bays with low temperatures sustaining specialized cold-water species at shallower depths not found in the Norwegian fjord systems with higher temperatures (Lande, 1971, naturforvaltning, 2007). Further research into semi-enclosed bays with these cold deep-water basins to map the species diversity and distribution is recommended, and the development of a system of characterization for semi-enclosed basins based on variables such as water exchange limitations, freshwater input and depth, temperature and oxygen content is recommended.

4.1 Description of biology versus depth gradient

The ROV-RGB was used to record macrofaunal species as function of depth gradient. Previously the use of underwater cameras to map benthic habitats and make estimates of biodiversity has been used for projects either by sinking a camera rig to the seafloor (Smith and Rumohr, 2005) pulling the camera-system on a rig, by SCUBA (Parry et al., 2003), or by attaching to underwater platforms (like ROVs and AUVs) (Amon et al., 2016, Conti et al., 2019, Marnor, 2022). Depending on the resolution of the camera and the distance from the seafloor these cameras can effectively record macrofaunal species residing on- and partially hidden by the sediments (Parry et al., 2003). Using underwater cameras to survey the seafloor eliminates disturbance of the sediments, but the tradeoff is the loss of sampling of burying organisms that are not visible or hard to estimate with cameras (Parry et al., 2003). Some organisms can be predicted based on the size and shape of hills and pits left in the soft sediment, or by siphon opening (Parry et al., 2003).

As shown in figure 3.12 (Ch. 3.6 Habitat description), some general trends at different depths were found during RGB video analysis. *Ascophyllum nodosum* was the prominent species in Karihavet at 0 m during low tide, with regions from 0 m to 5 m containing a cover of turf algae. The sediments here were a mix of gravel, sand and larger rocks. Both in November 2021 and March 2022 the region from 0 – 15 meters contained high densities of particles reducing visibility at these depths.

There was a change in coralline algae coverage and distribution at different depths, where coralline algae close to the surface (5-15 m) would occur in low to medium coverage patches, usually on the underside of rocks where it was shadowed from direct sunlight. The low coverage of coralline algae at this depth in comparison at deeper regions could be due to reduced salinity because of freshwater runoff. This is also supported by the turf algae observed at 0-5 m and the absence of kelp species. The surface of the rocks from 5-10 meters were covered by high densities of *G. prolifera* and calcareous

tubeworms. The coralline algae at this depth will be exposed to higher light intensity and longer wavelengths than at deeper depths, where longer wavelengths are attenuated. The low coverage of coralline algae in this region, especially in the region 10-15 meters could also be due to grazing from sea urchins, or due to competition for substrate with calcareous tubeworms, bryozoans and tunicates. The coverage of coralline algae increases to high coverage from 15 m down to the bottom of the wall, at 30 m. In this region most of the wall is covered in organisms like coralline algae, *B. balanus*, calcareous tubeworms and anemones with small regions covered in a thin layer of sediments indicating high productivity of phyto- and zooplankton at 25-30 m depth providing high biomass for benthic plankton filter-feeders. Along the vertical walls were small shelf-like structures containing softer sediments like sand with shell parts and soft sediment organisms such as brittlestars *Ophiura* sp. and burrowing polychaetes. *Ophiura* sp. was also observed on regions of the wall where thin layers of sediments were settling during fieldwork in March 2022.

A high-density scallop bed mainly dominated by *C. islandica* was observed at 25-30 meters at Nastadholmen, and single clams were observed on- and below the bedrock wall in Faksvågen. *Chlamys islandica* and *A. opercularis*, which are challenging to differentiate from video-footage due to being morphologically similar with similar habitats. The scallop shells were densely populated by epifaunal species of sponges, hydrozoa and bryozoans making it impossible to count radial stripes on the shells. By comparing high-resolution images from Nils Aukan with video footage from the ROV the species were distinguished by size, shape, and connection to the sediment. At 25 meters at Nastadholmen (low sloping angle) soft sediments (sand, gravel, and interspersed rocks) replaced the vertical wall, and there is a clear change in species composition. In this gradient, *Hormathia* spp. were observed on the bedrock wall, on gastropods *B. undatum* and *N. despecta*, and on rocks in the soft sediments. Both *H. nodosa* and *H. digitata* have previously been observed in Karihavet and are morphologically similar making it challenging to distinguish the species (Gulliksen and Svensen, 2004). *Hormathia* spp. were also observed in Faksvågen, but only attached to bedrock walls. Species burrowing within the soft sediments were not recorded as these were not visible to the ROV-RGB. The polychaete *Oxydromus flexuosus* were observed from 27 – 35 meters. This species of polychaete are carnivorous and eats small prey organisms off the sediments (Oug, 1980). *Ctenodiscus crispatus* was observed in the same region as *O. flexuosus* and was hard to identify due to being partially covered by sediments. Sea stars and sea urchins were observed using ROV-RGB, ROV-UHI and by SCUBA-specimens collected, in contrast to benthic life of similar habitats in the Barents Sea where large and long-lived predators within these taxas are absent (Gulliksen et al., 2009).

The reason for choosing a depth gradient was the use of Blueye's internal depth sensors to place specimens along a gradient with high accuracy (± 0.01 m). Since the ROV did not produce georeferenced data such as longitude and latitude, highest quality data by driving straight forward following an accurate heading combined with the variation in depth was preferred.

Temperature and salinity in Karihavet

The CTD measurements done in November 2021 and March 2022 showed a distinct layer of permanently cold water (<6 °C) at 30 meters depth and below. In November a thermocline was visible at 15 meters depth where warmer water masses (10 °C) were residing between the deep-water and the top layer. Surface waters (0-10 m) in this period had a temperature of 7.5 °C with a salinity of 29-30 (PSU). In March the following year the salinity in the surface waters was similar to the measurements done the previous year, but the temperatures were reduced to 4.5 – 5.3 °C. Salinity in November 2021 increased with depth and had a sharp increase at 10-20 meters where it leveled off at 20 meters with salinity levels of 32.5. In March the salinity levels increased with depth and had a less strong increase from 31.5 to 32.5 at 25 meters. The salinity measured in March 2022 was stable at 32.5 from 30 meters to 70 meters depth. The surface water in November was exposed to low air temperatures, while water masses at 10-20 meters were exchanged waters with the warmer fjord basin. The change in pycnocline from 20 to 30 meters from November to March indicates mixing of these upper water masses through the winter.

Observed *C. islandica* at 24 – 31m which is a cold water species, and together with CTD measurements and the observation of cold water species at 25 m depth it is predicted the temperature and salinity stays within range that *C. islandica* can tolerate. A similar cold-water system is also found in west Spitzbergen, in Billefjorden, where sill depth is at 40 m depth (constant temperature -1.8 °C), and all Atlantic-derived water is staying at surface levels 0-40 m depth. Typically, high biomass of polar cod is found in the cold-water masses in Billefjorden (Johnsen et al., 2020a).

Underwater hyperspectral imaging

It was possible to distinguish from sediment classes enabling the use of bioclastic sediment classification for quantification of high production in an area. The UHI was able to classify OOI in a transect in classes in benthic taxa based on their optical fingerprints we could estimate coverage of each class. SAM-classification identified less pixels as rocks and more pixels as soft sediments and bioclastic sediments, and provided an overall more accurate classification. SAM-classification also had a lower percentage coverage of organism groups. Using SVM-classification a higher percentage of the pixels (ca. 1% or ca. 960 pixels) were categorized as coralline algae, sea stars and brown algae. These pixels were pixels that the SAM-classification classified as mainly soft sediments and bioclastic sediments. 65-72 % of the pixels were classified as soft sediments, 3-8 % were classified as bioclastic sediments and 12-23% were classified as rocks. 3.0-4.1 % were classified as coralline algae, and 2.6-4.0% were classified as sea stars, while 1.5 -2.2 % were classified as brown algae. Bioclastic sediments were typically white shell due to containing calcareous material and were distinguished from other sediment types by having higher reflectance (λ). Coverage of bioclastic sediments strongly indicated this habitat is a productive area with high occurrences of filter feeding bivalves, mollusks, and calcareous tubeworms feeding on plankton in the water masses.

It was observed a dip (clear decrease in intensity at certain wavelengths) in intensity in spectral reflectance (λ) of OOI measurements *in-situ* and *in-vivo* at approximately 650 and 675 nm (see Figure 3.2 for rocks and soft sediment, and Table 3.6, for *C. islandica*, *M. modiolus*, *B. undatum* and *N. despecta*). This indicates epigrowth of photosynthetic algae on the shells of the organisms and on the sediments (Summers et al., 2022).

UHI has successfully been used previously to map high spatial coverage of different habitats like shallow benthic habitats (Mogstad et al., 2019), eelgrass (*Zostera* sp.)-meadows (Bjerkvoll, 2022, Sjøreng, 2022), kelp forests (Summers et al., 2022), deep sea benthic habitats (Dumke et al., 2018),

cold-water coral reefs (Mogstad et al., 2022) and has also been used for mapping of underwater archeological sites (Mogstad et al., 2020). Technical difficulties involving the altimeter of the ROV-UHI during fieldwork in November 2021 resulted in transects being recorded across varying distances from the seafloor. Areas of the transect with greater distance from the seafloor had a higher spatial coverage but had lower spatial resolution and were affected by more water attenuation resulting in lower signature intensity (low spectral to noise ratio). The transect was split into sub-transects where regions with optimal distance from the seafloor (ca. 1 m) were used. This resulted in a smaller portion of the seafloor was surveyed than initially planned due to manually correcting for altitude above the seafloor is challenging and reducing the quality of the data. Results from the sub-transect of 2.3 meters does not cover patch dynamics of biodiversity and species occurrence that a full transect of <30 m length is able to cover. This could result in an assumption of high productivity in this entire area but could only be relevant for specific patches within this habitat.

Underwater photogrammetry

By using ROV-RGB footage to create three-dimensional maps of the survey area it was possible to make estimations of size of organisms without the use of lasers, observe changes across the depth gradient across a continuous map and observe micro-habitats in three-dimensional structures. UPG has not been used for a lot of biological surveying. It is a relatively new method in underwater research and has been combined with SCUBA as handheld cameras (Capra et al., 2015, Capra et al., 2017, Piazza et al., 2018) and similar ROV and AUV setups (Price et al., 2019). Studies have done using multicamera imaging of sediments and marine-archaeological sites previously with success (Diamanti et al., 2021, Mogstad et al., 2020), and has been used for mapping of coral reefs using industrial-grade ROVs (Price et al., 2019). Newer research shows trials on combination of camera systems collecting RGB images and combining this with *in-situ* fluorescence (Rossi et al., 2022), and used for annual monitoring of change in tropical coral reefs (Nocerino et al., 2019). The use of UPG fits best in sites with rugged sediments and good lighting conditions to observe these habitats. This is shown in the models where 3D structures such as clams, anemones and sea urchins could be represented in the model itself not just the texture as colors (demonstrated in Appendix 3). These structures could also be measured giving a relative scale to other objects in the model.

Organisms measured in the lab were found to be of smaller size than organisms measured in the UPG models. The average length of *C. islandica* specimens collected from Karihavet measured in the lab was 7.9 cm in length and 7.4 cm in width, and average (for scallops) from the model were 10.1 ± 0.5 cm in length and 9.3 ± 0.5 cm in width. In comparison the biggest specimen length of *C. islandica* measured in the lab was 9.4 cm, which is close to the average length obtained in the measurements from the UPG models. Many factors can affect measurements done in the UPG models, some of these are the technique of the person doing the measurements, and the orientation of the object in the transect. Objects that were well-visible from the FOV of the ROV were selected for the measurements, but with 3D objects such as clams and sea urchins the measurements were experienced to be more challenging when parts of the objects being obscured or in shadows. In the case of *C. islandica* and *M. modiolus* measurements, it was challenging to identify “start” and “end” of the measurement, and the measurements are done in digital 3D space compared to using a physical ruler used in the physical samples. Measurements could also be affected by the grade of overlap throughout the transect due to manual operation resulting in variation of ROV speed and distance over the seafloor. This could be solved by driving partially autonomously like with the ROV-UHI, but this requires sensors such as altimeters and technology capable of adjusting to avoid obstacles.

By using synchronized multicamera systems higher reconstruction accuracy could be obtained. Using stereo-GoPro cameras mounted on top of the ROVs made it possible to collect stereo-footage, but the

quality of these videos was of lower spatial resolution than the ROVs internal camera system. Due to the difference in placement, the stereo-camera had less of its FOV illuminated by the ROVs artificial light system. This also meant the collected calibration footage was less than optimal for the stereo camera reducing camera parameter calibration quality and reconstruction accuracy for these cameras. The models presented in this thesis used the internal ROVs camera.

Shannon-Wiener biodiversity index

Shannon-Wiener biodiversity index was calculated on 60 x 60 cm squares measured in the UPG models, and the highest diversity index was found at 20 meters depth hard sediment vs. 14 meters depth hard sediment. Evenness was the highest in the square from 34 meters depth, followed by the square at 20 meters depth. Both SW-squares on the bedrock wall (14 m and 20 m depth) were dominated by calcareous tubeworms, but several different species were observed to compete for substrate at 20 meters depth and it was observed a generally higher density of filter-feeding organisms. Diversity at 34 meters depth likely had an underestimate of species as most macrofauna reside within the sediment at this depth. For biodiversity surveying, there is likely an underestimate of OOI due to poor spatial image resolution, difficulty identifying fauna from images, and the presence of cryptic species (Amon et al., 2016). This was experienced at both 14- and 20 meters depth where it was challenging to distinguish between individuals of calcareous tubeworms and bryozoans.

Use and optimization of camera systems

UHI enables collection of high-resolution spectral data to identify and classify species groups in big datasets based on smaller manually classified regions of interest. This enables mapping of big distances without the use of manual time-consuming analysis. Platforms can be customized to fit a study design based on what biological information is needed. These methods give a variation of biological information that can be used for different purposes. The use of remotely operated vehicles enables a new approach of surveying the seafloor with no risk on human operators lives.

UPG was found to be able to perform high quality reconstructions of the benthic habitats in shape and texture (Price et al., 2019). This method gives multiscale models and heightens our understanding for the seabed and performs well in seafloor with irregular or dramatic 3D structures that might be challenging for other methods. Information contained in the models could be visualized as orthomosaics and depth elevation maps to observe the 3D shapes of the seafloor. This information could assist in contextualizing the biodiversity observed in the transect and contribute with additional insight to the habitats. The models themselves can be used for visual purposes or quantitative analysis. Shannon-Wiener index can be used to estimate biodiversity and by counting in models compromised of several continuous images the risk of recounting the same specimen across images are eliminated. By adding georeferenced data, it is possible to obtain a more accurate reconstruction in scale and possibly reducing degree of manual processing. During processing of the models in this data several features in Agisoft software were tried to experiment with the extraction of biological data from the model. One of these were the use of color classes to classify pixels with similar color in the texture. This is like the features that can be extracted from hyperspectral imaging but is restricted to the wavelengths sampled by the RGB camera. Sorting based only on RGB-bands restricts the quality of the sorting, but photogrammetry is also possible with multi spectral imaging which was not attempted in this thesis. Rugosity measurements can be done *in-situ* by methods such as the chain-draping technique (Friedman et al., 2012), but similar measurements can be obtained in the UPG model by using polylines, potentially allowing for calculation of rugosity from underwater photogrammetry.

Further processing of the models can be done with third-party programs such as GIS. This information can then be combined with information from several different platforms and sensors. Observation from cross-platform and sensors combined into one enables their observation of patterns that had previously required analysis across datasets. One example of this is the combination of UPG models together with MBE models or UHI models of the same area enabling classification of sediment- and habitat types. On top of this additional data from environmental sensors can be added such as CTD-data.

Use of optical methods can be valuable for survey of smaller areas relative to the range of acoustic sampling. Acoustic sampling can be performed from greater distances from the subject and still get high quality results. With underwater imaging the distance from the subject is restricted by the light attenuation of the water masses. Acoustic sampling can cover areas of km² but cannot detect and identify OOI. In contrast, optical sampling, especially UHI, and can be used to identify and map OOI at high spatial resolution, but areal coverage is lower than 1 km² (Mogstad et al., 2022). Regions of interest detected by acoustic methods can subsequently be visited by optical sensor-carrying platforms to obtain a higher spatial resolution overview of the region.

A combination of challenging terrain and technical difficulties during fieldwork in November 2021 enabled the choice of exploration of another method (UPG) during the fieldwork in March 2022 due to the ROV-UHI being challenging to maneuver in complex 3D area. This resulted in many variations of platforms and sensors being used for mapping benthic habitats with high variation in 3D-dimensionality. In Table 4.1 an attempt at comparing the methods based on qualities such as availability in cost and technology knowledge, the quantity of data collected, the spatial coverage of this data as well as the time consumption in collection- and analysis of the data was used.

Table 4.1 Overview of estimated relative pros- and cons of methods used in this thesis. The given values are based on collected data from fieldwork and post-processing of data. GT = Ground truth (SCUBA), RGB = Red, green & blue, UHI = Underwater hyperspectral imaging, UPG = Underwater photogrammetry.

Method	Method availability	Quantity of data	Spatial coverage	Time consumption of post-processing
GT	High	Low	No	<5 hrs
Spectrometer	Low-medium	Low	No	<5 hrs
RGB-video analysis	Medium	High	Yes	+ 24 hrs
360-video analysis	Medium	Medium	Yes	+ 24 hrs
UHI	Low	Medium	Yes	+ 48 hrs
UPG	Low	High	Yes	+ 48 hrs

Utilizing mini-ROVs combined with optical sensors for benthic habitat mapping could be a nice entry level method or could be used more extensively with more industrial grade equipment. By using acoustic mapping equipment it's possible to return to an area for annual mappings making it highly relevant for annual environmental monitoring studies. Using the Blueye ROV for mapping the bedrock vertical wall was applicable and easily executable in comparison to industry-grade ROV platforms often requiring several operators. A student gets hands-on experience with the equipment and feeling of ownership over research.

Measurement of size of OOI was done in Agisoft and is the first step towards measuring of absolute (true) sizes. These measurements are accurate in relativity to each other, but the accuracy of the measurements compared to true size is not as accurate due to not having a reference point for scale throughout the entire transect, combined with no positioning data for latitude and longitude positions. With a measure of scale (e.g., two-point laser) it is possible to estimate the size of objects, and the width of the transect to ensure applicable scale points throughout the transect. The ROVs did at the time of sampling not feature a positioning system to supply georeferenced navigational data. Positioning sensors enables the revisiting of the same transect, which in turn enables environmental monitoring over time.

By combining several methods of mapping the benthic habitats to construct photomosaics and seascape maps it is possible to detect patterns and variations across different parameters and levels of remote sensing. In comparison with more traditional methods of benthic habitat mapping this gives more insight to the habitats as well as a bigger overview of gradients and patterns without intruding on their habitats and destroying the sample area. This allows for revisits over time and opens for a more controlled and specific monitoring of changes in marine benthic habitats due to human activity either directly or indirectly caused by our activity.

The 360-camera can record the area around ROV as we operate and gives us a new insight due to its high FOV. Light limitation is a challenge for observation; illumination evenness, area coverage, ambient vs artificial lighting, color composition greatly affects image quality. The 360-camera's high FOV contributes a new perspective to the mission and gives broader covering of our interaction with the environment when operating the ROV's. This enables the capture of more data. 360-cameras used for scouting missions prior to planning out trajectories can help with mapping of OOI for UPG or UHI missions.

The hyperspectral imager can capture the full $R(\lambda)$ of the sea floor in each image pixel. This gives information that can be used for calculating coverage of a specific organism and determine the ratios of and illustrate the distribution of species across the gradient. Used for mapping habitats and gives us a lot of information just from a single transect using RGB cameras. This level of mapping gives us a high level of insight into the benthic habitats and the biodiversity as well as their distribution and patterns. With the hyperspectral imager it is also possible to revisit the same site if we have the coordinates by using acoustic sensors. This makes hyperspectral imaging a good sampling method for annual environmental monitoring.

There was a great increase in model quality throughout the thesis work from November 2021 (Figure 3.4) until finished models in 2022 (Figure 3.5-3.10) due to continuous optimization based on trial and errors. In November 2021 no study design was planned for UPG, resulting in less-than optimal sampling methods with the Blueye Pioneer. As processing was done on the data it was found the data lacked some prerequisites for UPG. This data was used for trials and optimization to prepare for new fieldwork in March 2022. This data proved valuable as a source of information for further optimization and study design to further assess the use of UPG for benthic spatial mapping.

4.2 Camera factors affecting UPG result

It was found that the Blueye ROVs internal camera was able to perform alignment of images, even when cameras remained uncalibrated. To conduct photogrammetric methods the calibration of internal and external camera parameters (camera-specific residuals affecting image distortion) is important to obtain an accurate model (Diamanti et al., 2021). Through trial and errors when working with different cameras it was found the stereo-GoPro did not perform as well as the Blueye internal camera for alignment of UPG. One challenge was that the stereo camera was mounted on top of the ROV and had less of its FOV illuminated by the light of the ROV. The operator also views the OOI from the internal ROV camera, which is positioned further down (approximately 15 cm) on the ROV, and therefore footage that looks good on from the ROVs camera FOV does not necessarily look good from the stereo camera's FOV. The stereo camera therefore had weak footage when collecting data for camera calibration. Increasing the number of squares on the checkerboard-reference plate could solve this issue but was not possible for the timespan of this thesis. The calibration dataset should be collected through viewpoints from all directions where the perimeter of the reference is viewable (perimetrically oblique viewpoints, Diamanti et al., 2021).

The cause of the Blueye ROVs internal camera alignment performing well in alignment without camera calibration could be due to the Blueye camera lenses having less geometrical distortion than the GoPro cameras and the known exterior orientation values (from the IMU) aligning well and strengthening the alignment. To boost alignment one can, add a form of GT like ground control points, or conduct UPG on shorter trajectories with overlapping cross-trajectories. These are methods of increasing the robustness of the image geometry and assist in alignment of these stereo camera images.

4.3 Study design

When utilizing technology to provide biological information the study design depicts the ideal study site and mission. Biology is full of variation and non-ideal cases the challenges technology's skill at adaptation. During the fieldwork completed during this thesis this was experienced first-hand with challenges such as topography, hydrography, weather, and technological setbacks. Optimisation of methods for the given sampling area was needed to obtain high quality data. The learning curve was steep with lots of opportunities to improve.

UPG can be used to collect data on 3D surfaces and can be highly valuable for research on habitats with high rugosity affecting spatial distribution of organisms. Due to the high processing time required for constructing 3D models and the need for resources such as the ROV and ROV pilot, the use of UPG falls short in time to analysis of simple video-footage for flat surfaces. UHI on the other hand could be used to survey flat vertical surfaces and estimate coverage of different species. A combination of UHI and UPG could enable the recognition of patterns previously undetected by imaging-systems.

Habitat morphology will affect what data is collected by partially- to completely obscuring certain regions of the habitat, like cracks in walls, the underside of rocks or objects obscuring the view behind. In some of these cases, the "full picture" can only be acquired by physical sampling e.g., by SCUBA-diving.

4.4 Future prospect

The use of mini-ROVs reduces the threshold for utilization of marine technology and newer sampling methods. Smaller ROVs are relatively cheaper than their industrial-grade counterparts and has lower requirements in deployment and operation. Smaller ROVs can also access sites too challenging for bigger ROVs, like shallow habitats or portions with overhanging walls. This opens for new uses of ROVs in research and increases the method's availability. By combining mini-ROVs with open-source programs the economical requirements can be further reduced, with similar results being obtainable for analysis and visualization.

UHI has been used for several field missions proving its usefulness in benthic habitat mapping. UHI can also be used for several other approaches in mapping, and the use of mini-ROVs enables the use of UHI in shallow-habitat mapping.

UPG is a relatively new method for biological research. The biggest disadvantage of this method is the need for scale-references in the transect to get scaled models, and the high number of cameras needed for stereo imaging requires large platforms. Using optical methods enables capture of the variation in macrofaunal- as well as algal distribution across the sediment across varying depth and 3D structure that e.g., acoustics are not able to capture. Further work from this thesis would be testing the accuracy of scale obtained from single-camera imaging for UPG, and development of setups of multicamera systems for mini-ROVs conducting UPG.



This QR-code when scanned will lead you to the 3D model uploaded to Sketchfab of the habitat shown in Figure 3.9. The figure shows the scallop bed at Nastadholmen at 26-30 m depth. This gives the reader the opportunity to maneuver through the habitat and give further insight to underwater photogrammetry models. Also accessed through this link: <https://skfb.ly/oBzuO>, or by searching "Malne C3_UPG" in Sketchfab.

5. Conclusion

ROV-RGB video footage was able to record macrofaunal species across varying substrates ranging from flat soft sediment to vertical walls. Use of ROVs was a good platform for acquiring biological data often missing from crude high spatial scale acoustics, but also go into detail close to that of physical sampling.

UHI is more dependent on flat surfaces to acquire data and has a smaller niche than RGB video footage but performs well in classification of objects and interests and estimation of coverage. For statistics, UHI have many possibilities yet to be used (Johnsen et al., 2020b, Mogstad et al., 2022).

UPG is a new tool in benthic habitat mapping and was found to perform well in alignment and construction of orthomosaics to visualize video transects as continuous scaled maps. Further work could be done on the optimization of mini-ROV with payload sensors to better assess- and increase reconstruction accuracy. For habitats of high rugosity affecting distribution of species this method could be used to gain new knowledge into distribution patterns related to rugosity and 3 dimensionality.

Biology is a mosaic of variation, and not all habitats are “textbook-cases”. Use of optical methods covering high resolution spatial scale while still capturing biological information enables the observation of these mosaics of variations within sediment classes. On the other hand, the variety in habitats requires different optimizations of platform and payload sensors. Enabling technology optimizes for the desired biological data.

Cold-water species living along the Norwegian coast in areas such as Karihavet inhabits a narrow niche of deep (>25 m depth) cold water (<7 °C) habitats and may be exposed to reduced inhabitability of these habitats with time due to climate change causing temperature increase, human destructions of habitats and change in hydrography due to land rising and sills being closed off. Cold-water species such as *C. islandica* was found attached to rocks and bedrock wall at 24-31 meters depth. CTD measurements from Karihavet show the thermocline being as shallow as 20 m in November, allowing for *C. islandica* to survive at 24 meters. More CTD measurements during the summer would give insight if the temperature at these depths exceeds the measured 10 °C (measured at 15 m depth) and potentially decrease health in *C. islandica*.

References

References are given in Harvard citation style.

- AGISOFT 2022. Agisoft Metashape Professional Edition, User Manual (PDF). 1.6.4 ed.
- AMON, D. J., ZIEGLER, A. F., DAHLGREN, T. G., GLOVER, A. G., GOINEAU, A., GOODAY, A. J., WIKLUND, H. & SMITH, C. R. 2016. Insights into the abundance and diversity of abyssal megafauna in a polymetallic-nodule region in the eastern Clarion-Clipperton Zone. *Sci Rep*, 6, 30492-30492.
- AUKAN, N. 2021-2022. *RE: Photography and information on Karihavet bay, manuscript (unpublished) and personal communication.*
- AURE, J. & STIGEBRANDT, A. 1989. Fiskeoppdrett i fjorder. En konsekvensanalyse av miljøbelastning for 30 fjorder i Møre og Romsdal. *Temarapport 3. II. Næringsavdelinga, Møre og Romsdal Fylkeskommune: Havforskningsinstituttet, Rapport nr. FO 8803.*
- BERGE, J. & JOHNSEN, G. 2020. Life and Light at the Dead of Night. In: BERGE, J., JOHNSEN, G. & COHEN, J. H. (eds.) *Polar Night Marine Ecology*. Switzerland: Springer Nature.
- BJERKVOLL, M. 2022. *Aerial & Underwater Hyperspectral Imagery For Shallow Benthic Nature Type Mapping*. MSc thesis in biology, NTNU.
- BLAINVILLE, H. M. D. D. 1824. Mollusques, Mollusca (Malacoz.), pp. 1-392. In: Dictionnaire des Sciences Naturelles (F. Cuvier, ed.), vol. 32. Levrault, Strasbourg et Paris, & Le Normant, Paris.
- BLUEYE. 2022. *Blueye ROVs* [Online]. Available: blueye.no [Accessed 11.02.2022].
- BRAKSTAD, E., STRAUMSNES, B. & TINGVOLL, S. 1970. *Bygdehistorie for Tingvoll og Straumsnes : 1, Tingvoll, Bygdeboknemnda.*
- BRAKSTAD, E., STRAUMSNES, B. & TINGVOLL, S. 1975. *Bygdehistorie for Tingvoll og Straumsnes : 2, Tingvoll, Bygdeboknemnda.*
- BRUN, P. F. 1982. Forurensningsovervaking av fjordområde i Møre og Romsdal 1980-81. Rapport,. Fylkesmannen i Møre og Romsdal.
- BRUN, P. F. 1986. Overvaking av fjordar og vassdrag i Møre og Romsdal 1983 - 1985. Rapport nr. 7. Fylkesmannen i Møre og Romsdal.
- BRUZELIUS, N. 1805. *Dissertatio sistens species cognitae asteriarum, quamr. sub praesidio A.J. Retzii. exhibit N. Bruzelius. 1-37. Lundae (formerly know as Retzius, R.J.).*
- BUHL-MORTENSEN, L., AURE, J., ALVE, E., HUSUM, K. & OUG, E. 2006. Effekter av oksygensvikt på fjordfauna: Bunnfauna og miljø i fjorder på Skagerrakysten. *Fisken og havet*, nr. 3, 0-108.
- CAPRA, A., CASTAGNETTI, C., DUBBINI, M., GRUEN, A., GUO, T., MANCINI, F., NEYER, F., ROSSI, P. & TROYER, M. 2017. High Accuracy Underwater Photogrammetric Surveying. *Journal Name: 3rd IMEKO International Conference on Metrology for Archeology and Cultural Heritage*, Medium: X.
- CAPRA, A., DUBBINI, M., BERTACCHINI, E., CASTAGNETTI, C. & MANCINI, F. 2015. 3D reconstruction of an underwater archaeological site: Comparison between low cost cameras. *International Archives of the Photogrammetry, Remote Sensing and Spatial Information Sciences - ISPRS Archives*, 40, 67-72.
- CONTI, L. A., LIM, A. & WHEELER, A. J. 2019. High resolution mapping of a cold water coral mound. *Sci Rep*, 9, 1016-1016.
- DELLE CHIAJE, S. 1827. *[POLYCHAETA context. Vol.2] Memorie sulla storia e notomia degli animali senza vertebre del Regno di Napoli: Volume 2., Napoli, Stamperia delle Societa Tipografica.*
- DIAMANTI, E., LØVÅS, H., LARSEN, M. K. & ØDEGÅRD, Ø. 2021. A multi-camera system for the integrated documentation of Underwater Cultural Heritage of high structural complexity; The case study of M/S Helma wreck. *54 (16)*, 422-429.
- DUMKE, I., PURSER, A., MARCON, Y., NORNES, S. M., JOHNSEN, G., LUDVIGSEN, M. & SØREIDE, F. 2018. Underwater hyperspectral imaging as an in situ taxonomic tool for deep-sea megafauna. *Sci Rep*, 8, 12860-11.

- EHRENBERG, C. G. 1834. Beiträge zur physiologischen Kenntniss der Corallenthiere im allgemeinen, und besonders des rothen Meeres, nebst einem Versuche zur physiologischen Systematik derselben. *Abhandlungen der Königlichen Akademie der Wissenschaften, Berlin*, 1, 225-380.
- EKMAN, S. 1953. *Zoogeography of The Sea*, Sidgwick & Jackson.
- ELEFTHERIOU, A. & MOORE, D. C. 2005. Macrofauna Techniques. Chapter 5. 160-228. In: ELEFTHERIOU, A., MCINTYRE, ALASDAIR (ed.) *Methods for the study of marine benthos*. Oxford: Blackwell Publishing Company.
- FABRICIUS, J. C. 1779. *Reise nach Norwegen mit Bemerkungen aus der Naturhistorie und Oekonomie*, Hamburg, Carl Ernst Bohn.
- FABRICIUS, J. C. 1793. *Entomologia Systematica Emendata et Aucta. Secundum Classes, Ordines, Genera, Species Adjectis Synonymis, Locis, Observationibus, Descriptionibus. Christ. Gottl. Proft., Hafniae*.
- FRIEDMAN, A., PIZARRO, O., WILLIAMS, S. B. & JOHNSON-ROBERSON, M. 2012. Multi-Scale Measures of Rugosity, Slope and Aspect from Benthic Stereo Image Reconstructions. *PLoS one*, 7, e50440.
- GOSSE, P. H. 1859. Characters and descriptions of some new British sea-anemones. *Annals and Magazine of Natural History*, 46-50.
- GRANT, R. E. 1836. *Animal Kingdom*. In: Volume 1, 813.
- GULLIKSEN, B., HOP, H. & NILSEN, M. 2009. Benthic life. Chapter 15, 339-372. In: SAKSHAUG, E., JOHNSEN, G. & KOVACS, K. (eds.) *Ecosystem Barents Sea*. Trondheim, Norway: Tapir Academic Press.
- GULLIKSEN, B. & SVENSEN, E. 2004. *Svalbard og dyreliv i polare hav*, Kristiansund, Kom forlag.
- HANSEN, J. P., WIKSTRÖM, S. A. & KAUTSKY, L. 2008. Effects of water exchange and vegetation on the macroinvertebrate fauna composition of shallow land-uplift bays in the Baltic Sea. *Estuarine, coastal and shelf science*, 77, 535-547.
- HOLSETH, K. 2022. Dette skipet kan "håndplukke" fangsten fra havbunnen. *Gemini.no*, 22.11.2022.
- HSU, C.-W., CHANG, C.-C. & LIN, C.-J. 2003. A Practical Guide to Support Vector Classification, Last updated: May 19, 2016. Available: <http://www.csie.ntu.edu.tw/~cjlin/papers/guide/guide.pdf>.
- IHERING, H. V. 1876. Versuch eines natürlichen Systemes der Mollusken. *Jahrbucher d. Deutschen Malakozoologischen Gesellschaft*, 3, 97-148.
- J. L. GARRETT, S. BAKKEN, E. F. PRENTICE, D. LANGER, F. S. LEIRA, E. HONORE-LIVERMORE, R. BIRKELAND, M. E. GRØTTE, T. A. JOHANSEN & ORLANDIC, M. 2021. Hyperspectral Image Processing Pipelines on Multiple Platforms for Coordinated Oceanographic Observation. *11th Workshop on Hyperspectral Imaging and Signal Processing: Evolution in Remote Sensing (WHISPERS)*. Center for Autonomous Marine Operations and Systems.
- JOHANSEN, T. A. 2022. HYPISO-1 hyperspectral imaging satellite - Forslag til permanent nasjonal forskningsinfrastruktur - småsatelitter til nytte for havrommet. *Rapport fra arbeidsgruppe med NTNU, FFI og Andøya Space, i dialog med Norsk Romsenter*. Center for Autonomous Marine Operations and Systems (AMOS): NTNU, Trondheim.
- JOHNSEN, G., LEU, E. & GRADINGER, R. 2020a. Marine Micro- and Macroalgae in the Polar Night. Chapter 4, 67-112. In: BERGE, J., JOHNSEN, G. & COHEN, J. H. (eds.) *POLAR NIGHT Marine Ecology : Life and Light in the Dead of Night*. Cham: Springer International Publishing : Imprint: Springer.
- JOHNSEN, G., MOGSTAD, A. A., BERGE, J. & COHEN, J. H. 2020b. Operative Habitat Mapping and Monitoring in the Polar Night. Chapter 10, 277-306. In: BERGE, J., JOHNSEN, G. & COHEN, J. H. (eds.) *POLAR NIGHT Marine Ecology : Life and Light in the Dead of Night*. Cham, Switzerland: Springer International Publishing : Imprint: Springer.
- JOHNSEN, G., VOLANT, Z., DIERSSEN, H., PETTERSEN, R., ARDELAN, M. V., SØREIDE, F., FEARN, P., LUDVIGSEN, M. L. & MOLINE, M. 2013. Underwater hyperspectral imagery to create

- biogeochemical maps of seafloor properties. Chapter 20, 508-535. In: [EDS] WATSON, J. A. Z., O. (ed.) in: *Subsea optics and imaging*. Cambridge, UK: Woodhead Publishing Ltd.
- JONASSON, J. P., THORARINSDOTTIR, G. G., EIRIKSSON, H. & MARTEINSDOTTIR, G. 2004. Temperature tolerance of Iceland scallop, *Chlamys islandica* (O.F. Muller) under controlled experimental conditions. *Aquaculture research*, 35, 1405-1414.
- KRÖYER, H. 1856. *Afhandling om Ormeslaegten Sabella Linn., isaer med Hensyn til dens nordiske Arter [Alternate title: Bidrag til Kundskab af Sabellerne]*, Oversigt over det Kongelige danske Videnskabernes Selskabs Forhandling.
- LAMARCK, J. B. 1801. *Système des animaux sans vertèbres, ou tableau général des classes, des ordres et des genres de ces animaux; Présentant leurs caractères essentiels et leur distribution, d'après la considération de leurs rapports naturels et de leur organisation, et suivant l'arrangement établi dans les galeries du Muséum d'Histoire Naturelle, parmi leurs dépouilles conservées; Précédé du discours d'ouverture du Cours de Zoologie, donné dans le Muséum National d'Histoire Naturelle l'an 8 de la République*, Published by the author and Deterville.
- LAMARCK, J. B. M. D. 1816. *Histoire naturelle des animaux sans vertèbres, Tome troisième [in full: Histoire naturelle des animaux sans vertèbres présentant les caractères généraux et particuliers de ces animaux, leur distribution, leurs classes, leurs familles, leurs genres, et la citation des principales espèces qui s'y rapportent]*.
- LANDE, E. 1971. A new southern record of *Yoldia amygdalea* Valenciennes (Mollusca, Pelecypoda) in Pölen, North Trøndelag [sic]. *Skrifter (Det Kongelige norske videnskabers selskab : trykt utg.) Contribution No. 154.*, 15416-1971.
- LATREILLE, P. A. 1802. *Histoire Naturelle, Générale et Particulière des Crustacés et des Insectes*. Ouvrage Faisant suite à l'Histoire Naturelle Générale et Particulière, Composée par LeClerc de Buffon, et Rédigée par C.S. Sonnini, Membre de Plusieurs Sociétés Savantes. Dufart: Paris.
- LATREILLE, P. A. 1825. *Familles naturelles du règne animal, exposé succinctement et dans un ordre analytique avec l'indication de leurs genres*, Paris, J. B. Baillière.
- LINNAEUS, C. 1753. *Species plantarum, exhibentes plantas rite cognitatas ad genera relatas cum differentiis specificis, nominibus trivialibus, synonymis selectis, locis natalibus, secundum systema sexuale digestas*, Stockholm, Salvius.
- LINNAEUS, C. 1758. *Systema Naturae per regna tria naturae, secundum classes, ordines, genera, species, cum characteribus, differentiis, synonymis, locis*. 1: , 824.
- LINNAEUS, C. 1767. *Systema naturae per regna tria naturae: secundum classes, ordines, genera, species, cum characteribus, differentiis, synonymis, locis*, Holmiae [Stockholm], Laurentii Salvii.
- LUDVIGSEN, M., SORTLAND, B., JOHNSEN, G. & SINGH, H. 2007. Applications of Geo-Referenced Underwater Photo Mosaics in Marine Biology and Archaeology. *Oceanography (Washington, D.C.)*, 20, 140-149.
- MARGULIS, L. & SCHWARTZ, K. V. 1998. *Five Kingdoms: an illustrated guide to the Phyla of life on earth*. 3rd edition.
- MARION, P. V. 1996. Ecological studies in Hopavågen, a landlocked bay at Agdenes, Sør-Trøndelag, Norway. 31, *Gunneria* Vol. 71.
- MARNOR, C. M. 2022. *Mapping distribution patterns of brittle stars using ROV-based imaging*. Msc thesis in Biology, NTNU.
- MOEN, F. E. & SVENSEN, E. 2020. *Dyreliv i havet*, Kolofon Forlag AS.
- MOGSTAD, A. A. & JOHNSEN, G. 2017. Spectral characteristics of coralline algae: a multi-instrumental approach, with emphasis on underwater hyperspectral imaging. *Applied optics*, Vol. 56, No. 36, 19.
- MOGSTAD, A. A., JOHNSEN, G. & LUDVIGSEN, M. 2019. Shallow-Water Habitat Mapping using Underwater Hyperspectral Imaging from an Unmanned Surface Vehicle: A Pilot Study. *Remote sensing*, 11(6): 685.

- MOGSTAD, A. A., LØVÅS, H. S., STURE, Ø., JOHNSEN, G. & LUDVIGSEN, M. 2022. Remote Sensing of the Tautra Ridge: An Overview of the World's Shallowest Cold-Water Coral Reefs. *Frontiers in Marine Science*, 9, 18.
- MOGSTAD, A. A., ØDEGÅRD, Ø., NORNES, S. M., LUDVIGSEN, M., JOHNSEN, G., SØRENSEN, A. J. & BERGE, J. 2020. Mapping the historical shipwreck Figaro in the high arctic using underwater sensor-carrying robots. *Remote sensing* 12(6): 997, 997.
- MONTAGU, G. 1808. *Description of several marine animals found on the south coast of Devonshire*, Transactions of the Linnean Society of London.
- MÜLLER, O. F. 1776. *Zoologiæ Danicæ Prodromus, seu Animalium Daniæ et Norvegiæ indigenarum characteres, nomina, et synonyma imprimis popularium*, [Copenhagen]: Hallageri., Havnæ.
- NATURFORVALTNING, D. F. 2007. Kartlegging av marint biologisk mangfold. DN Håndbok 19-2001 Revidert 2007. 51.
- NOCERINO, E., NEYER, F., GRUEN, A., TROYER, M., MENNA, F., BROOKS, A., CAPRA, A., CASTAGNETTI, C. & ROSSI, P. 2019. Comparison of diver-operated underwater photogrammetric systems for coral reef monitoring. *International Archives of the Photogrammetry, Remote Sensing and Spatial Information Sciences - ISPRS Archives*, XLII-2/W10, 143-150.
- NORNES, S. M., LUDVIGSEN, M., ØDEGÅRD, Ø. & SØRENSEN, A. J. 2015. Underwater photogrammetric mapping of an intact standing steel wreck with ROV. *IFAC-PapersOnLine*, 28, 206-211.
- NORSE, E. A. & CROWDER, L. B. 2005. *Marine conservation biology : the science of maintaining the sea's biodiversity*. 2nd ed. Washington: Island Press.
- OUG, E. 1980. On feeding and behaviour of *Ophiodromus flexuosus* (Delle Chiaje) and *Nereimyra punctata* (O.F. Müller) (Polychaeta, Hesionidae). *Ophelia*, 19, 175-191.
- PARRY, D. M., KENDALL, M. A., PILGRIM, D. A. & JONES, M. B. 2003. Identification of patch structure within marine benthic landscapes using a remotely operated vehicle. *Journal of experimental marine biology and ecology*, 285, 497-511.
- PHILIPPI, R. A. 1837. *Pododesmus, ein neues Genus der Acephalen*, Archiv für Naturgeschichte.
- PIAZZA, P., CUMMINGS, V., LOHRER, D., MARINI, S., MARRIOTT, P., MENNA, F., NOCERINO, E., PEIRANO, A. & SCHIAPARELLI, S. 2018. Divers-operated underwater photogrammetry: Applications in the study of antarctic benthos. *International Archives of the Photogrammetry, Remote Sensing and Spatial Information Sciences - ISPRS Archives*, 42, 885-892.
- PRICE, D. M., ROBERT, K., CALLAWAY, A., LO LACONO, C., HALL, R. A. & HUVENNE, V. A. I. 2019. Using 3D photogrammetry from ROV video to quantify cold-water coral reef structural complexity and investigate its influence on biodiversity and community assemblage. *Coral reefs*, 38, 1007-1021.
- RAFINESQUE, C. S. 1815. *Analyse de la nature ou Tableau de l'univers et des corps organisés.*, Palermo, (self-published).
- RELLING, B. & OTNES, B. 2000. *Miljøkartleggingar i fjordar og kystfarvatn i Møre og Romsdal pr. 01.01.2000*, Molde, Fylkesmannen i Møre og Romsdal, Miljøvernavdelinga.
- RETZIUS, A. J. 1783. Anmärkningar vid. *Asteriae* genus. *Kunliga Svenska Vetenskapsakademiens handlingar*, 4, 230-248.
- ROSSI, P., RIGHI, S., PARENTE, L., CASTAGNETTI, C., CATTINI, S., DI LORO, G., FALVO, E., GRASSI, F., MANCINI, F., ROVATI, L., SIMONINI, R. & CAPRA, A. 2022. Photogrammetric and fluorescence solutions for monitoring of habitat forming organisms. *International Archives of the Photogrammetry, Remote Sensing and Spatial Information Sciences - ISPRS Archives*, Volume XLIII-B2-2022 XXIV ISPRS Congress
- SAKSHAUG, E., JOHNSEN, G., KOVACS, K. M. & PRO, M. 2009. *Ecosystem Barents Sea*, Trondheim, Tapir Academic Press.

- SARS, M. 1835. Beskrivelser og lagttagelser over nogle moerkelige eller nye i Havet ved den Bergenske Kyst levende Dyr af Polypernes, Acalephernes, Radiaternes, Annelidernes og Molluskernes classer, med en kort Oversigt over de hidtil af Forfatteren sammesteds fundne Arter og deres Forekommen. [book]. Thorstein Hallagers Forlag hos Chr. Dahl, R.S., xii + 81 pp., 15 plates.
- SHANNON, C. E. & WEAVER, W. 1949. *The mathematical theory of communication*, Urbana, University of Illinois Press.
- SMITH, C. J. & RUMOHR, H. 2005. Imaging techniques. Chapter 3, 87-111. In: ELEFThERIOU, A., MCINTYRE, ALASDAIR (ed.) *Methods for the study of marine benthos*. 3 ed. Oxford: Blackwell Publishing Company.
- SNELI, J. A. 2007. Poller og relik fauna fra istiden i Nord-Trøndelag og langs norsk vestkyst. TBS-Rapport No.1-2007. *unpublished work, Trondhjem biologiske stasjon, NTNU*.
- SØRENG, M. O. 2022. *Mapping of Zostera habitat in the Sublittoral Zone using Underwater Hyperspectral Imaging and Unmanned Surface Vehicle*. MSc thesis in Biology, NTNU.
- SØRENSEN, A. J., LUDVIGSEN, M., NORGRÉN, P., ØDEGÅRD, Ø. & COTTIER, F. 2020. Sensor-Carrying Platforms. Chapter 9, 241-276. In: BERGE, J., JOHNSEN, G. & COHEN, J. H. (eds.) *POLAR NIGHT Marine Ecology : Life and Light in the Dead of Night*. 1st 2020. ed. Cham: Springer International Publishing : Imprint: Springer.
- STANDARDIZATION, C. E. C. F. 2012. Water quality - Visual seabed surveys using remotely operated and/or towed observation gear for collection of environmental data. *BS EN 16260:2012*.
- STRØM, K. M. 1936. *Land-locked waters : hydrography and bottom deposits in badly-ventilated Nordwegian fjords with remarks upon sedimentation under anaërobic conditions*, Oslo, I kommisjon hos Dybwad.
- SUMMERS, N., JOHNSEN, G., MOGSTAD, A., LØVÅS, H., FRAGOSO, G. & BERGE, J. 2022. Underwater Hyperspectral Imaging of Arctic Macroalgal Habitats during the Polar Night Using a Novel Mini-ROV-UHI Portable System. *Remote sensing* 14(6): 1325.
- TELFORD, M. & MOOI, R. 1986. Echinoderms, Babel and the Confusion of Nomenclature. *Systematic Biology*, 35, 254-255.
- THENDRUP, A. 1991. KRIFAST. Bergsøysundet bru. Resultat fra hydrografiske målinger i 1989/90. OCEANOR rapport OCN R-91073.
- UNDERWOOD, A. J. & CHAPMAN, M. G. 2005. Design and Analysis in Benthic Surveys, Chapter 1, 1-42. In: ELEFThERIOU, A., MCINTYRE, ALASDAIR (ed.) *Methods for the study of marine benthos*. Oxford: Blackwell Publishing Company.
- WIBORG, K. F. 1963. Some observations on the Iceland scallop *Chlamys islandica* (Müller) in Norwegian waters : 1963 Fisk. Skrift., Ser. Havund., 13 (6): 38–53.
- YOUNG, G. C., DEY, S., ROGERS, A. D. & EXTON, D. 2017. Cost and time-effective method for multi-scale measures of rugosity, fractal dimension, and vector dispersion from coral reef 3D models. *PLoS One*, 12(4), 18.

Appendix

Appendix 1: Species overview from ROV video transects, samples collected by SCUBA and species measured for in-vivo spectral reflectance (λ) in the lab.

Table A1 Overview of species within morphological groups (grouped by functional groups) observed in ROV-transect video analysis, by physical samples done with SCUBA, and which of these species were measured for in-vivo spectral reflectance (λ) in the lab using the QEPro spectrometer March 2022. Observed is indicated by an “x”. Not observed indicated by “\”.

Morphogroup	Species	Author	ROV-transect	SCUBA	In-vivo reflectance
Annelida	<i>Chone infundibuliformis</i>	(Kröyer, 1856)	x	\	\
	<i>Myxicola infudibulum</i>	(Montagu, 1808)	x	\	\
	<i>Oxydromus flexuosus</i>	(Delle Chiaje, 1827)	x	\	\
	<i>Sabellidae</i> sp.	(Latreille, 1825)	x	\	\
	<i>Serpula vermicularis</i>	(Linnaeus, 1767)	x	\	\
	<i>Serpulidae</i> sp. (<i>Placostegus tridentatus</i> & <i>Spirobranchus triqueter</i>)	(Rafinesque, 1815, Fabricius, 1779, Linnaeus, 1758)	x	\	\
Bivalva	<i>Aquiptecten opercularis</i>	(Linnaeus, 1758)	x	x	\
	<i>Chlamys islandica</i>	(Müller, 1776)	x	x	x
	<i>Modiolus modiolus</i>	(Linnaeus, 1758)	x	x	x
	<i>Pecten maximus</i>	(Linnaeus, 1758)	\	x	\
Bryozoa	<i>Bryozoa</i> sp.	(Margulis and Schwartz, 1998)	x	\	\
Chordata	<i>Pododesmus</i> sp.	(Philippi, 1837)	x	\	\
Cnidaria	<i>Alcyonium digitatum</i>	(Linnaeus, 1758)	x	\	\
	<i>Ascidacea</i> sp.	(Blainville, 1824)	x	\	\
	<i>Goniactinia prolifera</i>	(Sars, 1835)	x	\	\
	<i>Hormathia</i> spp.	(Gosse, 1859)	x	x	x
	<i>Urticina</i> sp.	(Ehrenberg, 1834)	x	\	\
Crustacea	<i>Balanus balanus</i>	(Linnaeus, 1758)	x	\	\
	<i>Galathea</i> sp.	(Fabricius, 1793)	x	\	\
	<i>Paguridae</i> sp.	(Latreille, 1802)	x	\	\
Echinoderm	<i>Asteroidea</i> sp.	(Telford and Mooi, 1986)	x	\	\
	<i>Ctenodiscus crispatus</i>	(Bruzelius, 1805)	x	x	x
	<i>Ceramaster granularis</i>	(Retzius, 1783)	x	x	x
	<i>Marthasterias glacialis</i>	(Linnaeus, 1758)	x	x	\
	<i>Porania pulvillus</i>	(Müller, 1776)	x	\	\
	<i>Ophiura</i> sp.	(Lamarck, 1801)	x	x	x
	<i>Echinus esculentus</i>	(Linnaeus, 1758)	x	x	\
	<i>Gracilichinus acutus</i>	(Lamarck, 1816)	x	x	\
<i>Strongylocentrotus droebachiensis</i>	(Müller, 1776)	x	x	\	
Gastropoda	<i>Buccinum undatum</i>	(Linnaeus, 1758)	x	x	x
	<i>Neptunea despecta</i>	(Linnaeus, 1758)	x	x	x
	<i>Polyplacophora</i>	(Ihering, 1876)	x	\	\
Phaeophyceae	<i>Ascophyllum nodosum</i>	(Linnaeus, 1753)	x	\	\
Porifera	<i>Porifera</i> sp.	(Grant, 1836)	x	x	x
Rhodophyta	<i>Corallinade</i>	(Linnaeus, 1758)	x	x	x

Appendix 2: Full overview over measurements of length and width of organisms.

Table A2.1 Measured length (cm) and width (cm) of physical samples from Karihavet March 2022. Each measurement is categorized into a morpho group. Echinoderms are measured in diameter for urchins, and from center-arm for sea stars. *Ophiura* sp. are shown as disk diameter due to arms being incomplete for both specimens. The more specimens measured of each species measured contributed to a more accurate representation of mean size for the species in Karihavet. Not measured indicated by “\”.

Morphogroup	Species name	Length (cm)	Width (cm)
Bivalva	<i>Aquiptecten opercularis</i>	5.9	5.9
	<i>Chlamys islandica</i>	6.6	6.6
	<i>Chlamys islandica</i>	6.8	6.5
	<i>Chlamys islandica</i>	6.9	6.1
	<i>Chlamys islandica</i>	7.9	7.5
	<i>Chlamys islandica</i>	8.1	7.8
	<i>Chlamys islandica</i>	8.1	7.6
	<i>Chlamys islandica</i>	9.1	8.6
	<i>Chlamys islandica</i>	9.4	8.7
	<i>Modiolus modiolus</i>	10.3	4.9
	<i>Modiolus modiolus</i>	11.7	6.9
	<i>Modiolus modiolus</i>	13.0	6.8
	<i>Modiolus modiolus</i>	13.8	7.9
	<i>Modiolus modiolus</i>	14.6	6.8
	<i>Modiolus modiolus</i>	14.7	6.5
	<i>Modiolus modiolus</i>	15.7	8.0
	Cnidaria	<i>Hormatia</i> spp.	3.0
<i>Hormatia</i> spp.		3.8	\
Echinoderm	<i>Echinus acutus</i>	5.9	\
	<i>Echinus acutus</i>	7.6	\
	<i>Echinus acutus</i>	7.6	\
	<i>Strongylocentrotus droebachiensis</i>	2.8	\
	<i>Strongylocentrotus droebachiensis</i>	3.1	\
	<i>Strongylocentrotus droebachiensis</i>	3.3	\
	<i>Strongylocentrotus droebachiensis</i>	3.5	\
	<i>Strongylocentrotus droebachiensis</i>	3.7	\
	<i>Strongylocentrotus droebachiensis</i>	3.8	\
	<i>Strongylocentrotus droebachiensis</i>	3.9	\
	<i>Strongylocentrotus droebachiensis</i>	5.2	\
	<i>Ceramaster granularis</i>	2.7	\
	<i>Ctenodiscus crispatus</i>	2.4	\
	<i>Ctenodiscus crispatus</i>	2.5	\
	<i>Ctenodiscus crispatus</i>	2.6	\
	<i>Ctenodiscus crispatus</i>	3	\
	<i>Ctenodiscus crispatus</i>	3.1	\
	<i>Ctenodiscus crispatus</i>	3.2	\
	<i>Ctenodiscus crispatus</i>	3.5	\
	<i>Ctenodiscus crispatus</i>	3.6	\
<i>Ctenodiscus crispatus</i>	4.1	\	

	<i>Marthasterias glacialis</i>	23.7	
	<i>Ophiura</i> sp.	0.8	
	<i>Ophiura</i> sp.	1.4	
Gastropoda	<i>Buccinum undatum</i>	5.7	3.4
	<i>Buccinum undatum</i>	6.6	3.4
	<i>Buccinum undatum</i>	7.3	3.9
	<i>Buccinum undatum</i>	7.8	3.9
	<i>Buccinum undatum</i>	8.1	3.9
	<i>Neptunea despecta</i>	7.9	4.6
	<i>Neptunea despecta</i>	11.4	5.8
	<i>Neptunea despecta</i>	12.1	6.8
	<i>Neptunea despecta</i>	14.4	7.5

Table A2.2 Measured sized of specimens within transect R25 done as illustrated in Figure 3.14. For Echinoderms, the sea urchins were measured in diameter, and the brittlestars were measured from central disk to tip of the arm similar to specimens measured in-vivo. Not measured indicated by “\”.

Molluscs	Length (cm)	Width (cm)	Echinoderm	Lenght (cm)
<i>C. islandica</i> 1	9.9	8.5	<i>E. esculentus</i> 1	6.6
<i>C. islandica</i> 2	10.2	9.8	<i>E. esculentus</i> 2	5.8
<i>C. islandica</i> 3	9.3	8.8	Average <i>E. esculentus</i>	6.2 ± 0.5
<i>C. islandica</i> 4	8.0	7.3	<i>G. acutus</i> 1	7.0
<i>C. islandica</i> 5	10.4	8.8	<i>G. acutus</i> 2	8.3
<i>C. islandica</i> 6	10.7	10.2	<i>G. acutus</i> 3	6.9
<i>C. islandica</i> 7	11.7	11.6	Average <i>G. acutus</i>	7.4 ± 0.5
<i>C. islandica</i> 8	10.4	10.2	<i>Ophiura</i> sp. 1	8.8
<i>C. islandica</i> 9	9.2	7.9	<i>Ophiura</i> sp. 2	7.9
<i>C. islandica</i> 10	11.2	10.0	<i>Ophiura</i> sp. 3	4.4
Average <i>C. islandica</i>	10.1 ± 0.5	9.3 ± 0.5	<i>Ophiura</i> sp. 4	9.4
<i>M. modiolus</i> 1	21.1	12.4	<i>Ophiura</i> sp. 5	7.2
<i>M. modiolus</i> 2	21.8	9.4	<i>Ophiura</i> sp. 6	7.8
<i>M. modiolus</i> 3	18.3	8.8	<i>Ophiura</i> sp. 7	5.2
Average <i>M. modiolus</i>	20.4 ± 0.5	10.2 ± 0.5	<i>Ophiura</i> sp. 8	5.9
<i>B. undatum</i> 1	6.5 ± 0.5		Average <i>Ophiura</i> sp.	7.1 ± 0.5

Appendix 3: Collection of ROV-video for underwater photogrammetry and further details on workflow in Agisoft Metashape Professional

Agisoft Metashape Professional is a standalone software that uses images to generate 3D spatial data.

Agisoft has ways of generating and measuring point clouds, texture, models, orthomosaics and Depth Elevation Maps (DEM) (Agisoft, 2022). This was used to measure objects of interest. During the work conducted for this thesis a series of trials using ROV and stereo camera to collect video footage for underwater photogrammetry (UPG) were conducted. During these trials there were challenges and discoveries that were used to improve the UPG results used for this thesis. Due to the extent of the methods, key methods are described in the main methods of the thesis, and additional information can be found in this appendix to show how the results were reached describing method in detail.

This appendix is heavily referenced to the Agisoft Metashape Professional user manual (see Agisoft, 2022). This appendix describes the in-depth data collection process and Agisoft workflow used by Malin Bø Nevstad for underwater photogrammetry. The purpose of this appendix is to include details excluded from the main thesis that will be helpful in further insight into the use of underwater photogrammetry for the duration of this thesis.

Details on data acquisition using RGB-ROV

There are several software configurations that were controlled before deployment or any collection of data. The Blueye-system has configurations that "hardcode" the metadata into the collected video, making the utilization of the video more challenging in UPG as this creates a permanent overlay of metadata obscuring view for parts of the video FOV. Turning off adaptive streaming for ROV-livefeed was done as this was found to possibly reduce the video quality of the video files (Blueye, pers. com. 2022). Both the camera's spatial resolution quality and frames of the video were controlled and properly logged to keep same standard for all data collection across deployments. When using multiple camera systems, potentially differences in camera quality when pairing them on the same system or when comparing systems were considered.

Before deployment of the ROV it was ensured all hardware is connected and functioning correctly. If the battery were stored separately, battery installation and watersealing were checked for any damage in the o-rings and sealed tightly. Keeping a toolbox for hardware fails and installing is wise for field redundancy. The ROV communication were tested on land to ensure proper communication between the ROV itself, the surface unit (server) and the operator's mobile device (Figure A3.1).

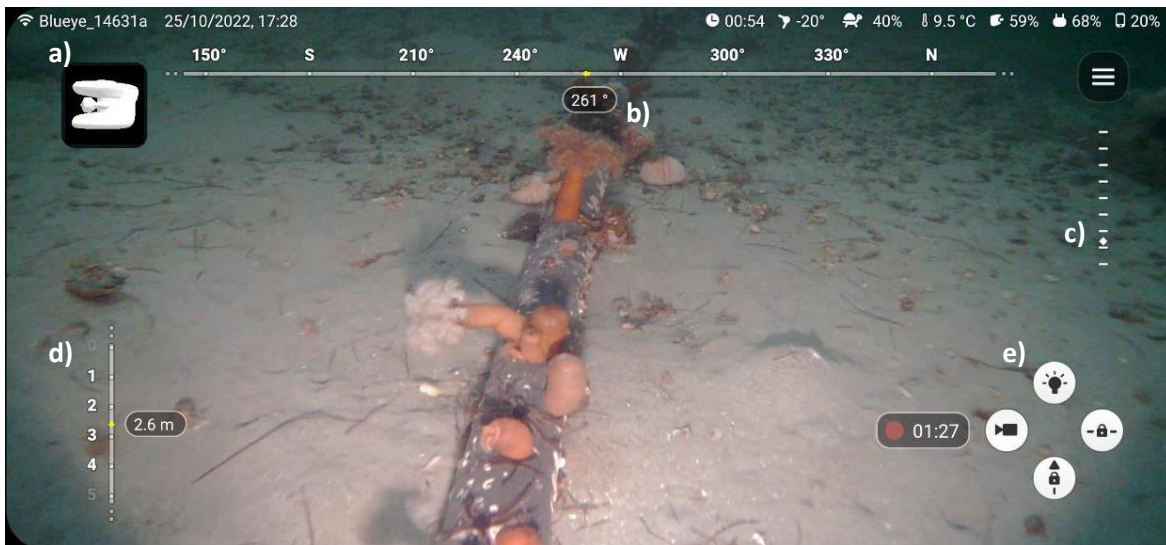


Figure A3.1 User interface overlay for the Blueye operator-app. A Bluetooth-connected controller is used to manoeuvre the vehicle, while a mobile unit communicates with the Blueye server. a) visualization of the ROV in the water updated in real-time based on the yaw, pitch and roll. b) Heading overview for the ROV. Yellow point indicates input “autoheading” and in this case current heading. c) Camera tilt level. Current tilt also displayed in the metadata bar on top of the image. d) gives depth in meters of the ROV based on internal pressure-sensor. Yellow point indicates auto-input depth and in this case current depth. e) Shows overview of current functions used during the mission. Top is light, left is camera, right is autoheading and bottom is autodepth. Image: Malin Bø Nevstad, 2022.

Weather may affect the effect of the ROV. Wind and temperature that can risk damage to the hardware of the ROV. Temperatures below -5 °C can potentially damage the batteries (recommended by Blueye, 2021). The batteries might be better secured in its own heated storage prior to deployment. Winds and corresponding water current speed/direction may affect the ROV’s pitch, roll, yaw and altitude. This is a bigger issue with a modified rig (e.g., ROV-UHI rig, see table 2.1) with mounted payload equipment and should be properly tested before deployment in field. A modified rig with mounts can potentially be destabilized more quickly and this should be kept in mind when testing, piloting and when considering the weather.

Driving method:

Study design took into consideration that the Blueye X3 did not have a geographical positioning sensor (per March 2022). Blueye company announced in spring 2022 the introduction of a compatible Doppler Velocity Logger (DVL) and global positioning for the Blueye enabling altitude control, which was not used for this fieldwork (Blueye, 2022). The Blueye model X3 has a depth sensor making driving along depth gradient best option to obtain scale compared to driving horizontally (see figure 2.4). Driving for collecting video for UPG should be done in a slow manner to reduce motion blur. Slow driving forward or sideways, using auto heading and auto depth (making the ROV keep the heading and depth set by the operator) was used to get smooth video for equal overlap between frames. For high spatial coverage, the optimal solution was found to start the transect at the deepest point of the survey area and follow a set heading while ascending in depth. This optimizes the area of the FOV viewing the seafloor.

By extracting image frames from the continuous video of transect C2 in Faksvågen an orthomosaic and a depth elevation map (DEM), if properly scaled. To obtain scale it is important to have a reference plate of known dimensions in transect video, and for this thesis a checkerboard-reference-plate of black and white squares (See camera calibration). The calibration should be done by throughout

covering the whole FOV of the camera with the checkerboard-reference-plate. Pre-calibration was also done before the fieldwork to assure that everything is in working order and up the date that we collect is going to be high quality. For separate ROV-missions across different locations in time and depth, as well as demounting- and remounting of external cameras a new set of calibration data should be collected.

When collecting video data for 3D models of objects of interest (OOI), high quality reconstructions can be acquired by filming from different viewpoints of the OOI by maneuvering the ROV in left-right motions as well as up-down motions. This makes it possible to construct a high-quality 3D reconstruction of OOI area/habitat. This eliminates “blind spots” of the ROV from only viewing an object from one direction. This was attempted in November 2021 (see figure 3.4) and later again in February (see figure 2.16).

Camera calibration

Correcting and optimalisation of cameras

Each camera have different camera parameters affecting camera video and imaging. Some of these parameters are intrinsic (internal), focal length, format size, principal point, and lens distortion. Correcting for these parameters increase reconstruction accuracy but non-calibrated cameras will also perform well in alignment and produce accurate reconstructions at sub-centimeter spatial scale (Young et al., 2017, Price et al., 2019).

The trials in camera calibration done for this thesis is described in appendix. For RGB-cameras video-data for camera calibration was collected in the sea water basin at Trondheim biological station (TBS) by using a checkerboard-reference plate. (Figure A3.2) For calibration a reference plate with squares of 4x4 cm (5 x 3 squares total) was used, giving a usable calibration surface of 20 x 12 cm for



Figure A3.2. Setup for recording the reference video used to calibrate the internal- and external camera parameters for the Blueye ROV in 2021. Here the checkerboard is quite far away and as a result does not cover enough of the screen to be used sufficiently for camera calibration. See figure 2.8 for a closer view of the checkerboard-reference plate. Image: Malin Bø Nevstad, 2021.

The ROV-RGB carrying the stereo camera is a multi-camera system consisting of the main camera (internal Blueye camera) that is assigned the navigational data (which is for this particular ROV also the body coordinate system, BCS, due to low translation). The other cameras (here this is the stereo-camera) are slave-cameras, and extrinsic (external) parameters must be calculated to adapt navigational data to the offset of the slave-cameras (giving camera coordinate system, CCS). By capturing images simultaneously by all cameras of the checkerboard-reference plate it is possible to calculate this offset. To get the CCS the rotation (R) and translation (t) between the coordinate systems must be found by calibration external parameters of the cameras. This gives the vector [T] used to generate navigational data for each of the slave-cameras (Diamanti et al., 2021). High-quality image-frames of the checkerboard-reference plate taken from different angles was used for the camera calibration done in MATLAB with the Computer vision toolbox. It was found that the data collected for the camera calibration of the stereo cameras during tests in the sea water basins and fieldwork in Karihavet March 2022 was not sufficient to calibrate external camera parameters, and further work on calibration of these were not done. For further work on this topic a bigger reference area to collect reference data more easily is recommended.

Table A3.1 shows the intrinsic camera calibration parameters used for underwater photogrammetry reconstruction from RGB-video imageframes from the internal Blueye camera.

Parameters	Definition
Fx, fy	Focal length in x- and y direction
Cx, cy	Coordinates of principal point in camera model
K1, k2	Radial distortion coefficients
P1, p2	Tangial distortion coefficients

Agisoft workflow

The workflow of Agisoft Metashape Professional (Figure 2.12) consist of these general steps: Add photos from video, align photos, build the dense cloud, build mesh, build texture, build Digital Elevation Model (DEM) and build orthomosaic (scaled photomosaic) (Agisoft, 2022). These results are then exported for use in the master thesis.

Extracting frames from video

This method of collecting data with the ROV results in video-data, and from these image frames are extracted to start the processing of UPG. This is done by importing the video. The videos extracted from the Blueye X3 is 30fps, HD video. Agisoft allows for the user to select the degree of overlap as the defining factor for the extraction of frames, or with a set “framestep” (Figure A3.3). For this thesis the “framestep” input was used. It was found that framestep 30 was sufficient for alignment of most of the transect, but in some areas the overlap was not sufficient due to high 3D structure, and these models were reconstructed with a framestep of 15, doubling the number of frames and resulting in sufficient overlap for accurate reconstruction (Table A3.2) (Agisoft, 2022).

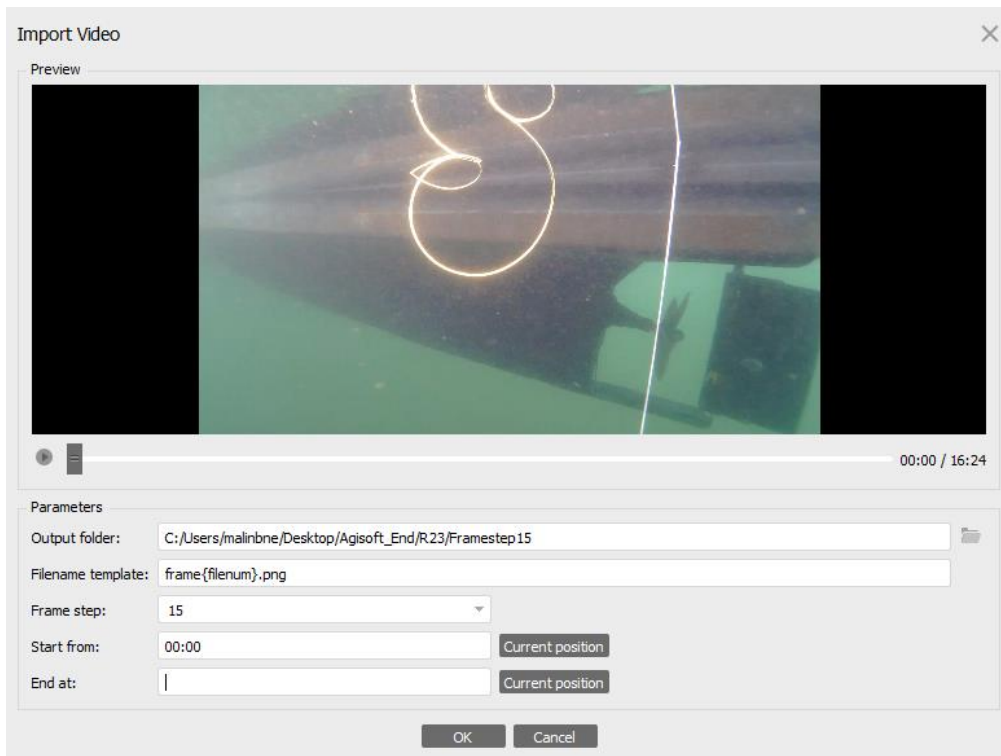


Figure A3.3 Importing video in Agisoft. The output folder will contain the frames picked out from the video, named with numbers like the filename template. Here the video image framestep is 15 meaning 2 frames are extracted per second of video where the original number of frames are 30 (fps). The images are extracted from the start of the video to not shift the numbering from the navigational dataset numbered in the same manner.

Table A3.2 showing different transects with corresponding framestep used for aligning in Agisoft.

Transect	Framestep = FPS
A1	60
C2	15
C3	15

The Blueye X3 also included an internal navigational dataset with orientation (yaw, pitch, roll) and depth (Z), which needed to be assigned to specific photo frames to be usable in Agisoft processing (Agisoft, 2022). Blueye has produced and offered a set of programmes hosted on their servers available for Blueye users. These programs were used for aligning the navigation data with the video material recorded during field (Blueye, 2022). This was accessed by connecting to the Blueye-drone’s own network as this allowed access of server 192.168.1.101. During the fieldwork in November 2021 this program was not used, which resulted in a lot of manual labor to extract navigational data for alignment. This assures that the frames were aligned with their corresponding navigational data while reducing the amount of manual labor.

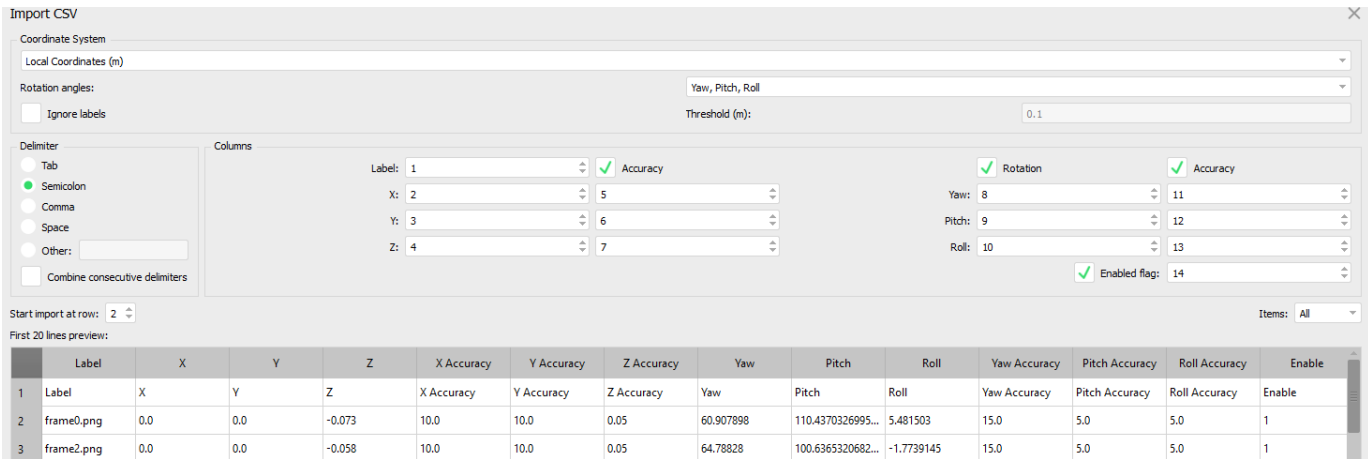


Figure A3.4 Importing a navigation-dataset adapted through Agisoft nav.data aligner into Agisoft. This dataset was extracted from the complete navigational dataset from the Blueye X3 using Blueye’s program for correctly assigning navigational data to its corresponding frame.

The navigational data is used to support placement of frames in 3D space. Accuracy for each parameter in the navigational data is shown in table A3.3 below, based on recommended values from Blueye (Blueye, 2022).

Table A3.3 Input accuracy (in meters) parameters for longitude (X), latitude (Y), depth (Z), yaw, pitch, and roll for image alignment in Agisoft.

Parameter	Accuracy (meters)
X, Y	5 – 10
Z	0.5
Yaw, Pitch & Roll	0.5

After importing the cameras and corresponding navigational data the dataset can be inspected for any low-quality images (of low spatial resolution) that could affect the model negatively. Low-quality images can be the result of motion blur or camera interpolation. With sufficient overlap single low-quality frames can be removed from further processing by disabling the specific frames (Agisoft, 2022). For the manual processing, the video was processed in Agisoft frames every two seconds were extracted for initial testing. This dataset was aligned manually assigning navigational data from the Blueye divelog masterfile. This was found to be a time-consuming process. Due to the time-consuming aligning and higher-quality imaging being obtained using a newer ROV in 2022 the dataset from November 2021 has less focus in this thesis.

After importing and aligning the video frames with the corresponding navigation data the initial alignment was done, the construction of the sparse point cloud (Figure A3.5). Here it was important to tell Agisoft what kind of data input was imported (Agisoft, 2022). The original data was in the form of a video transect with a moving platform recording different areas of a relatively permanent and immobile object of interest. This was important to note as the algorithm could prioritize frames that were close to each other in timestamps (sequential) rather than relatively far spaced from each other. Since there were no positional (X, Y) data for the whole transect the algorithm would rely on relative aligning by comparing closer frames and recording the points and manually placed markers as they shifted across neighboring frames. To save time during this stage from incorrect alignments, the “low” setting (downscaling spatial resolution of images by 16) was used first to find challenging areas where more assistance is needed in alignment, saving time spent finding high-spatial resolution features.

When all images were able to align in low-accuracy settings, the same set of images were re-aligned with high accuracy (using full spatial resolution) settings (Agisoft, 2022).

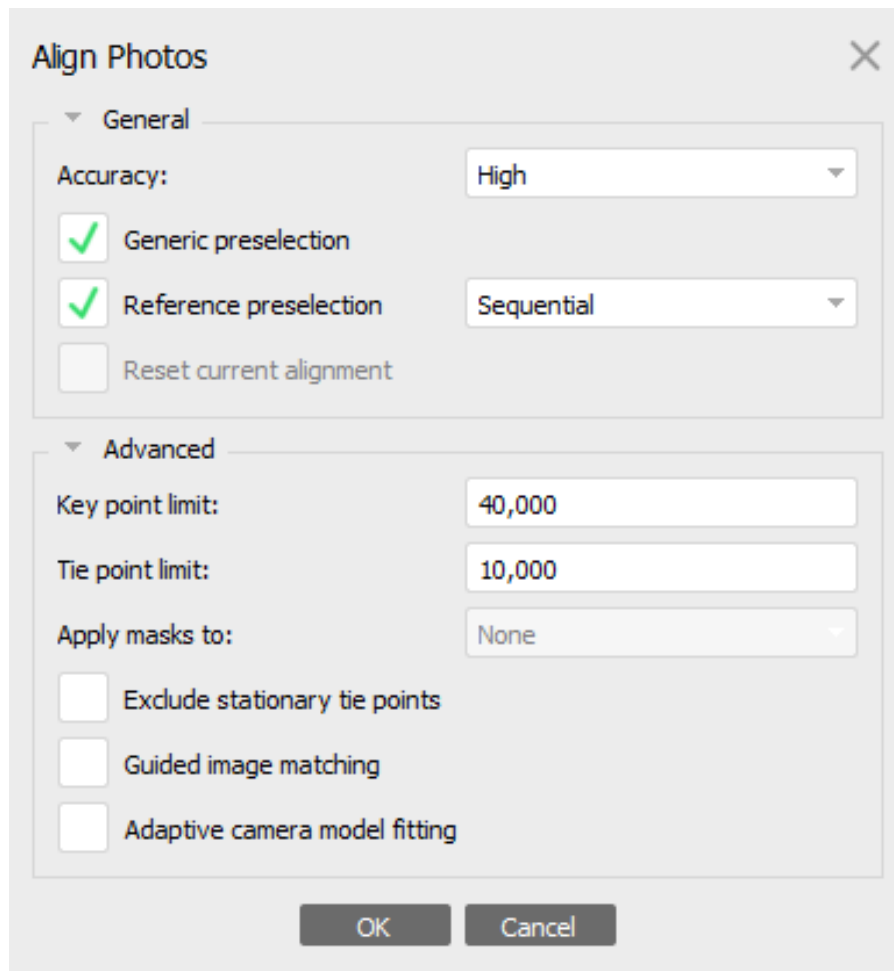
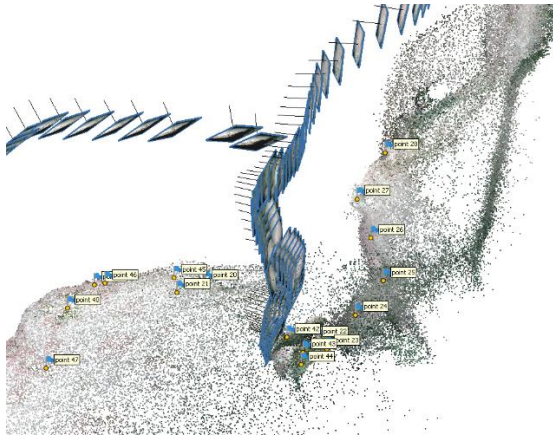


Figure A3.5 Aligning of photos and navigational data in Agisoft professional. For testing model overlap the accuracy was set to low to reduce processing time by scaling down the spatial resolution of the images by 16 times to estimate crude placement of images (see the Agisoft manual for more info). For final models the accuracy was set to high (using original-spatial resolution images) as this was the recommended accuracy setting for video and HD-cameras from Agisoft.

To increase the accuracy of the reconstruction flags and landmarks were marked in the model to help with recognition and optimize the amount of data reconstruction for an area of interest (Agisoft, 2022). In some regions it was challenging for Agisoft to align the images resulting in inaccurate alignment (Figure A3.6 a). After placement of markers (OOI visible in several overlapping images) the alignment were re-run and accurate alignment was obtained (Figure A3.6 b).

a)



b)

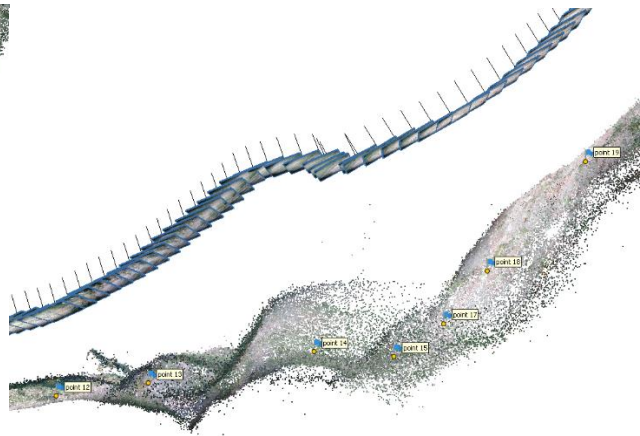
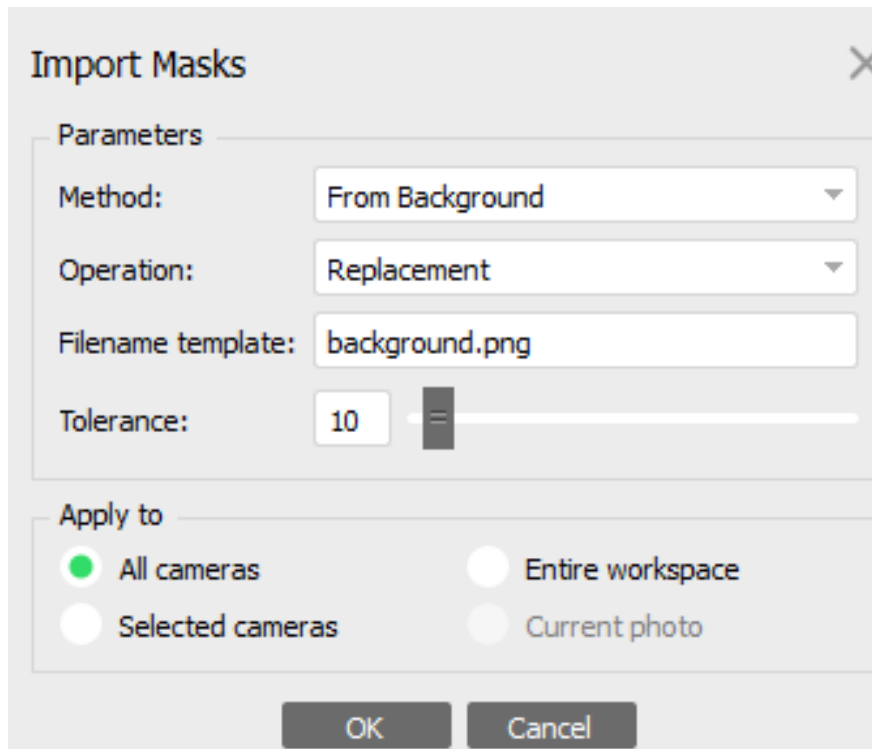


Figure A3.6 An example where markers are used to help align challenging areas in the transect a) Placement of markers did not help with the alignment of the point cloud on the left. The issue here lies in the topography. The camera on the Blueye sits higher than the light source, which in some cases with rocky substrate and being too close to the seafloor will result in a lot of shadow in the picture frames, resulting in lower overlap and a challenge in aligning two portions of the transect. This point cloud projects the difficult area from two different imaging angles, missing the middle frames due to high shadow during ascend of the ROV. b) How markers can successfully be used in challenging areas (steep areas with many obstacles) to help with alignment. In the case shown in the right figure the area with markers was previously unable to align and construct a point cloud, resulting in a failed alignment similar to the failed alignment on the left. After marking out landmarks in the individual neighboring pictures this area was aligned in the point cloud. This issue in alignment could be due to the readjustment of the ROV to the seafloor, shown by the frame legend (frames) hovering above the point cloud.

Cleaning up the point cloud

Operating in low-light to dark areas proved additional challenge due to the difference in illumination evenness due to differences in light intensity in the middle of the FOV compared to the edges of the FOV. The low-light and dark areas would affect the alignment process by making the program think the landscape was sloped. This resulted in the transect taking on a “banana shape” (Diamanti, E., prs. com. 2022). By using masks to mask out the darker parts of the frames, Agisoft performed better in aligning photos in the low-light conditions and in areas with parts shadowing over others (Agisoft, 2022). The mask was created by using a background file and running the mask to be applied to all cameras in the selected chunk as shown in Figure A3.7.



A3.7 Using masks to remove dark backgrounds in images in Agisoft. The mask used is a background filter, removing the darkest part of the surrounding water as well as some shadow from being used for point cloud construction.

Dense point cloud

The dense point cloud (Figure A3.8 a) is generated from depth maps (see Figure 2.13) which are calculated from overlapping image pairs and estimating their relative orientation parameters. Every point in the dense point cloud contains a confidence value (Figure A3.8 b) based on the number of depth maps contributing to the point (Agisoft, 2022).

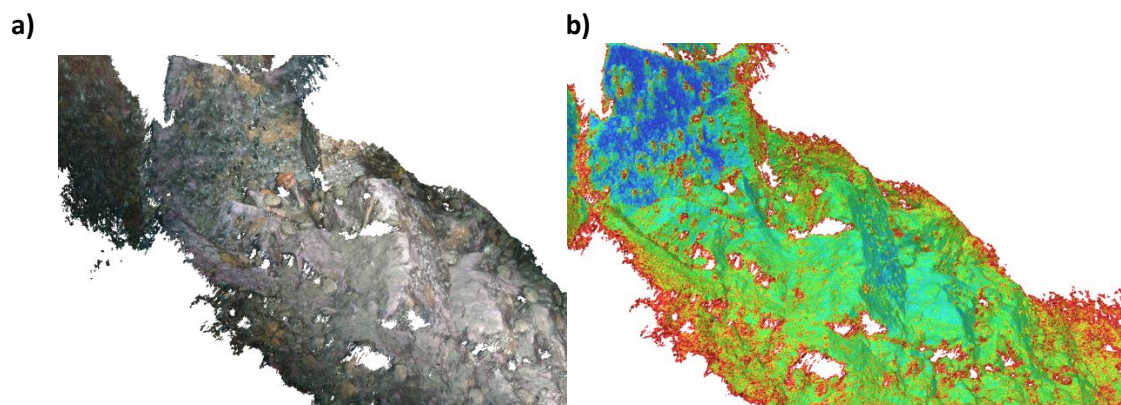


Figure A3.8 transect C3 of Nastadholmen a) Dense point cloud and b) reconstruction accuracy in the dense point cloud.

Mesh and texture construction

The mesh is a polygonal mesh model and was created based on the dense point cloud information. High quality mesh output were generated using the dense point cloud as source data (Figure 3.9 a). Surface type arbitrary could be used for any kind of modeling, while height field was recommended for aerial photography, and for the high rugosity walls were not used as much. Quality of the mesh was based on the quality in the dense cloud (here, the dense cloud used is of high quality, using full spatial resolution of the source images). Similar was done for face count, specifying the maximum number of polygons in the final mesh. Interpolation was disabled as this will lead to accurate reconstruction results without interpolated surface areas. Calculate vertex colors gave a viewable color for mesh in its own view (Agisoft, 2022). By building texture the colors of images were built onto the mesh (Figure 3.9 b). The results of the construction of the mesh and texture is seen in figure A3.10.

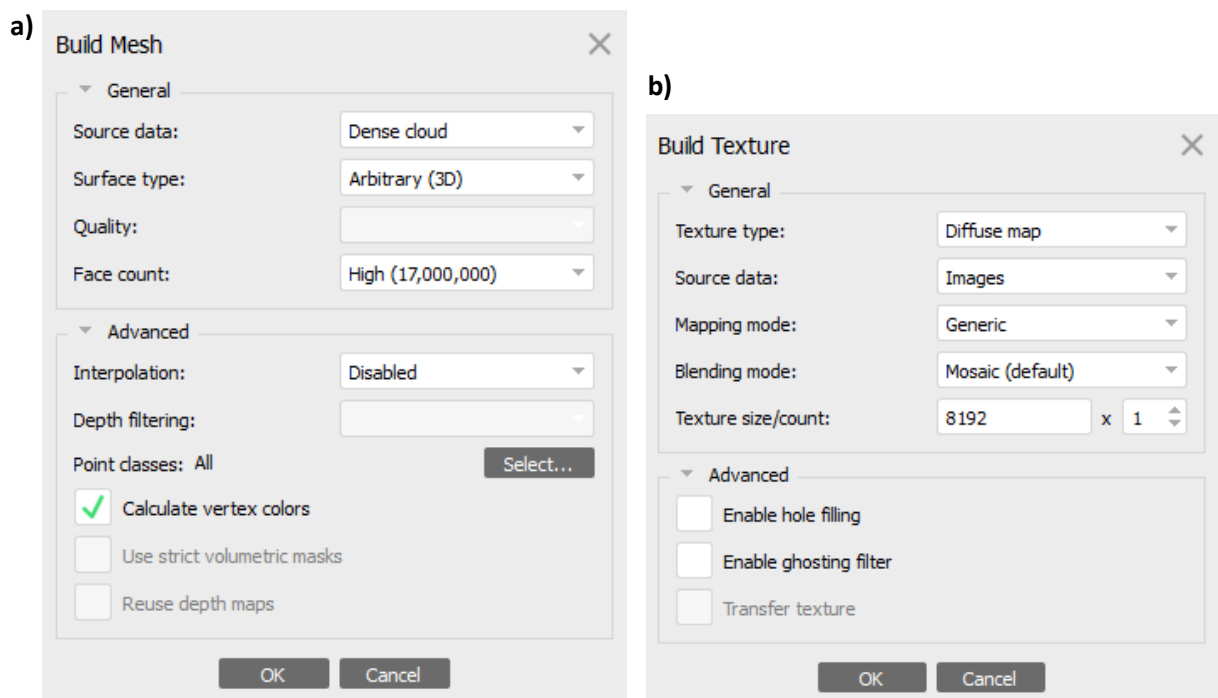


Figure A3.9 transect C3 a) building mesh from dense cloud b) adding texture from images to the mesh

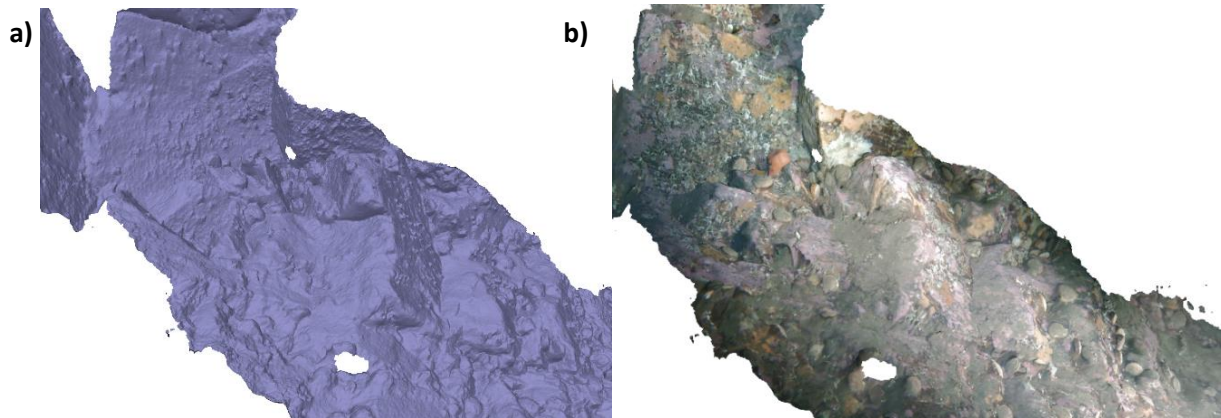


Figure A3.10 Transect C3 a) mesh b) mesh with texture.

Contours can be added as a shapelayer in the model based on navigational data assigned to their representative estimated depth based on navigational data and depth maps. The levels can be changed to preferred intervals (Agisoft, 2022). Figure 3.9 has an interval of 0.1 m per contour.

Depth elevation model (DEM) and orthomosaic construction

Depth elevation model (DEM) is a 2.5D model of a surface with height values visualized in a heat map. The DEMs in figure 3.5-3.7 was generated from the dense point cloud with planar projection type in the “Top XY” projection plane (bird’s eye view) (Agisoft, 2022). Geographic projection type was not used due not having a geographical coordinate system. No hole filling or interpolation was added as only the accurate reconstruction was wanted.

Orthomosaics are scaled, combined images providing a seamlessly merged map of the transect. Similar settings for generating the orthomosaics, but instead of being generated from the dense point cloud it was generated from the mesh (Figure A3.11). Blending mode mosaic was the default blending mode, only blending edges of the seamline between images (Agisoft, 2022).

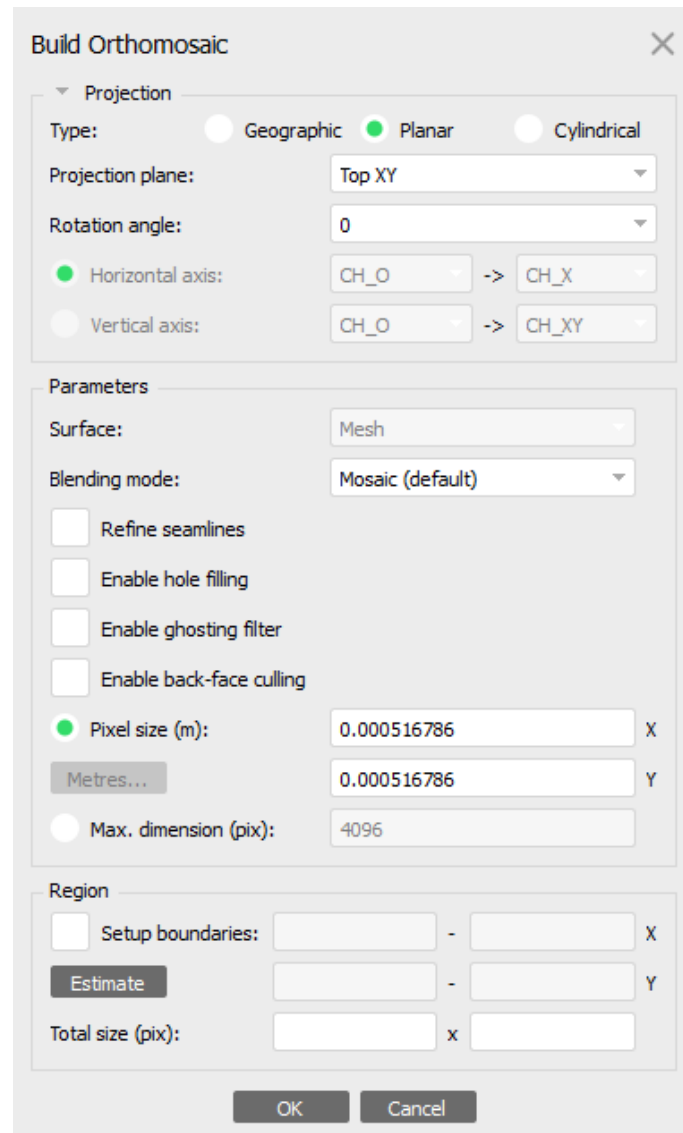


Figure A3.11 Orthomosaic construction from top-XY view. For transects it was found the planar setting was best fitting.

The model was exported in .TIF and .shp file and corresponding texture files (.png + .jpeg) making it compatible to Sketchfab (online platform for publishing of 3D models). Analysis of the models were done in Agisoft, but further analysis and extraction of biological information can be done using third-party softwares not explored in the work of this thesis.



 **NTNU**

Norwegian University of
Science and Technology